INTENSIFIED BIOCATALYSIS FOR PRODUCTION OF FUEL AND CHEMICALS FROM LIPIDS

A DISSERTATION
SUBMITTED TO THE FACULTY OF THE GRADUATE SCHOOL
OF THE UNIVERSITY OF MINNESOTA
BY

XUEYAN ZHAO

IN PARTIAL FULFILLMENT OF THE REQUIREMENTS
FOR THE DEGREE OF
DOCTOR OF PHILOSOPHY

PING WANG, ADVISER

MARCH 2010

ACKNOWLEDGEMENTS

I would like to express my deepest gratitude to my advisor, Dr. Ping Wang for his continuous support, guidance, and encouragement throughout my study and research. He has been a great mentor with his enthusiasm, understanding and willingness to help students professionally and personally.

I am very grateful for having an exceptional doctoral committee and wish to thank Drs. Daniel Bond, Shri Ramaswamy, Jonathan Schilling and William Smyrl for serving as my committee members and for their valuable and inspiring suggestions to my research. I am also indebted to Dr Jungbae Kim for his mentoring and hosting of my visiting research work at Pacific Northwest National Laboratory. I owe a special note of gratitude to Dr Xin Lu for her assistance and expertise in the electrochemical characterization work of this study. I appreciate the friendship from all my group members and the helps from the colleagues worked with me.

I wish to thank University of Minnesota Graduate School – Doctoral Dissertation Fellowship for the financial support in my last year of study.

Most of all, I am eternally grateful to my best friend and beloved husband – Xiaodong and our dearest son -- Anthony for their love, understanding and all the joys bring to me.

ABSTRACT

Triglycerides, the most well-known fatty acid esters of glycerol, are a subgroup of lipids found in vegetable oils and fats, which are abundant biorenewable resources. The effective utilization of triglycerides is one of the key interests in developing renewable fuels and products. However, natively occurring triglycerides are difficult and inefficient for use as fuels directly for regular combustion engines. The area of biodiesel synthesis therefore concerns reactions converting triglycerides to methyl or ethyl monoesters for better fuel properties. That process also releases glycerol as a byproduct, a versatile chemical promises many industrial applications. This thesis research aims at developing novel biocatalytic conversion of triglycerides and glycerol for the production of fuels and chemicals.

One key challenge in realizing efficient biocatalytic synthesis of biodiesel is to improve the reaction velocity and catalyst efficiency (in terms of amount of biodiesel produced per unit mass of biocatalyst). Toward that, this research explored a unique approach by developing organic-soluble enzymes for a one-pot synthesis-and-use strategy. Specifically, a lipase, lipase AK, was selected and chemically modified to enhance the solubility in organic media in order to catalyze a homogeneous transesterification reaction for maximum reaction velocities. The productivities of the modified lipase in a water-free reaction system were found to be over two orders of magnitude higher than previously reported results in literature. The effects of several key factors including water content, temperature, and solvent were examined for the

solubilized enzyme in comparison with several other commercially available lipases. Whereas native lipases showed no activity in the absence of added water, the organic soluble lipase demonstrated reaction rates of up to 33 g-product/g-enzyme-h. The biocatalyst remains soluble in the biodiesel product, and therefore, there is no need to be removed because it is expected to be burned along with the diesel in combustion engines. This provides a promising one-pot mix-and-use strategy for biodiesel production.

As for the byproduct (glycerol) from biodiesel synthesis, current research has mostly focused on derivation of value-added chemicals instead of being used as a simple additive in processing of food and personal care products. Key issues centered on how to produce the desired products most efficiently and selectively from glycerol. Enzymatic conversion of glycerol can generate a variety of products by selective oxidizing the hydroxyl group(s) of glycerol. The most exciting route of the selective oxidation of glycerol is the production of 1,3-dihydroxyacetone (DHA), a unique and versatile chemical with a broad range of application potentials. DHA has an annual global market of around 2000 tons with a market price ~$240/kg. In this work, DHA production was tackled through a novel biocatalytic process. Focus was placed on several aspects in understanding and optimizing the process including selection and improvement of biocatalyst, development of novel carbon electrode materials for cofactor regeneration, and reactor design.

To simplify purification and immobilization process of biocatalyst and thus reducing overall production cost, a recombinant glycerol dehydrogenase (GDH) tagged with 6xHis was produced. The successful insertion of *gld*A gene into a pET151/D-TOPO

vector with T7 promoter was confirmed through PCR amplification, DNA sequencing, and restriction digestion. Following the transfection, the BL21(DE3) *E. coli* strain produced GDH dominantly in the induced culture, with yields over 10 mg of enzyme per gram of cell paste. The success in expression of recombinant GDH was evaluated with immunodetection and amino acid sequencing. The specific activity (80 unit/mg) and stability of isolated GDH were also examined. The activity of the recombinant GDH was slightly higher than that of commercially available products.

GDH requires a cofactor to catalyze the desired biotransformation of glycerol. Cofactor NAD(H) is needed by more than 300 dehydrogenases including glycerol dehydrogenase. Unlike enzymes, cofactors are stoichiometrically consumed. Taking the high price of NAD(H) into consideration, it is apparently not viable for any large-scale enzymatic catalysis without regeneration or reuse of the cofactor. Among all the cofactor regeneration methods, electrochemical regeneration offers faster reactions and easy operations. However, the energy efficiency still needs improvements for practical application. One fundamental way is to reduce overpotentials involved in cofactor regeneration by developing highly active electrodes. In this research the development of 3-D carbon material by using carbonized of cellulosic fibers with branched CNT was achieved. The specific surface area of the resulted fibers reached 291 m^2/g as determined by using BET method, about 30-fold of improvement over regular carbon fibers. It was also discovered that this novel material showed improved electrochemical activity toward oxidation of NADH. The oxidation potential of NADH decreased from above 0.8 V to 0.6 V as a result of the introduction of CNT. Mediated cofactor regeneration methods

were also investigated by using Meldola's blue and poly(methylene green). Both approaches can reduce the oxidation potential of NADH to 0.1 V desired to avoid inactivation and dimerization of the cofactor in addition to energy consumption.

To examine the efficiency of the targeted glycerol oxidation reaction for large scale applications, cofactor regeneration was tested for two reaction processes. In one process, glycerol oxidation reaction with immobilized GDH in a fixed bed bioreactor was operated along with a separated electrochemical cofactor regeneration unit. The immobilized enzyme catalyzed the glycerol oxidation reaction with continuously fed glycerol substrate solution, which reduced the product inhibition effect significantly by immediate removal of the product. The reduced cofactor (NADH) from the enzymatic reaction unit was oxidized on a 3-D CNT-carbon electrode at 0.6 V in the cofactor regeneration unit, was then recycled back to the reaction unit. With the regeneration of cofactor, the TTN of cofactor reached over 5 in 15 cycles of operation based on the original amount of cofactor added. In a second process, regeneration of cofactor was realized *in situ* in the enzymatic glycerol transformation reactor. Glycerol oxidation reaction was catalyzed by GDH immobilized on microparticles. NAD^+ was again regenerated electrochemically, releasing protons carried over from glycerol oxidation reaction. The protons was converted to water by introducing another immobilized enzyme—laccase. With this design, the total turnover number (TTN) of cofactor reached over 3500.

To demonstrate the vast potentials of using the biorenewable carbon electrodes developed in this work for a variety of bioprocessing, research on using the carbon

fibrous electrodes were conducted for biosensing and carbon capture. In one effort, a model microfiber biosensor was constructed to demonstrate the possibility of detecting biochemical compounds and enzymes by taking advantage of the ubiquity of NADH in biocatalysis. The reaction system showed a linear response for glycerol detection up to 0.25 mM with a detection limit of 0.04 mM. For the measurements of glycerol dehydrogenase activity, the linear range was found between 0.004 and 0.05 U/ml. In another thrust, the reduction of carbon dioxide to formate was examined by applying the modified carbon material as a working electrode. The results showed that formate concentration was as high as 30 mM with over 50% current efficiency. Toward that, the 3-D carbon electrode was further modified with Sn by electroless plating to improve the selectivity toward formate production. Compared to its parent carbon fiber electrode, the Sn-modified electrode demonstrated a 5-fold higher current efficiency. In addition to the effect of CNT, it is believed that the introduction of Sn also afforded much improved adsorption of protons and electrode activity, and thus improving the overall efficiency toward formate production.

One potential advantage of using bioelectrochemical method for cofactor regeneration is the possibility to integrate the biochemical process with biofuel cells for simultaneous chemical production and power generation. That represents an exciting future technology. Toward that, this thesis explored the necessary fundamental issues, including the construction and study of a model glucose/oxygen biofuel cell. The kinetics of the glucose biofuel cell was investigated to determine the limiting factors. The reaction kinetic parameters were applied to predict the current generation from an

enzyme-based bioanode successfully when it was examined as a single electrode, however, the biofuel cells only reached a power density equivalent to <40% of reaction capability of the enzyme immobilized on the electrode. It appeared to us that factors such as electron and proton transfer resistances rather than catalytic reaction rate are overwhelming in limiting the power generation of the biofuel cell.

TABLE OF CONTENTS

Page

LIST OF TABLES

LIST OF FIGURES

Figure Page

CHAPTER I

INTRODUCTION

1.1 Research Topics and Significance

Lipids constitute a large group of natural molecules which have important biological functions. Their main functions are for energy storage, structural components of cell membranes, and signaling molecules. Triglycerides, a subgroup of lipids contribute to the bulk of storage fat in animal tissues for energy storage purpose. Another major source of triglycerides is vegetable oil. The breakdown of triglycerides in biological systems is controlled by enzymes, lipases[1]. This reaction releases fatty acids and glycerol and provides high caloric content (38 kJ/g), which is more than twice the energy release from the breakdown of carbohydrates and proteins. Free fatty acid can readily react with simple alcohols such as methanol and ethanol forming monoesters, which can be applied directly to combustion engines and thus are called biodiesel. The theme of this thesis research is to explore effective utilization of triglycerides by deploying novel biocatalysis in renewable energy generation and chemical production areas. Topics including enzymatic biodiesel synthesis, catalytic oxidation of glycerol, and direct conversion of CO_2 will be explored.

1.1.1 Biodiesel

Biodiesel synthetic reaction can be catalyzed chemically with acids or bases, or enzymatically. In the industrial synthesis of biodiesel from triglyceride, all types of vegetable oils and animal fats can be utilized. At present, commercial production of biodiesel is mainly achieved through alkali-catalyzed transesterification of soybean oil. Albeit its conversion efficiency, several issues in that process are subject to further improvement. These issues include the removal of inorganic salt from the products, the recovery of glycerol, dehydration, and the treatment of alkaline wastewater[2, 3]. The use of lipase-catalyzed transesterification reactions in low water media has pursued recently as a promising approach to overcoming these problems[4]. It was expected that the application of lipases could afford high conversion yields of oils and simplify downstream product purification at the same time[5, 6]. As reported so far, however, native or immobilized lipases require the addition of certain amount of water to redeem in most cases only moderate activities. According to these works, a least water content of 0.48% (wt) is required to activate the enzymes. Therefore, additional dehydration steps will still be needed for such lipase-catalyzed synthesis of biodiesel. Anhydrous transesterification reactions are hence desirable. One way to improve enzyme activity in anhydrous organic media is to solubilize the enzymes and thus achieving homogenous reactions. One effort of this thesis research is to explore the possibility of a water-free biodiesel synthesis process using alkyl-modified lipases.

1.1.2 Glycerol processing

The major byproduct in biodiesel synthesis is glycerol. Glycerol is a very versatile and valuable chemical[7]. However, the glycerol market is currently undergoing radical changes, driven primarily by the very large supplies from biodiesel production. That have driven researchers to explore new uses for glycerol as a source of raw material replacing petrochemicals[8]. Glycerol can be produced into high varieties of chemicals via many reactions, including oxidation, reduction, and dehydration reactions. Among other synthetic routes, glycerol can be selectively oxidized into 1,3-dihydroxyacetone (DHA), a valuable chemical intermediate and additive a pharmaceutical and personal care products, with a market value of about 200-fold higher than that of glycerol. Currently the popular methods for the production of DHA are chemical synthesis and microbiological fermentation. Most of the industrial production of pharmaceutical and food grade DHA was preformed through fermentation conversion of glycerol with only moderate yields (~20 g/l) and complicated purification and separation requirements[9, 10]. DHA can also be produced through chemical catalysis from formaldehyde or glycerol[11, 12]. Such synthetic routes involve the production of undesired byproducts due to the low selectivity of the catalysts. Although fine tuning of reaction conditions and composition of catalysts may improve the selectivity[13, 14], yields of the desired product are still generally low[15]. Generally speaking enzymes promise much faster reactions than microbial processes, and offer precise molecule control of the products. The oxidation reaction of glycerol can be catalyzed by an enzyme, named glycerol dehydrogenase (GDH, EC 1.1.1.6), which can be found in a broad variety of bacteria

strains such as *Enterobacter aerogenes*, *Cellulomonas sp.*, and *E. coli*. The glycerol oxidation catalyzed by GDH has been demonstrated before[16]. In fact the systematic studies of GDH may date back to 1953[17, 18]. However, the enzymatic method of DHA production is still at an early research stage. GDH requires either NAD(H) as a cofactor. The cofactor acts as an electron carrier during the enzyme catalyzed redox reactions. Most of previous studies have been conducted for chemistry and analytical interests[19], for which neither cofactor regeneration nor proton accumulation was a critical consideration. Sustainable chemical production has to provide efficient means in dealing with those issues. Investigation of DHA production from glycerol constitutes another important part of this thesis.

1.1.3 Cofactor Regeneration

Another bottleneck problem for enzymatic production of DHA is the high production cost of the cofactor, NAD^+. Unlike enzymes, cofactors are consumed stoichiometrically in biochemical reactions. They are often much more expensive than the desired products, which costs ~$1,000/kg in the case of NAD(H). Accordingly, efficient regeneration and reuse of the cofactors is vitally important to their large-scale applications[20]. Methods including microbial, enzymatic, chemical, photochemical, and electrochemical have all been developed for cofactor regeneration[21]. Among these regeneration methods, electrochemical approach has advantages over other methods in that it provides low cost, easy product isolation, *in situ* monitoring of reaction progress etc. The reaction on the electrode can be expressed as $NADH \leftrightarrow NAD^+ + H^+ + 2e^-$. The

theoretical redox potential of NAD(H) is +0.32 V vs. standard hydrogen electrode (SHE). However, it has been shown that the redox reaction of NADH on electrodes tends to involve high overpotentials (potentials above the theoretical redox potential of the reaction). For examples, direct electrochemical oxidation of NADH at pH 7.0 was observed at 1.1 V on carbon electrode[22] and 1.3 V on the platinum electrode[23], much higher than the ideal case of 0.32 V. High overpotentials reduce the process efficiency, and in many cases, introduce undesired side reactions. In case of NAD(H), such high potentials tend to denature the cofactor and cause the electrode fouling (due to the adsorption of denatured NADH and NAD^+). Therefore, many analytical methodologies favor the use of highly active mediators to reduce the redox potentials on electrodes[24]. A number of mediators were developed to realize NADH oxidation at lower potentials, but they are generally associated with poor stability, complicated and time-consuming modification procedures, and complication with product recovery, making the utilization of mediators a daunting task for large-scale bioprocessing applications. Alternatively, the use of nanostructured electrodes can also reduce the redox potential on electrodes without using mediators. Several recently published studies have revealed that carbon nanotube (CNT) and nanoparticles could enable efficient regeneration of NAD(H)[25-27]. In this study, a novel fabrication method of carbon electrode was realized by using cellulosic material. The electrochemical properties of such material will be tested for the potential applications in many fields including cofactor regeneration, biosensing, and biosynthesis.

1.1.4 Nanocarbon Electrode Material

One additional goal of this research is to utilize renewable resources for the preparation of nanostructured carbon electrodes. Previous studies of the fabrication of carbon fiber electrode based on synthetic polymers lack the potential of low cast scale-up for applications in biochemical processes. A feasible approach could be carbonization of cellulosic materials. There have been no reported attempts so far in growing CNT on surfaces of cellulose-derived carbon fibers to produce nanostructure materials. This work explores the use of naturally derived cellulose materials for preparation of hierarchical carbon materials. Metal-catalyzed growth of nanotubes has been applied widely in recent years for preparing a variety of nanostructured materials, such as the fiber-tube and fiber-fiber[28] hybrid carbon materials, for the purposes of increasing surface area, providing higher sensitivities and easy preparation for many applications including field effect transistors[29]. The introduction of CNT in this kind of nanostructured materials for electrochemical applications has resulted in a great improvement in electrochemical properties. All of these reported fibers for CNT growth are synthetic materials for larger scale application, and it is therefore necessary to investigate the use of renewable materials for sustainable production of CNT-based electrodes. A new and facile fabrication production method of CNT-carbon fibers is developed through carbonization of cotton wool fibers and growth of CNT in the presence of Fe/Ni.

1.1.5 Extended Applications of Nanostructured Carbon Electrodes: Biosensor and CO_2 Reduction

Combining with the development of nanoscale materials and other electrochemical means, biological electrochemical devices, ranging from microscale to macroscale have boosted in both research and application fields. Cellulosic carbon materials with CNT content is promising in both kinds of applications, since single fiber can be fabricated into a microscale electrode, and larger pieces of carbon materials can be used as 3-D macroscale electrode for many electrochemical applications.

Microelectrodes are of great interests because it can be used in many microelectronic applications including microbiosensor[30-32] and miniature fuel cells[33]. One drawback in using single carbon fiber microelectrodes is that only limited surface area is available and thus very weak electronic signals can be detected. This setback is a result of the diameter of carbon fibers are usually in the range of several micrometers to tens of micrometers. Depositing CNT on the surface of fiber can improve the overall surface area; therefore, can be helpful to overcome this drawback without substantially changing the size of the electrode. Several approaches have been tested and reported in literatures, for examples, CNT was deposited on single carbon fiber microelectrode[34] and nanoelectrode[35] by dipping carbon fiber electrodes into CNT suspension with the aid of other chemicals, by dip-coating[36]on the electrode in Nafion® suspension, and by electrochemical deposition[37]. In addition to surface area improvement, CNT can also introduce many favorable properties desired for electrochemical applications[38]. For instance, CNT have been found capable of

promoting electron transfer, minimizing electrode fouling[39], enhancing electrocatalytic activity, and facilitating the immobilization of biomolecules[40, 41]. Nevertheless, the reported preparations of CNT-containing electrodes do not promise to fully capitalize the potentials of CNT, as the fabrications generally led to CNT that are bundled together or embedded inside other supports such as polymers, exposing only a portion of CNT for reactions.

In this work the use of carbon-fiber and CNT hierarchical electrodes with nanotubes branched out from the surface of the fibers was explored. A single CNT-modified carbon fiber was then used as a microelectrode, and tested for the efficiency of oxidation reaction of NADH generated from the glycerol oxidation reaction to explore its potential in large scale electrochemical applications involving NADH reuse and regeneration. It is expected that the single CNT-modified carbon fiber will provide sensitive detection corresponding to the concentration changes of NADH in glycerol oxidation reaction, lower the overpotential of NADH on carbon electrode and reduce the electrode fouling. For sensor applications, single carbon fiber electrodes are especially appealing in that they require only a small amount of samples, but provide high signal/noise ratios and render short responding times[119-121]. Such sensors have found a variety of applications.

The production of bioproducts and bioenergy attracted attentions from researchers and government agency for the biorenewable, biodegradable, and sustainable concerns. Moreover, the environmental matter of greenhouse gas has been focused on for decades. The solidification of CO_2 becomes the challenge tasks[42, 43], and new technology for

such application is highly on demand. CO_2 can be regarded as a kind of carbon source and reduced to chemicals and fuels. Reduction methods such as chemical[44], photochemical[45], enzymatic[46] and electrochemical[47] approaches have been developed. For example, reduction of CO_2 to syngas and fuel has been realized under high temperature and pressure by chemical method[44]. Photochemical and enzymatic catalyses could reduce CO_2 at a relative ambient condition, but the concentration of redox product is too low to be economical in the practical applications. Comparing to other methods, electrochemical way of CO_2 reduction sounds to be a promising route, since electricity is currently in low price compare with other energy sources and can be generated from renewable substances, such as wind and water power. On the other hand, the concentration of product in electrochemical reduction can be relevantly high and suitable for practical applications. Formic acid/formate is not only the one step reduction product of CO_2, but also the useful chemical as a fuel or used in fuel cell. In this study, the fabricated carbon based material which composed by carbon fiber with carbon nanotubes was used as electrode for CO_2 reduction. CNT-modified electrodes have showed some advancement in catalytic ability.

1.1.6 Biofuel cells

DHA production from glycerol can be designed as a biofuel cell. The total reaction in glycerol biofuel cell is described as $glycerol + \frac{1}{2}O_2 \rightarrow DHA + H_2O$. The theoretical potential of glycerol biofuel cell will be: 0.56 V. Although many potential applications have been proposed since the invention of biofuel cells, no biofuel cells were

commercially available for power generation other than in research labs currently. This is mostly due to the lower performance of biofuel cells, compared to conventional fuel cells. So, how to transfer electrons efficiently from the biocatalysts reaction active sites to the electrodes becomes the critical issue in direct biofuel cells. Usually, it is difficult for direct electron transfer to the enzymatic electrodes due to the non-conductive protein hull which covers active sites of enzymes. Direct electron transfer was observed only in cytochrome c, laccase and several peroxidases[48-51]. Methods of chemical modification were also developed to help increasing the enzymes conductivity. Other than the above approaches, mediator also could be used to shuttle between the active site and the electrode; therefore, the resistance of enzymatic electrode could be reduced. When mediator was used, usually much higher cell efficiency could be reached. A glucose biofuel cell was used as model to study the kinetic limitation, including the mass transfer and electron transfer rates in enzymatic biofuel cells. The knowledge generated from this study will be used in the development of glycerol biofuel cell.

1.2 Objectives

This research focuses on production of valuable chemicals in an economical and environmental friendly way. Glycerol was oxidized into DHA which has a market price about 200 folds that of glycerol and being widely used as an intermediate in pharmacy and chemical engineering areas. The reaction is catalyzed by GDH and use NAD^+ as cofactor. The reduced form of cofactor (NADH) was oxidized on carbon based electrode at the potential ~0.6 V. This work will provide a brand new approach in electrochemical

application, which combines chemical production and electrochemical regeneration of cofactor. The understanding of the parameters in this process will benefit the biochemical and electrochemical society. The knowledge developed from this study will be able to realize the optimization the whole production procedure and promote advancement in bioprocessing technologies. The schematic illustration of the whole process is shown in Figure 1.1. This study started from triglyceride biomass (soybean oil) and produce biodiesel and DHA with the electrochemical regeneration of cofactor. The whole project can also be combined with other operational unit for the production of electricity and biodegradable polymers in expanded research.

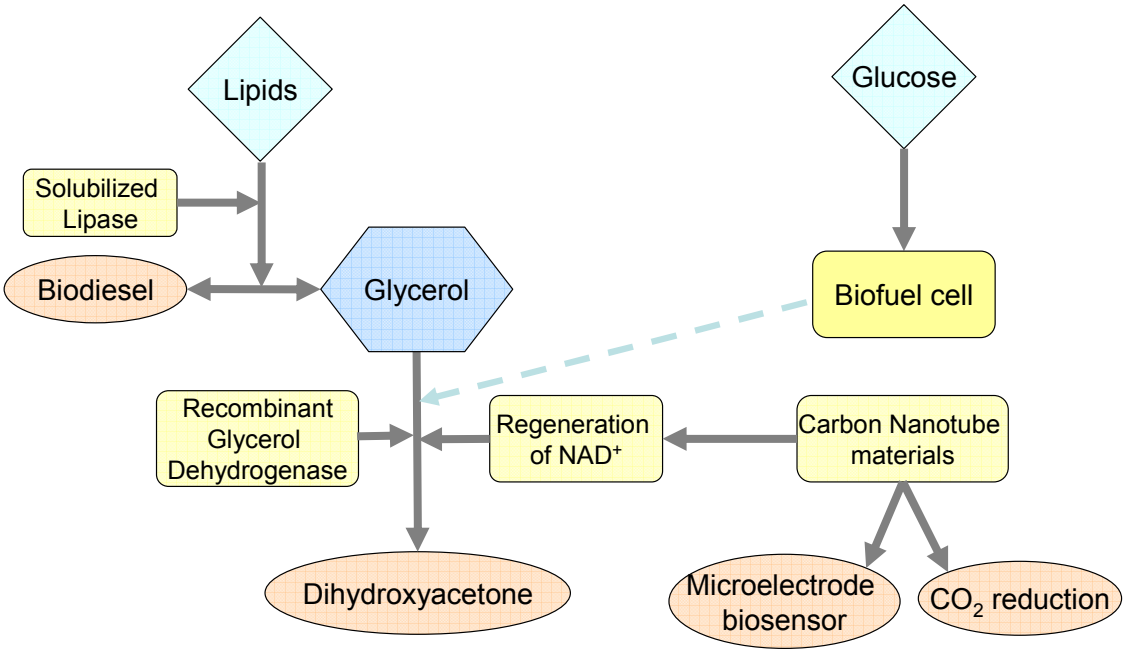

Figure 1.1 Schematic illustration of this research.

The primary focus of this research is to achieve the production of DHA from glycerol, a byproduct from biodiesel industry, with the assistance of electrochemical technology of cofactor regeneration. The key challenge is realization of efficient regeneration of cofactor NAD^+ in the production system with competitive rate of catalytic reaction. Accordingly, the specific research objectives include:

(i) Synthesis of biodiesel from soybean oil with enzyme catalyst;

(ii) Production of recombinant GDH by overexpress *gld*A gene in *E. coli*;

(iii) Production of 3-D carbon based material from cotton with the attachment of carbon nanotubes, and the application of carbonized cotton material in microfiber biosensing;

(iv) Exploration electrochemical regeneration methods of cofactor NAD^+/NADH on carbon based electrodes;

(v) Evaluation of limitations in enzymatic biofuel cells; and

(vi) Application of carbonized cotton material in CO_2 reduction to formate.

1.3 Major Approaches

1.3.1 Synthesis of Biodiesel with Solubilized Enzyme

In the enzymatic synthesis of biodiesel, native or immobilized lipases require the addition of certain amount of water to redeem their activities. Several recently reported works have examined the influence of water on the transesterification activities of lipases, which a least water content of 0.48% (wt) is required to activate the enzymes. That is

about 10 times of the regulated 0.05% water allowance for biodiesel in U. S. [52]. Anhydrous transesterification reactions are hence desirable, as the same for many other synthetic purposes[53]. To improve the enzyme activity in anhydrous organic media, lipase was solubilized by modification with hydrophobic chemical, thus synthetic reaction of biodiesel was achieved in homogenous reactions. A one-pot water-free biodiesel synthesis process was developed using alkyl-modified lipases. Lipases from different sources were screened to improve the conversion of transesterification reactions. In this water-free biodiesel synthesis reaction system, factors such as co-substrate, temperature, pH, and water content were evaluated. The efficiency of enzyme catalyst and the conversion of biodiesel synthesis reaction were analyzed with GC.

1.3.2 Production of Recombinant Glycerol Dehydrogenase

An important consideration in biodiesel industry is to utilize the byproduct of the reaction – glycerol. Converting glycerol into value-added product or energy could facilitate the sustainable blossom of biodiesel industry. Glycerol can be converted into many chemicals including 1,3-dehydoxyacetone catalyzed by biological catalysts. Among those biocatalysts, GDH catalyzes the oxidation reaction of glycerol with the assistance of cofactor, NAD^+. GDH is highly pricy in current market due to the low production yield in bacteria culture, low specific activity, and easy to denature. To use enzyme in the industrial scale production, an easy immobilization method should be provided. Recombinant GDH was produced by overexpress the *gld*A gene into *E. coli* with pET151/D-TOPO vector, and tagged with 6x-His for the easy purification and

immobilization. The insertion of *gld*A gene was confirmed with restriction digestion, Polymerase Chain Reaction (PCR) reaction, DNA sequencing, and amino acid sequencing analysis. The recombinant GDH produced was immunodetected with western blotting, and purified with affinity chromatography. The yield of the bacteria culture was evaluated in term of activity per culture volume.

1.3.3 Production of Carbon Based Electrode Material from Cotton Wool

The biooxidation of glycerol can produce various valuable products, including several chemical intermediates for pharmaceutical or synthetic applications. However, the price of cofactor usually limits the usage of GDH as catalyst, since one NAD^+ will be consumed for the production of one molecule of product, i.e. DHA in this study. This makes the regeneration of cofactor necessary for the realization of biocatalytic DHA production from glycerol. Cofactor can be regenerated with many methods, including chemical, microbiological, and enzymatic approaches. Electrochemical regeneration of cofactor have shown the advantages of low cost, no consumption of stoichiometric regenerating reagent, readily controlled redox potential, and easy monitoring of reaction progress. The concerns, however, lie in the incompatibility with many biochemical systems, poor selectivity (especially for reductive regeneration), complex apparatus and procedures, requirement in many systems for mediating redox dyes or enzymes, most of all, the rapid fouling of expensive metal electrodes. Carbon based electrode material was produced by carbonization of cotton wool in a high temperature oven for the regeneration of cofactor in glycerol oxidation system. The surface area of the material was improved

with the formation of multi-wall carbon nanotubes on the surface of carbon fiber introduced by metallic nano particles. The morphology of carbon based material and carbon nanotube layer was observed by Scanning Electron Microscope (SEM) and Transmission Electron Microscopy (TEM). The BET surface area of carbon material was examined with gas adsorption technique.

1.3.4 Construction of Single Microfiber Electrode for Biosensors

Single carbon fiber electrodes are greatly promising for microelectronic applications, and are especially appealing in sensor applications because of fewer amounts of samples, higher signal/noise ratios and shorter responding times. CNT is well known as high specific surface area material. In addition to that, CNT also impart many favorable electronic properties desired for biosensing, which includes promoting electron-transfer reactions, minimizing fouling of electrode surfaces, enhancing electrocatalytic activity. The carbon-fiber with carbon nanotubes branched out was prepared by using renewable resources (cotton wool) as described in section 1.2.3. A single CNT-modified carbon fiber was then fabricated into a microelectrode, and tested for the efficiency of oxidation of NADH generated from glycerol oxidation reaction. The electrocatalytic activity of microfiber electrode was evaluated by the oxidation potential of NADH employing a cyclic voltammetry analysis in an electrochemical cell. The detect limit and dynamic range of such biosensor for the detection of glycerol and glycerol dehydrogenase were measured by amperometry technique (I-t) in the electrochemical cell. The reusability of microfiber biosensor was tested, and the potential

of applying 3-D hierarchical carbon material in large scale electrochemical applications involving NADH reuse and regeneration was also explored.

1.3.5 Electrochemical Regeneration of Cofactor and DHA Production

The reversible one-proton redox potential for the couple of NAD^+/NADH is -0.32 V *vs.* hydrogen electrode[54] at pH 7, higher applied potentials are required to achieve an appreciable electron-transfer rate due to the slow heterogeneous kinetics at unmodified metal and carbon surfaces[55, 56]. The adsorption of NAD^+ and the occurrence of uncontrolled side reactions may also cause severe interferences[57, 58]. Due to the high overpotential and considerable dimerization, NAD^+/NADH cannot direct react on the surface of solid electrodes electrochemically. Therefore, efforts in preparing modified electrodes with electrocatalytic activity in NADH oxidation were focused on either using electropolymerized films or novel electrode materials to lower the overpotential. The regeneration of cofactor in glycerol oxidation reaction system was studied with both approaches. One approach used was the modification of carbon electrode with poly-(methylene green); the other was the realization of carbon nanotubes growth on the surface of carbonized cotton fiber to develop a new kind of electrode material with increased specific surface area. Both methods were evaluated by the term of NADH oxidation overpotential, which was measured with cyclic voltammetry. Cofactor regeneration efficiency was evaluate by regeneration cost, stability of the operational process, separation cost of the products, and the kinetics parameters of enzymatic reactions[59].

Techniques developed including recombinant enzyme production, carbonized electrode material production, and electrochemical regeneration of cofactor were integrated into a bioprocess for production of DHA from glycerol. The process included two operation units: catalytic reaction unit and cofactor regeneration unit. Conversion yield, cofactor regeneration efficiency, and some other operational factors were optimized.

1.3.6 Construction of 3-D Carbon Electrode for Reduction of CO_2

Formic acid/formate is not only the one step reduction product of CO_2, but also the useful chemical as a fuel or used in fuel cell. Producing formate by CO_2 reduction seems to be a promising way with easy equipment and high efficiency. Chaplin[60] reviewed the effects of reaction conditions and electrode material on the pathways of electrochemically reduction of CO_2, especially the formation of formate. Some favorite reduction products were found occurring at specific electrodes in electrochemical reduction of CO_2 in previous research[47, 60, 61]. For example, formate was favorably produced on a sp transition metal electrode[47]. To a large extent, the electrode properties determine the product of electrochemical reduction of CO_2. Stannum electrode has been proven to be an electrode with high current and good selectivity, which are the important properties for large scale production of formic acid/formate. Hori[62] revealed that formate was the predominantly product of CO_2 reduction on Sn electrode. Formate is produced on the electrode with high overpotential. According to the theory about electrochemical reduction of CO_2, the quantity of active site and adsorption of CO_2 anion

radical on the surface of electrode determines the productivity of CO_2. Nanostructure materials were proven to have more active site and higher surface area to realize CO_2 reduction[63]. In addition to that, nanopores can help to create a virtual higher pressure on the surface of electrode, therefore, increase the productivity. We have developed a carbon based material being composed of CNT-carbon fiber by carbonization of cotton wool fiber deposited with metal catalyst in a high temperature furnace followed by the growth of CNT. Electroless plating of Sn on CNT was designed to improve electrode selectivity of formate. The developed materials were fabricated into a CF-CNT electrode to realize CO_2 reduction. The reaction conditions were optimized with formate yield and current efficiency as targets. The reaction kinetic parameters were determined for the understanding of the complicated electrochemical reaction mechanism. Potentials of operation were selected by using cyclic voltammetry. The current efficiency and conversion yield was calculated based on the current applied in I-t technology. The products from the reaction were measured in a Gas Chromatography.

1.3.7 Evaluation of Reaction Kinetics in Enzymatic Biofuel Cells

Currently, use of renewable energy and low-carbon fossil energy technologies are highly desired to ensure energy security. Moreover, clean and efficient energy technologies were also demanded for the environment concerns. The most recognized efficient process of using fossil fuels is the conversion of chemical fuels stored in fossil fuels directly to electricity. This process could be realized by fuel cells. The theoretical efficiency of fuel cell process could reach 100%. In addition to all the advantages of

chemical fuel cells, biofuel cells provide much more options in the fuel selections. Biofuel cells are even more environmental friendly because both the catalysts and the fuels are renewable. The low power density and stability narrowed the biofuel cells to the areas, such as clinic, health care and biomedical applications, which fuel cells were not considered. There were no biofuel cells commercially available in application due to the lower performance, compared to conventional fuel cells. Much more interests had been gathered to improve the performance of the direct biofuel cells, in which biocatalysts are directly involved in the redox reactions for electricity generation. Usually, it is difficult to achieve direct electron transfer to the enzyme molecules from the surface of electrode due to the non-conductive protein hulls of enzymes. Direct electron transfer was observed only with small enzymes such as cytochrome c, laccase and several peroxidases [48-51]. Methods of chemical modification were also developed to help increasing the enzymes conductivity. Other than the above approaches, mediator also could be used to shuttle electron transfer between the active sites of enzyme and the electrode; therefore, the resistance of enzymatic electrode could be reduced. When mediator was used, usually much higher cell efficiency could be reached. A glucose biofuel cell was used as model to study the kinetic limitations, including the mass transfer and electron transfer rates in the enzymatic biofuel cells. Parameters, such as Michaelis-Menten coefficients, were calculated using Ping-Pong Bi-Bi kinetic model. Both mass transfer and electron transfer rates were evaluated in finding out the kinetic limitation in enzymatic biofuel cell for further applying glycerol oxidation reaction in a similar device.

1.4 Outline

The outline of this dissertation is given as follows: Chapter II reviews literatures about biocatalysis, industrial applications of glycerol and DHA, and cofactor regeneration, biosensor and biofuel cells. The synthesis of biodiesel with solubilized enzyme is depicted in Chapter III. Chapter IV involves the development of recombinant GDH in *E. coli*. Chapter V reveals the production of carbon based electrode material from cotton wool, and the application of single carbonized cotton fiber microelectrode in the application of biosensing. Chapter VI explores the feasibility of regenerate cofactor on carbon based electrode with/without the assistance of mediator, and the process of DHA production from glycerol with electrochemical regeneration of cofactor. Chapter VII discusses the kinetic limitation of enzymatic biofuel cell with glucose biofuel cell as study model, providing further information for future research. Chapter VIII investigates the application of carbonized cotton wool electrode material in electrochemical reduction of CO_2. The conclusions are summarized in Chapter IX.

CHAPTER II

BACKGROUND

In this study, the research focused on production of valuable chemicals in an economical and environmental friendly way by utilizing the excessive glycerol from the extensive biodiesel production. With the objectives of this project, key background knowledge and previous research related to the studies conducted in this research are summarized in this chapter, including the non-traditional enzymatic catalysis, applications of glycerol and 1,3-dihydroxyacetone (DHA), nanostructured materials, cofactor regeneration, biosensors and biofuel cells.

2.1. Non-Traditional Enzymatic Biocatalysis

Biocatalysis can be defined as reaction processes using microbes or isolated enzymes as catalysts[64-66]. One traditional example of biocatalysis is the production of ethanol via yeast fermentation[67]. The presence and action of enzymes were first been recognized in 18th century. Enzymes have been used for various applications since then, such as textile, leather and food industries for a fairly long period. Nowadays enzymes have been applied broadly in human's daily life, as well as in the fields of analytical medicine, pharmaceuticals, food, animal feed, crop protection, pulp and paper, chemicals and mining[68]. Enzymes have also been found capable of producing a great variety of valuable products in controlled *in vitro* environments. Comparing with chemical

catalysts, enzymes have shown remarkable advantages in selectivity, efficiency and environmental friendly. These superiorities allowed enzymatic technology to attract the research interests consistently for centuries. . In exploring large scale bioprocessing for production of renewable materials and fuels, people still need to substantially improve the art of biocatalysis in terms of reducing the cost of enzymes production and improving the enzyme activity and stability.

Enzymes were traditionally considered as biocatalysts limited to aqueous environment, considering their biological origins. When used directly in organic solvents, native enzyme molecules tend to aggregate leading to greatly reduced accessibility for reaction and consequently unfavorable catalytic efficiency. However, it was reported that enzymes still maintained their catalytic activity in nearly anhydrous conditions[69]. This observation made a breakthrough impact on the application of enzymes. A whole new era of biocatalysis has been revealed. It benefits many biosyntheses involving organic substances that are not soluble in aqueous solutions. Advances in enzymatic synthetic technology over the last 3 decades showed a good focus on nonaqueous biocatalysis, including the development of active and stable biocatalysts in organic phase[53, 70-73]. One way to improve enzyme activity in anhydrous organic media is to solubilize the enzymes and thus achieving homogenous reactions. Solubilization of enzymes in organic solvents requires modification of native enzyme to increase their surface hydrophobicity to prevent it from aggregation or denaturation. Chemical modification implies altering the side groups of amino acid or attaching additional chemical groups to enzymes[74]. It is an effective way to tune the properties of the enzyme molecules towards desirable

applications. Typical reagents such as small molecules, surfactants, and polymeric materials have been used to increase the solubility or stability of enzyme in organic phase[75]. PEG-modified enzymes are probably the most extensively studied enzymes for organic-phase homogeneous reactions[76, 77]. However, pegylated enzymes have usually limited solubilities. One work conducted by Distel et al. from our research lab reported that enzymes modified with short alkyl chains could achieve very high organic solubilities and thus afford high enzyme activities in organic solvents[78].

Enzyme can also be altered leading to new catalytic features by chemical modification. The redesign of enzyme activity through the chemical modification of amino acid side chains is currently a common technique. It is an intriguing approach for catalyst development because chemical modification altered both physical properties and catalytic efficiency and provides the enzyme enormous range of functionality[75, 79, 80], which was needed in many industrial applications.

2.2. Glycerol and its Industrial Applications

Glycerol is one of the most versatile and valuable chemical known so far[7]. The traditional applications of glycerol, either directly as an additive or as raw materials range from food, tobacco and food additive to synthesis of polymers, are shown in Figure 2.1.

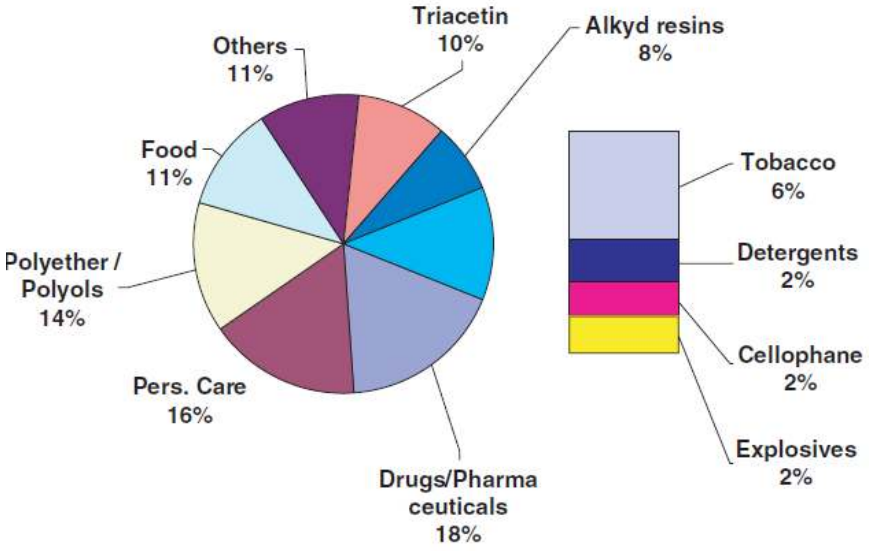

Figure 2.1 Usage of glycerol in industries. [8](Source: Novaol, May 2002).

The glycerol market is currently undergoing rapid changes, driven by very large supplies of glycerol from biodiesel production. Researchers have been looking at new uses for glycerol as a source of raw material[8]. The price of pure glycerol is very low (less than ~$1/kg), in some cases, industrial grade glycerol is considered as a waste. Glycerol can be converted into various chemicals via selective oxidation, reduction, halogenation, dehydration, etherification and esterification reactions[8]. Some examples of the products derived from glycerol reaction are shown in Figure 2.2.

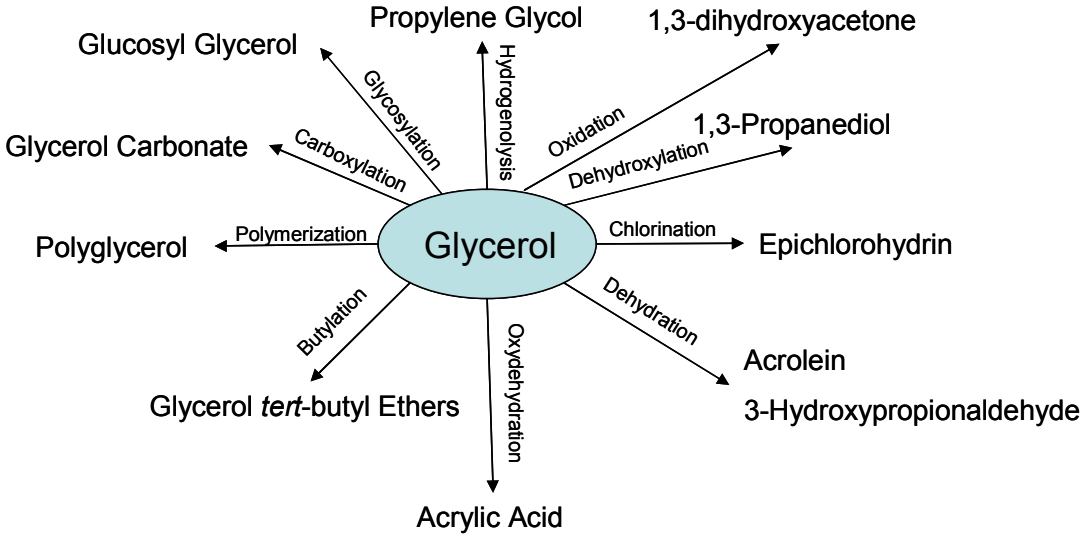

Figure 2.2 Example of chemicals can be produced from glycerol.

Selective oxidation of glycerol has been shown very powerful in generation a spectrum of valuable chemical products. Chemical, electrochemical and biological oxidation methods have been explored vigorously during the last decade to seek a market outlet for the large surplus of biodiesel glycerol. As a result, several major glycerol derivatives as shown in Figure 2.3 have been achieved. One of the most exciting routes of the selective oxidation of glycerol is the production of 1,3-dihydroxyacetone (DHA) production. Among the chemicals shown in Figure 2.3, DHA has an annual global market of around 2000 tons with a market price of $240/kg. DHA is a unique and versatile chemical with a broad range of applications in cosmetic, pharmaceutical and food industries[81]. Section 2.3 provides more background information regarding DHA.

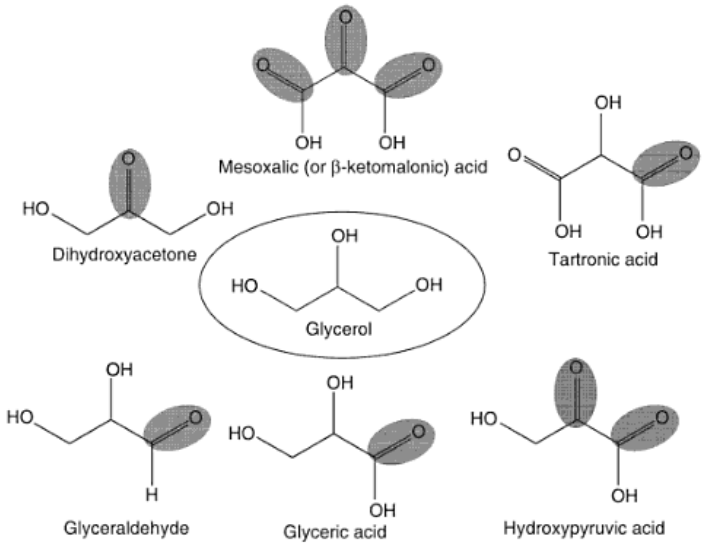

Figure 2.3 Oxidized glycerol derivatives [8].

2.3. The Structure and Applications of 1,3-Dihydroxyacetone

2.3.1 Structure of DHA

The DHA monomer is a ketone with three carbon molecules, produced by oxidizing the 2'–OH group of glycerol into carbonyl group, as shown in Figure 2.3. Recent research has shown that pure DHA occurs as a mixture of monomers and dimers in which the dimers predominate[82]. When DHA dimer dissolves in water, the conversion to monomer takes within 30 minutes in aqueous solution[83-86]. Usually commercial package of DHA contains DHA dimer.

2.3.2 Applications of DHA

Coppertone® introduced the first consumer sunless tanning lotion containing DHA into the market in the 1960s[87, 88]. Since then, various methods have been used for the

production of DHA in larger amount and at cheaper rates because of its commercial value. DHA was added to the list of approved cosmetic ingredients the Food and Drug Administration (FDA) by in the 1970s [89]. The mechanism of DHA tanning effect is based on Maillard reaction[90, 91], according to which carbohydrates react with amino acids of proteins to produce a golden to brown pigmentation. DHA reacts with the $-NH_2$ group of the amino acids present on the uppermost layer of skin, i.e., stratumcorneum to produce a darkening effect. Due to the penetration only up to the dead layer of skin, DHA does not cause any harmful effects on the skin. Thus, DHA provides a tanning without the harmful effects of UV rays.

DHA is also used to treat vitiligo in practice and has been well accepted due to the ability of causing pigmentation[92]. Vitiligo is an autoimmune disease in which pigment cells (melanocytes) are destroyed resulting in irregularly shaped white patches on the skin. The patients suffer from disease called variegate porphyria[93, 94] can also benefit from the use of DHA based products as their skin is overly sensitive to sunlight and DHA can provide some protection against UVA by react with skin and produce melanoidin pigment[95-97]. Although DHA has not been accepted as a sunscreen, a study[98] reveals that application of DHA in high concentrations on the hairless mice may lead to a delay development of skin cancer with moderate UV doses. The protection effects of DHA against UV is better than most of the natural pigmentation enhancers. Other than application in photoprotection, Niknahad et al.[99] found DHA has antidotal effect against cyanide poisoning[100].

DHA is an important C3 building block in industrial chemical productions. Other than easily to be oxidized to other ketones[101], DHA can be converted into many derivates, such as 1,3-di-o-benzyldihydroxyacetone[102] and 1,3-o-cyclohexylidenedihydroxyacetone 1,3-diphenylacetone[103] utilizing the –OH groups on 1' and 3' positions. These derivates can be widely used in generating sugars and other chemical compounds by reacting with organic chemicals such as aldehydes[104]. With the increasing concern of environment, biodegradable materials attract more and more attentions in research and development. Building blocks such as lactic acid and ester has been researched for cheaper prices and more applications. DHA also has been used in the production of lactic acid[105] with a conversion of 86%, catalyzed by Cu^{2+} and Zn^{2+} at 300 ^{o}C and 25 MPa. The routes of using DHA directly as building blocks to produce biodegradable materials were also been researched and developed recently. Since DHA has two free hydroxyl groups, it can be polymerized with the amino or carboxylic group on other chemicals. DHA derivates can also be added to the biodegradable material to accelerate the degradation rate. For example, DHA derivate, hydroxymalonic acid, has been used to fulfill such task[106].

2.3.3 The Production Routes of DHA

The production methods of DHA can be divided into chemical, microbiological and enzymatic methods by the catalyst used. Current industrial processes apply the first two methods. Enzymatic method is still under development. DHA can be produced through chemical catalysis from formaldehyde or glycerol[11, 12]. Precious metals, such

as Au and Pt are the most commonly used catalyst. Even though, pure Pt can be used as catalyst, composite catalysts are always preferred for their low cost and better performance. For example, composite catalysts consisting of Au and carbon[107] or Pt[108], Pt-Bi[109], Pt-carbon[110] had been used in glycerol oxidation reaction for DHA production. Chemical route for DHA production has the advantage of short reaction time, but the disadvantages of low selectivity, low conversion, and high energy requirement. Such synthetic routes involve the production of undesired byproducts due to the low selectivity of the catalysts. Although fine tuning of reaction conditions and composition of catalysts may improve the selectivity[13, 14], yields of the desired product are still generally low[15]. Most of all, the oxygen content in the oxidation reaction of glycerol often cause the poisoning of the metal catalyst easily.

Microbiological route of producing DHA involves fermentation or mixed fermentation of strains such as *Gluconobacter oxydans*[111] and *Acetobacter Suboxydsns*[111]. The principal is to utilize glycerol as substrate as a result of the activity of glycerol dehydrogenase (GDH), the enzyme in glycolysis process inside the microbes. The result of the glycolysis is the oxidation of glycerol at the 2' position to form a carbonyl group and thus leading to DHA. The problems inherent with the large scale application of microbiological production of DHA lies in processing operations, since the fermentations processes are usually in batch operations, which are associated with long running cycles, high energy consumption on sterilizing the reactor, difficult in products separation, low yield and the environmental impacts of the biowaste. Most of the industrial production of pharmaceutical and food grade DHA was preformed through

fermentation conversion of glycerol with only moderate yields (~20 g/l) and complicated purification and separation requirements[9, 10]. Even though some improved fermentation processes can be done continuously in membrane bioreactor[79] and with enhancement of products separation, the environmental concerns still exist. Generally speaking enzymatic synthesis promises much faster reactions than microbial processes, and offer precise molecule control of the products.

Compared to microbial and chemical approaches, enzymatic conversion of glycerol to DHA has advantages such as high selectivity, high yield, and mediate reaction conditions. In 1950s, Burton and Asnis found GDH in the strain of *Aerobacter aerogenes*[112] and *Escherichia coli*[18] separately. Following that, GDH has been successfully extracted not only from strains such as *Schizosaccharomyces pombe*[16, 113], *Cellulonomas*.sp[114-116], and *Bacillus stearotermophilus*[117, 118], also from animal muscle[119]. GDH can be divided into three groups according to different cofactor required: NAD^+-dependent glycerol dehydrogenase (EC 1.1.1.6) which exists inside bacteria cell in most of the cases; pyrroloquinoline quinone (PQQ) dependent glycerol dehydrogenase (EC 1.1.99.22), which is membrane-bound protein[120, 121]; and $NADP^+$-dependent glycerol dehydrogenase (EC 1.1.1.72). The NAD^+-dependent glycerol dehydrogenases from different microorganisms are shown in Table 2.1.

Table 2.1 Glycerol dehydrogenase structure from different microorganisms[122]

Microorganism	Subunit number	Molecular weight (kDa)
Bacillus megaterium	4	152
Candida valida	2	76
Cellulomonas sp.	8	336~344
Escherichia coli	8	309~320
Hansenula polymorpha	2	72
Klebsiella aerogenes	4	160
Schizosaccharomyces pombe	8	376

The NAD^+-dependent glycerol dehydrogenase was widely studied and used since it is easily obtained in separation and purification compare to PQQ-dependent glycerol dehydrogenase, which is membrane bounded. The oxidation reaction of glycerol to DHA catalyzed by GDH is shown in Figure 2.4[113]. This reaction was regarded as ordered Bi-Bi mechanism[114]. The enzyme binds with cofactor (NAD^+) first, forming GDH-NAD^+ complex. The GDH-NAD^+ complex then bind with glycerol forming triple intermediate complex, followed by the conversion of glycerol to DHA. After releasing DHA from the active site, reduced form of cofactor (NADH) is released as well. GDH is readily to catalyze another reaction again.

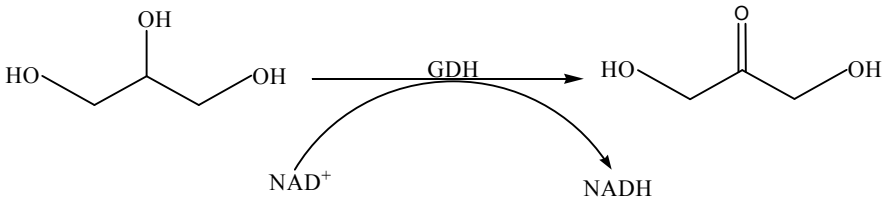

Figure 2.4 Conversion of glycerol to DHA by NAD^+-dependent glycerol dehydrogenase.

The bottle neck in commercializing enzymatic production of DHA is the pricy of enzyme and cofactor, NAD^+. For example, NAD(H) costs ~$1,000/kg, while NADP(H) can be 5-fold more expensive. Unlike enzymes, cofactors are consumed in biochemical reactions stoichiometrically to substrates reacted. Accordingly, efficient regeneration and reuse of the cofactors is vitally important to their large-scale applications[20]. A total turnover number (TTN) of cofactor in the order of over 10^3 is usually desired to make the process economically feasible.

2.4. Cofactor Regeneration

Methods including microbial, enzymatic, chemical, photochemical, and electrochemical have all been developed for cofactor regeneration[21]. Cofactors can be divided into two broad groups: organic cofactors and inorganic cofactors. Organic cofactors are often vitamins or are made from vitamins, including nicotinamide adenine dinucleotide (phosphate) ($NAD(P)^+$), flavin adenine dinucleotide (FAD), flavin mononucleotide (FMN), and coenzyme A (CoA). NAD^+ is also called coenzyme I, and $NADP^+$ is named as coenzyme II[123]. The research of regeneration, recycling, and reuse of cofactors are mostly focused on $NAD(P)^+$ and NAD(P)H, because of their high frequency of occurrence in enzymatic reactions.

The enzymatic conversion of glycerol to DHA has the advantages of fast conversion rate, less byproduct, easy product purification, and mild reaction conditions. However, the regeneration of cofactor – NAD^+ is necessary for the applications of this reaction system for the economic considerations of process because the price of cofactor.

Other than that regeneration of cofactor also favorite of the forward reaction by removing the competitive inhibiter – NADH generated from the reaction[124]. The major regeneration methods available now are chemical, microbiological, and enzymatic approaches[123]. The summary and comparison of these methods are shown in Table 2.2.

Table 2.2 Comparison of cofactor regeneration methods[125]

Cofactor regeneration method	Advantages	Disadvantages
Microbiological	• Low operational cost, self-assembling enzyme activity • Low price regenerating reagents (O_2, glucose) • high selectivity	• Relatively primitive state of development • low reactor volume productivity • complicated product isolation • poor stability • difficulty in controlling relative activities of enzymes • possible incompatibility with some chemical or biochemical components
Enzymatic	• High selectivity, especially for $NAD(P)^+$ to NAD(P)H • compatibility with enzyme-catalyzed syntheses • high rates for some systems • easy monitoring of reaction progress	• High cost and instability of enzyme • complexity of product isolation in some cases
Chemical	• Use inexpensive and commercially available reagents • No requirement for added enzymes • High redox potentials	• Limited compatibility with biochemical systems • complexity of product isolation in some cases • low product yields • low TTN • Slow rate for some systems (especially for oxidative regeneration)
Photochemical	• No stoichiometric regenerating reagent in some systems • no requirement for added enzymes	• Complex apparatus, limited compatibility with biochemical systems • limited stabilities • requirement for photo-sensitizers and redox dyes
Electrochemical	• Low cost of electricity • no stoichiometric regenerating reagent • readily controlled redox potential • easy product isolation • easy monitoring of reaction progress	• poor selectivity (especially for reductive regeneration) • complex apparatus and procedures • rapid fouling of electrodes • requirement in many systems for mediating redox dyes or enzymes

2.4.1. Microbiological Method

For microbial cofactor regeneration, cofactor is regenerated inside living cells. To achieve that, substrates and products need to pass through the cell membrane to reach the enzymes which catalyze the reaction cycles[126] (Figure 2.5). Usually the reaction rate is controlled by the diffusion rate of substrate/product. This method has been used in industrial scale for its easy operation and low cost of energy source (sugar). The enzyme systems in microorganisms, such as *Saccharomyces cerevisiae*[125], recombinant *E. coli*[125, 127], and *Klebsiella*[128], have been studied and utilized for the regeneration of cofactors.

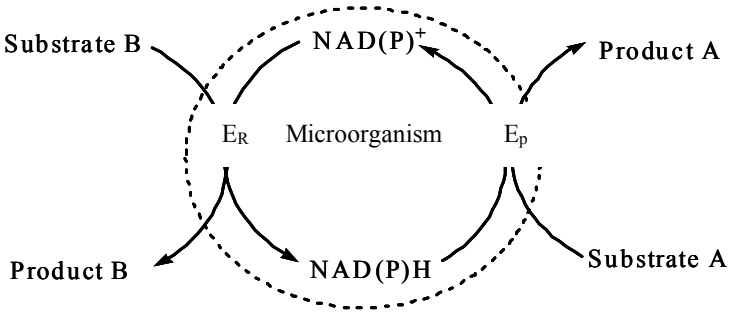

Figure 2.5 Cofactor regeneration in microorganism[126]. The dashed line indicates the cell membrane of microorganism. Ep: Producing enzyme; E_R: Regenerating enzyme in microorganism.

2.4.2. Enzymatic Method for Cofactor Regeneration

The enzymatic method mimics the reaction pathways inside microorganism for the regeneration of cofactor. Several reaction routes have been examined for enzymatic regeneration of NAD(H). Enzymatic regeneration of cofactor can be divided into substrates coupled regeneration system and enzymes coupled regeneration system. Usually, each system includes two reactions, one is synthetic (producing) reaction, and

the other is cofactor regeneration reaction. The synthetic reaction is used to produce the products, and the regeneration reaction catalyzed by the same enzyme regenerating cofactor back to its original form for the purpose of continuous operation[127]. In substrates coupled regeneration system, another substrate was provided to the regeneration reaction, utilizing the same enzyme to realize the regeneration of cofactor (Figure 2.6). The directions of production reaction and regeneration reaction are reverse, and this method is commonly used in cofactor reduction reactions[127].

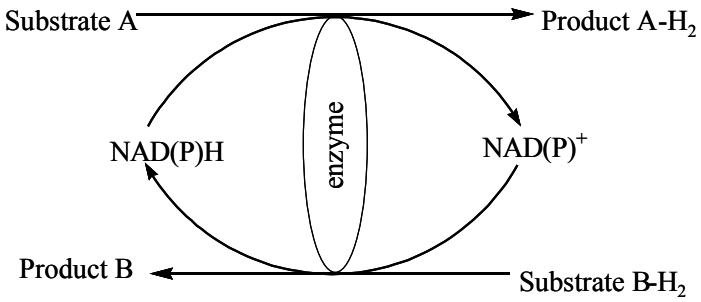

Figure 2.6 Substrates coupled regeneration of cofactor[126].

Enzymes coupled cofactor regeneration system pairs two enzymatic oxidize/reduce reactions, one produce the product desired, another realize the regeneration of cofactor (Figure 2.7)[59]. Enzymes coupled cofactor regeneration system usually involves formate dehydrogenase, glucose dehydrogenase, alcohol dehydrogenase, and amino acid dehydrogenase.

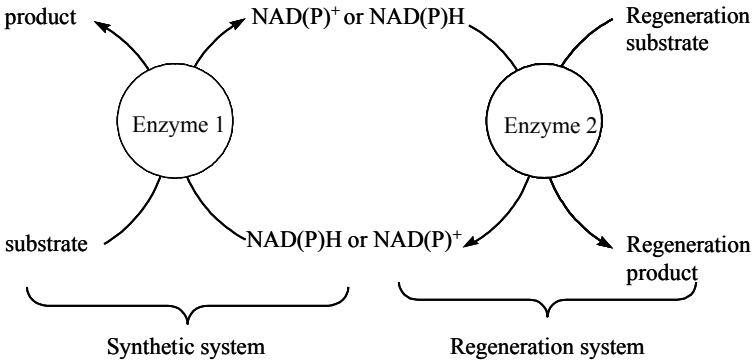

Figure 2.7 Enzymes coupled regeneration of cofactor[126].

2.4.3. Electrochemical Method for Cofactor Regeneration

Chemical and biochemical regeneration methods are generally realized by using a second chemical which has to be reactive and cheap. Those criteria have been difficult to satisfy in most large-scale bioprocessing applications, although that is acceptable for most analytical applications which require the use of only small amounts of chemicals. However, electrochemical regeneration which can make use of renewable energy sources such as sun light via photovoltaic cells (photoelectrochemical regeneration) and renewable redox species such as hydrogen and oxygen (electrochemical regeneration) promises a much more sustainable approach for biofuel and bioproduct industry.

Photochemical method for cofactor regeneration utilizes visible lights inducing the photosensitization reaction of photo sensitizer, such as $[Ru(bpy)_3]^{2+}$[129], the electron is transferred to cofactor by mediator, which reduces cofactor to its redox form (Figure 2.8). The drawback of this method is the photo sensitizer usually is not stable in the system, and can be easily degraded. The prevention of such degradation is to use semi-conductive materials such as titanium dioxide[126] as photo sensitizer. The regeneration

of cofactor with photoelectrochemical method still stays in the experimental stage due to complication of system and low efficiency of regeneration. With the low price of solar energy, this method may bring more exciting aspect to current research of cofactor regeneration.

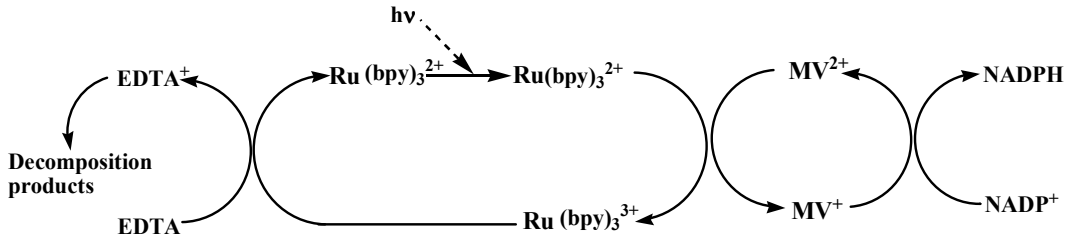

Figure 2.8 Photoelectrochemical regeneration of cofactor[129].

With the wide use of enzyme and cofactor on electrodes for the development of bioelectronic devices, electrochemical regenerations of cofactor became more and more important among the regeneration methods mentioned above. Electrochemical regeneration of cofactor is to oxidize/reduce cofactor to its preferred status by the overpotential of electrode. Electrochemical regeneration method can be divided into direct and indirect regeneration[126]. Direct electrochemical regeneration of cofactor use overpotential to oxidize/reduce cofactor on the electrode directly. Electrons transfer between cofactor and electrode directly. The process requires high overpotential which makes the fouling of electrode easily. In order to decrease the potential needed for the regeneration of cofactor, dyes such as viologen[130] and metal composite like rhodium[131] are often involved as mediator, which could be immobilized on the electrode[125]. This method is called indirection regeneration of cofactor (Figure 2.9).

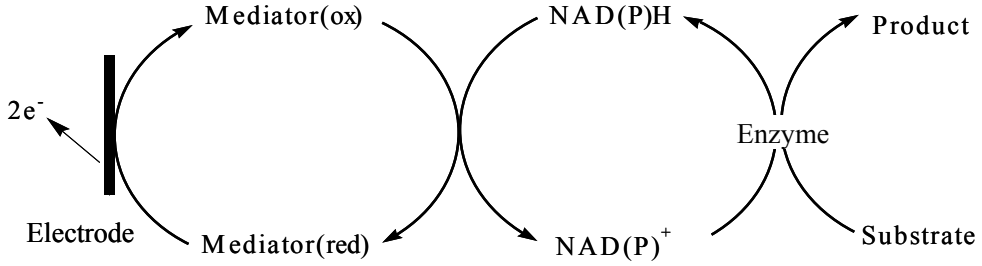

Figure 2.9 Indirect electrochemical regeneration of cofactor.

2.5. Biosensor

One area closely related to bioelectrochemical catalysis is biosensing. The most frequently used biosensor is glucose biosensor which is used by diabetic patients to monitor their blood sugar level. The fundamental subject in manufacturing the enzyme electrodes is to improve electron exchange between the enzyme active site and the electrode cross the non-conductive protein shell. Based on this principal, two subgroups of biosensor were classified by electron transfer methods: (1) Biosensors using a soluble or immobilized mediator; and (2) Biosensors with direct electron transfer (mediatorless).

Traditionally, biosensors are based on the amperometric detection of the reaction products. This kind of biosensors may suffer from several disadvantages. For example, dissolved gas species, such as oxygen may cause the deviation of the current response to substrate concentration. The dynamic range of detection could also be limited by depletion of oxygen in the solution [132]. Diffusion mediators, such as quinines and ferrocenes, are commonly used for helping the electron transport of enzyme electrodes to overcome the oxygen dependence[133-136]. However, because these diffusion mediators are small, the leaching issue of the mediator will be a serious concern in clinic

applications. To eliminate mediator leaching, several larger-size novel diffusion mediators, such as 3-methyl-4-hydroxycyclobut-3-ene-1,2-dione (methylsquarate, OHME) and 3-phenyl-4-hydroxycyclobut-3-ene-1,2-dione (phenylsquarate, OHPH), were fabricated and studied for better electrochemical characteristics[137]. Moreover, mediators were also immobilized to reduce the leaching issue[138-141]. For example, Ghica et al. described a methyl viologen-mediated amperometric biosensor[142]. The mediator, methyl viologen, was directly entrapped with the enzyme together by Nafion® cation-exchange polymer.

Mediator entrapment could alleviate the mediator leaching problem during some of the biosensor operations, but could not completely eliminate the possibility of leaching. Further studies have been exploited to address this issue, such as the employment of conducting polymers to directly wire the enzyme active site with the electrode[143]. Novel nanostructured materials also were investigated to enhance the electron transfer in a biosensor. For their unique properties in electronic, chemical, and mechanical application, the synthesizing nanostructured materials were interested considerably in recent years. Different materials, such as metal, carbon, and polymers, have been used to prepare nanostructured materials, nanoparticles[144, 145], nanotubes[146, 147], and nanofibers[148]. Three major methods have been investigated in recent years to improve the electrode reactivity for the application in biosensors: (1) Carbon nanotubes and conductive nanoparticles; (2) Conductive polymers; and (3) Multienzyme system.

Carbon nanotubes (CNT) have been used in electronic applications and chemical and biological detections for the unique structure and property, such as conductivity.

Recent studies indicated that CNT could enhance the biological molecular electrochemical reactivity and promote the electron transfer in protein reactions[149-151]. The remarkable high conductivity and high surface absorbent of CNT make it a promising candidate in making nanostructured biosensors. Lim et al.[144, 152] reported co-deposit enzyme with palladium nanoparticles onto a Nafion-solubilized CNT film, and the resulting electrode allows for fast and sensitive quantification.

When conductive polymer was used to wire the enzyme active site and the electrode directly, polymer could be formed by electrochemical deposition. Shin et al.[153] reported using electrochemical deposition to form polypyrrole/enzyme film. Linke et al.[154] described that cross-link enzyme into a 3-dimensional network. They found that in the presence of redox polymer, the formed redox hydrogel electrode has high sensitivities. Besides of direct wiring, multi-enzyme working pathway also could be used to replace the mediated reactions in biosensor. Multi-enzyme biosensor was initiated in the late 70s[155], in which different enzymes were coupled either in sequence or in cycles on the electrode. In this way, not only a wider range of species could be measured by bioelectroanalytical approach, but the selectivity and sensitivity of biosensors could be enhanced[156].

2.6. Biofuel Cells

Clean and efficient power generation is actively sought worldwide, as the demands in energy rapidly grow while concerns over environment pollution and petroleum resources remain potent. Fuel cells, as an alternative power generation

technology to thermo-mechanical processes, directly convert chemical energy of non-nuclear fuels into electricity with a theoretical efficiency of 100% and almost zero pollution emission. Even though the concept of the technology has been demonstrated for decades, there are several challenges to overcome to make fuel cells economically competitive for general-purpose applications. For example, conventional fuel cells typically use noble metals such as platinum for catalysts on electrodes. But the precious Pt costs about $38,000 per kg, which makes the fuel cells too expensive for many large-scale applications. Metals are not renewable and resource-limited. In addition, metallic catalysts usually have to be operated at high temperatures; they are subject to inactivation by trace amount of impurities such as CO and sulfur in fuels; and may cause pollution to the environment upon discarded[157]. Biofuel cells refer to a class of fuel cells that utilize microbial or enzymatic biocatalysts, which can effectively catalyze redox reactions under ambient conditions and neutral pH values. In contrast to noble metals, biocatalysts are renewable and the cost of production can be very low, as microorganism and enzymes such as detergent enzymes can be economically produced from large-scale fermentation processes once the market is developed. In addition, because of the unique catalytic activity of biocatalysts, biofuel cells can use a variety of special fuels such as carbohydrates and organic pollutants in wastewater[158-160].

One major challenge in the development of biofuel cells is their low power output density, typically 2-3 orders of magnitude lower than that of chemical fuel cells. Many factors may contribute to that. Among others, the inefficiency of electron conduction between biocatalysts and electrodes is believed to be critical. In chemical fuel cells,

metallic catalysts are deposited on electrodes and, because both catalysts and electrode materials are conductive, electrons can transfer between the catalytic sites and the surface of electrodes. Such direct electron transfer (DET) is available only for a few biocatalysts. Bacteria including *Rhodoferax ferrireducens*[161], *Geobacter sulfurreducens*[162] and *Shewanella putrefaciens*[163], along with several small enzymes such as laccase and hydrogenase, were found capable of conducting electrocatalysis with DET. Enzymes that are capable of DET have been mostly examined for biosensors[48, 50, 51, 164-166], although biofuel cells using physically adsorbed laccase and hydrogenase have been also reported[167]. However, these biofuel cells generally produced low power and current output[168].

Electron transfer between two sites separated by nonconductive medium is possible should the distance between them is short enough[169, 170]. For most enzymes, except the smaller enzymes such as laccase and hydrogenase, the protein shells surrounding the active sites are often too thick for DET. One strategy to overcome this barrier is to transform the protein shell to be conductive by chemical modification[171-174]. Another popular approach is the use of redox mediators, which carry the electrons and shuttle between the enzyme active sites and the surface of electrodes. Many of such mediated catalytic systems have been reported for both microbial and enzymatic biofuel cells[158-160, 175]. Even though the mediators introduce an additional step in the redox reaction chains from fuel to electron generation, much higher performance of biofuel cells was usually observed. One shortcoming of such systems lies in the fact that redox mediators are usually small molecules and are difficult to retain during continuous

operations. To address this issue, substantial efforts have been made during the last decade to co-immobilization of enzyme and mediators[176-182].

The past decade also witnessed the explosive growth of nanotechnology. Progresses in synthetic and fabrication methods have greatly extended the application of nano-structured materials for many purposes such as the development of electronic, optoelectronic, biomedical, and sensing devices. It has been demonstrated that catalysts supported by nano-structures well performed for nitrooxide reduction[183], hydrogenation[184], hydroformylation[185], and electrochemical catalysis in sensors[186] and fuel cells[187]. Recently various configurations of nanomaterials such as nanofibers[148, 188, 189], nanotubes[190-192], nano-particles[193, 194] and nanoporous materials[195-198] have been reported for use as the supports for enzymes. Many of this type of "nanobiocatalysts" displayed enhanced performance in terms of catalytic efficiency and durability in comparison with their native parent enzymes[199]. The emergence of nanobiocatalysts may also bring up chances for the fabrication of high-performance bio-electrodes for biofuel cells. Particularly, electrodes based on conductive nanomaterials may offer promising opportunities to improve the power output of biofuel cells. An example has been reported by Xiao et al[200]. In that work, glucose oxidase (GOx) was "wired" to electrode by gold nanoparticles and showed higher activities than native enzymes. Although the electrode was not suited for biofuel cell application due to the high over potential, it did show the potentials in developing novel biocatalysts using nanoscale manipulation approaches. Carbon nanotube (CNT) attracted a lot of attention for its unique physical, chemical and mechanical properties. Previously, CNT has been

extensively studied for biosensing and many CNT-based biosensors showed better selectivity and/or improved sensitivity[160, 172, 191, 201-207]. CNT also represents a class of ideal materials for electrochemical applications for the good conductivity and extraordinary stability.

CHAPTER III

AN ORGANIC SOLUBLE LIPASE FOR WATER-FREE SYNTHESIS OF BIODIESEL

3.1 Introduction

Biodiesel is pursued not only for the consideration of the future shortage of petroleum, but also for the consideration of environment since the growth of its biological origin consumes at least the same amount of CO_2 as that of emission from the combustion of biodiesel. The European Union's Directive published in 2003 estimated that a content 5.75% of biodiesel would be used for transportation fuels by the end of 2010[208]. The National Biodiesel Board of the United States estimated that biodiesel industry would reach 650 million gallons annually by 2015, and would add $24 billion to the U.S. economy between 2005 and 2015[209]. Although raw vegetable oils can be used directly as fuels, their high viscosity and low volatility make them inefficient for most combustion engines. Biodiesel which has a molecular weight of about one third of their parent oils in form of either methyl or ethyl monoesters of fatty acids is, on the other hand, much easier to handle as a liquid transportation fuel. All types of triglycerides, including vegetable oils and animal fats can be utilized for production of biodiesel.

At present, commercial production of biodiesel is mainly achieved through alkali-catalyzed transesterification of soybean oil. Albeit its conversion efficiency, several issues in that process are subject to further improvement. These issues include the

removal of inorganic salt from the products, the recovery of glycerol, dehydration, and the treatment of alkaline wastewater[2, 3]. As reported so far, however, native or immobilized lipases require the addition of certain amount of water to redeem in most cases only moderate activities. Several recently reported works have examined the influence of water on the transesterification activities of lipases, which a least water content of 0.48% (wt) is required to activate the enzymes. That is about 10 times of the regulated 0.05% water allowance for biodiesel in U. S.[52]. Anhydrous transesterification reactions are hence desirable, as the same for many other synthetic purposes[53].

One way to improve enzyme activity in anhydrous organic media is to solubilize the enzymes and thus achieving homogenous reactions. PEG-modified enzymes are probably the most studied enzymes for organic-phase homogeneous reactions[76, 77]. However, pegylated enzymes have usually limited solubilities (mostly much less than 1 mg/ml). Distel et al. reported recently that enzymes modified with short alkyl chains could achieve very high organic solubilities (up to 44 mg/ml) and thus afford high enzyme activities in organic solvents[78]. In this work, a one-pot water-free biodiesel synthesis process using alkyl-modified lipases is examined.

3.2 Materials and Methods

3.2.1 Materials

Several commercial available lipases were kindly provided as gifts from Amano Enzyme Inc. (Nagoya, Japan). The sources and protein contents of these enzymes are

tabulated in Table 3.1. Soybean oil, decanoyl chloride, oleic acid, ethyl oleate and methyl oleate were obtained from Sigma-Aldrich (St Louis, MO, USA). Iso-octane, methanol and ethanol was purchased from Burdick & Jackson (Muskegon, MI, USA); and 1-Ethyl-3-(3-dimethylaminopropyl)-carbodiimide (EDC, 98%) and N-Hydroxysuccinimide (NHS, 98%) were products of Alfa Aesar (Ward Hill, MA, USA). Unless specially mentioned, all other reagents used in the experiments are ACS grade.

Table 3.1 Transesterification reaction catalyzed by different lipases.

Lipase	Source	Protein Content (wt-%)	Observed conversion (v/v%)	Normalized conversion (v/v% / h·mg protein)
AH	*Burkholderia cepacia*	39.2	0.5	0.26
AK	*Pseudomonas fluorescens*	53.3	35.5	13.3
AY	*Candida rugosa*	42.9	0.5	0.30
F-AP	*Rhizopus oryzae*	70.5	1.7	0.48
G	*Penicillium camembertii*	11.0	0.0	0.04
M-10	*Mucor javanicus*	93.7	0.3	0.06
R	*Penicillium requeforti*	6.9	0.8	2.35

The conversion was measured with 2 ml of soybean oil, 2 ml methanol in the presence of 1 ml water and 5 mg lipase.

3.2.2 Preparation of Solubilized Lipase

The solubilized lipase AK (S-AK) was prepared according to the previously reported procedure[78]. Typically, 30 mg of lipase was dissolved in 3 ml of phosphate buffer (0.2 M, pH 10) contained in a 20 ml glass scintillation vial. To start the

modification reaction, 6.0 ml of chloroform containing 15% (v/v) decanoyl chloride was added, and the mixture was magnetically stirred at room temperature for 8h. The pH value of the aqueous solution was maintained at 10.0 by adding sodium hydroxide solution (10 wt-%) periodically. The reaction was stopped by centrifugation. The concentration of solubilized lipase in the organic phase was determined by absorbance at 280 nm. A typical concentration of modified lipase in the organic was around 4 mg/ml, indicating a modification yield of 80%.

3.2.3 Biodiesel Synthesis Reactions

The transesterification reactions were conducted in 20 ml glass scintillation vials under shaking (180 rpm) in water bath (for elevated temperatures) or air (for room temperature reactions). Soybean oil and alcohols were mixed in a molar ratio of 3:1 unless specified otherwise. Since the oil and alcohol are not miscible, iso-octane was used to generate monophase solutions. The ratio between iso-octane and alcohol-soybean oil mixture was 1:1 (v/v) if methanol was used, and 4:1 (v/v) for ethanol with a total volume of 5 ml. Both native and solubilized lipases were used with an amount equivalent to 1 mg/ml. The reaction was analyzed by monitoring changes in the concentration of product. Typically aliquots of 1 ml sample were taken from the well mixed reaction medium, and were centrifuged at 14,000 g for 10 min. Five hundred micro-liter of supernatant was diluted by 4 times with iso-octane and was analyzed by using gas chromatography (Shimadzu GC-17A, Kyoto, Japan) equipped with a RTX-5 column (15m×0.35nm×1.0μm, Restek, MD, USA). The column temperature was kept at 200°C,

while the injector and detector were kept at 250°C. Ethyl oleate and methyl oleate were chosen as a biodiesel standard for GC analyses. The conversion of soybean oil was calculated in this work by accounting the volume ratio of the detected monoester products versus the volume of soybean oil added to the reaction.

3.3 Results and Discussions

3.3.1 Transesterification Reactions with Different Lipases

It has been well demonstrated that hydrolases such as lipases and proteases catalyze the reversed reactions of their hydrolytic reactions once they are placed in organic media, because of the shift in thermodynamics of reaction equilibrium[69, 210]. Although most of the hydrolyases can catalyze the esterification and transesterification reactions of a wide range of substrates in organic media, enzymes may show very different preferences of reaction conditions for a given reaction. Although all lipases are efficient enzymes evolved over time in their biological origins to hydrolyze lipids, they are expected to show very different efficiency when they are required to function in an artificial reaction medium that is very different from their native biological environments. In this work, seven commercially available lipases, most of which were developed for use as detergent enzymes, were first tested for the transesterification reaction between soybean oil and methanol at the same reaction conditions (Table 3.1). The reaction was monitored by detecting the production of biodiesel using gas chromatography (GC). In a typical GC chromatogram using the analytical method described in this work, two product peaks were determined (separated by ca. 2 min) with the larger peak matching

that of the methyl oleate standard. The smaller was believed to be corresponding to the monoester product of lighter lipid acid components, since the refined soybean oil contains ~15% of C16 and ~85% of C18 lipids. Both peaks are accounted as products in the subsequent analysis of reaction rates.

Although most of the enzymes showed detectable activities, lipase AK showed the highest activity with over 35% of soybean oil converted within 1 h of reaction (Table 3.1). The gross amounts of enzymes instead of effective enzyme contents were controlled in these reactions to keep the phase ratio of liquid to solid of the suspension reactions (since enzymes were not soluble in the reaction media) consistent. After normalizing the conversion with the actually protein content of each lipases tested, lipase AK still gives the highest activity. Lipase AK was then selected for further transesterification studies.

3.3.2 Factors that Affect the Activity of Native Lipase AK

In order to examine the primary factors that control the performance of lipase AK, experiments were conducted according to a factorial design with respect to 4 factors including temperature, water content, pH and molar ratio of substrates, with two levels of variations. Figure 3.1 shows the factorial design and testing results. Changes in all the factors except the substrate molar ratio impacted evidently the production yield of the biodiesel. These sensitive factors were then examined further in the following tests.

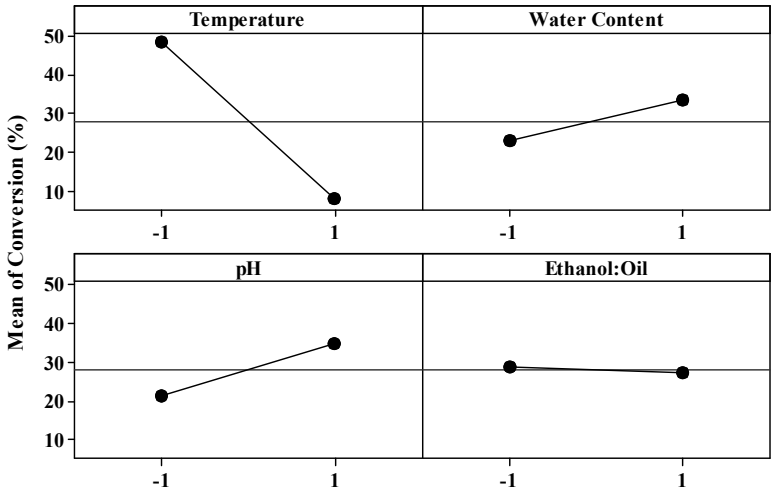

Figure 3.1 Factorial screening tests for factors that impact the activity of lipase AK for transesterification reactions. The lower level and higher level of the factors used in this experiment are described as following: 25^{o}C and 50^{o}C for temperatures; 2 v/v% and 5 v/v% for water contents; pH 3 and pH 7 for pH values; and 3:1 and 9:1 in ethanol to oil molar ratios.

Temperature may impact the reaction rate through two different mechanisms. On one hand, it promotes faster reactions through Arrhenius relationship; on the other hand, it may denature and inactivate the enzyme and thus significantly slow down the reaction. The effect of temperature on the activity of lipase AK was further examined in the presence of 2% (v/v) water (Figure 3.2). For the reaction with ethanol, the temperature impacts the reaction as expected. The reaction rate increased first with increase in temperature, indicating the effect of thermal reaction kinetics; but it dropped sharply after reached a peak activity at 30 ^{o}C, implying significant enzyme inactivation at temperatures higher than that. Interestingly, the activity of the enzyme toward the transesterification reaction with methanol did not change much within the temperature range tested. The mechanism for that was not clear to the authors, although we tend to believe that the

effect of substrate (methanol) inhibition in the case with methanol is more prominent than any other factors, as indicated by its low reaction rates. As to be shown in the following, the transesterification reaction with ethanol also showed greater sensitivities than that with methanol to changes in pH and water content. Overall, these observations indicate that ethanol is a much more efficient substrate than methanol for the enzymatic production of biodiesel with lipase AK.

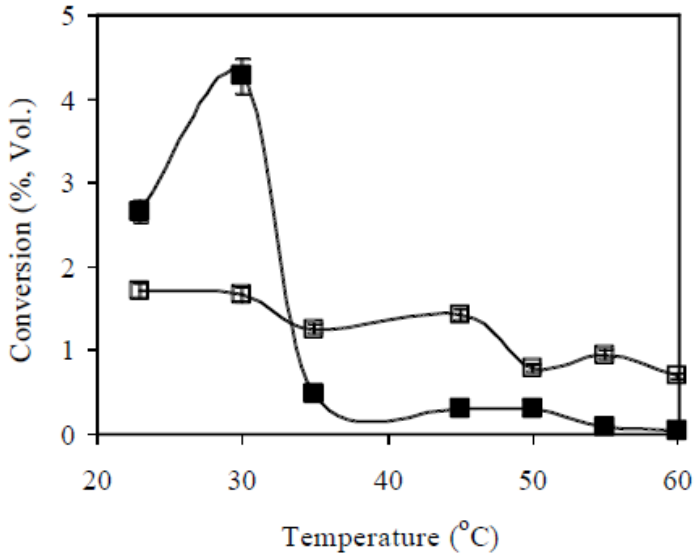

Figure 3.2 Effect of temperature on the transesterification activity of lipase AK. Reactions were executed in water bath for 1 h. Water (2 v/v %) was added into vials and pH of the reactions is 7.0. (□) – Methanol; (■) - Ethanol.

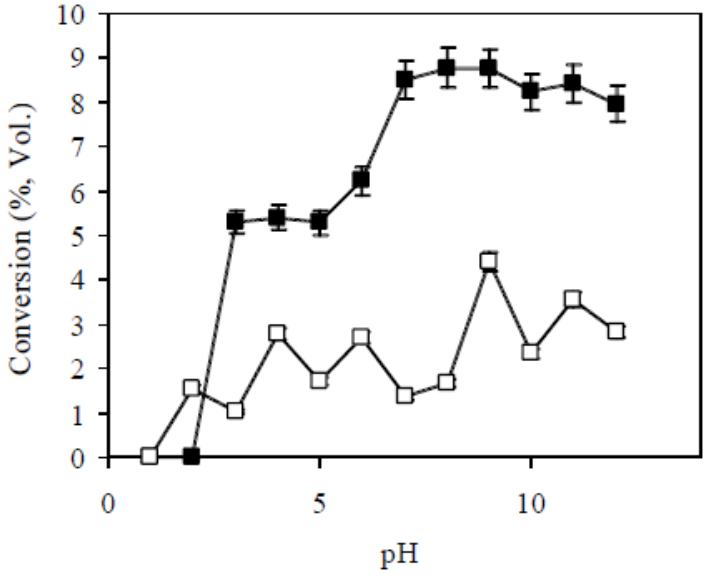

Figure 3.3 Effects of ph on the transesterification activity of lipase AK. One hundred micro-liters of aqueous buffer solutions of variable pH values (1-12) were added to 5 ml of the reaction mixture (oil, alcohol, and enzyme). Reactions were conducted at room temperature for 1 h. (□) – Methanol; (■) - Ethanol

The effect of pH on the activity of lipase AK is shown in Figure 3.3. It appeared that the reaction preferred alkaline conditions, and higher conversions were observed when the pH value reached above 7. The effect of water content was then examined with pH fixed at 7.0 (Figure 3.4). No product was detected within the reaction time with either ethanol or methanol without addition of water (aqueous buffer) to the reaction media. The reaction rate with ethanol increased sharply with increase in water content and reached a peak high value of 57% at the water content of 10% (v/v). Subsequent increase in water content did not help to accelerate the reaction and the conversion at water content of 20% was slightly lower than that at 10%, indicating an adverse effect of excess amount of water to the transesterification reaction. A similar trend was observed for the reaction with methanol, only the reaction rate did not change as dramatically as

that with ethanol. The highest enzyme activity was observed at water content of 5% (v/v) for methanol, the same optimal water content as reported in a study of methanolysis activities of different lipases for synthesis of biodiesel from soybean oil[211].

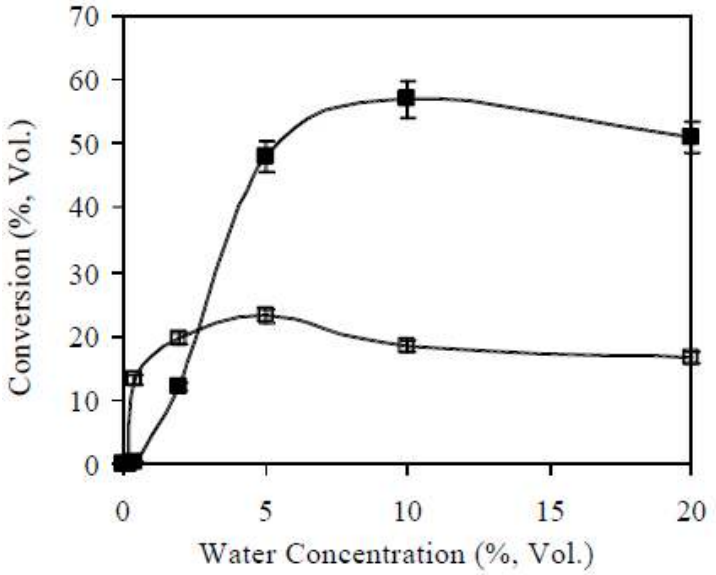

Figure 3.4 Effect of water content on the activity of lipases. Reactions were performed at room temperature for 21h. (□) – Methanol; (■) - Ethanol.

As water is not desired in the final biodiesel product and has to be removed to satisfy the regulated quality requirement, it is ideal to achieve the reaction without any use of additional water. Since the soybean oil and alcohols are not miscible and that can limit the achievable reaction velocity, one possibility to achieve nonaqueous synthesis of biodiesel is to dissolve both the oil and alcohol into one common organic solvent to improve their availability for reaction. Accordingly we further tested the use of organic solvents for lipase AK. Solvents including acetone, dichloromethane, tetrahydrofuran (THF), chloroform, hexane and iso-octane, were tested for the transesterification reaction between soybean oil and ethanol with a volume ratio of solvent vs. substrates as 3:1 with

1% of water added to ensure the activity of the enzyme. No product was detected the reactions conducted with acetone, dichloromethane, THF and chloroform, while reactions were observed with hexane and iso-octane over the 24-h screening tests. The results are in agreement with the expectation that solvents of higher Log P values afford better nonaqueous activities for hydrolyases[212].

3.3.3 Synthesis of Biodiesel with Solubilized Lipase AK

Although the use of organic solvents can help to achieve a monophasic reaction medium, native enzymes are not soluble in the organic phase and thus the reaction velocity is still limited by the heterogeneous nature of the reaction. Our previous study has shown that enzymes modified with short alkaline chains can significantly improve the organic compatibility of the enzymes, thus achieving high nonaqueous solubility and activity[78]. Since alkaline molecules should present no adverse contamination to biodiesel product, such a modification for lipase AK was explored in this work. Figure 3.5 compares the performances of native and solubilized lipase AK (S-AK) for the transesterification of soybean oil with ethanol in iso-octane in the absence of water. Within the tested reaction time of 21-h, the native enzyme did not produce any detectable products with either methanol or ethanol. However, the solubilized enzyme catalyzed the conversion of the added soybean oil up to 7.3% and 21.3% with methanol and ethanol, respectively.

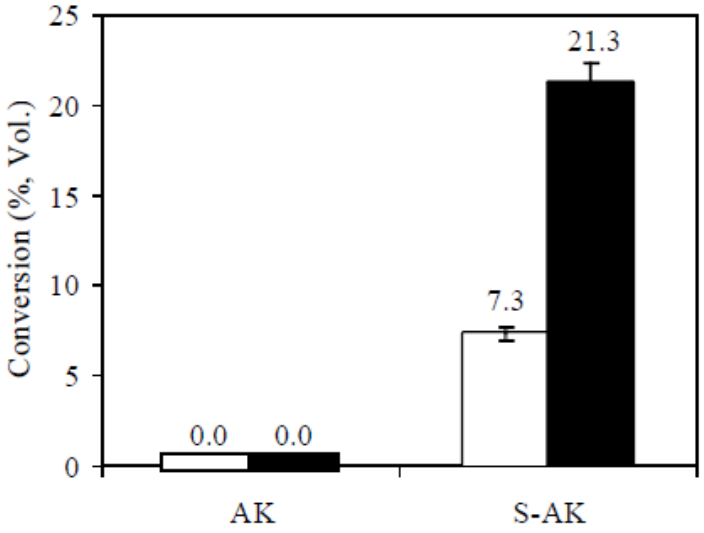

Figure 3.5 Transesterification reaction catalyzed by lipase AK and solubilized lipase (S-AK) in water-free reaction media. Reactions were at room temperature for 21h. . (□) – Methanol; (■) - Ethanol.

To further improve the reaction rate, the temperature effect on the catalysis of S-AK was also studied (Figure 3.6). Interestingly, the solubilized enzyme in the homogeneous nonaqueous solution showed much better thermal stability than the native enzyme tested in the soybean oil-alcohol-water heterogeneous system (Figure 3.3). The activity of S-AK generally increased with increase in temperature within the temperature range from room temperature up to 70 ^{o}C. The highest conversions of the reaction were observed at 70 ºC with the maximum conversions of 9.8% and 25.2% for methanol and ethanol, respectively.

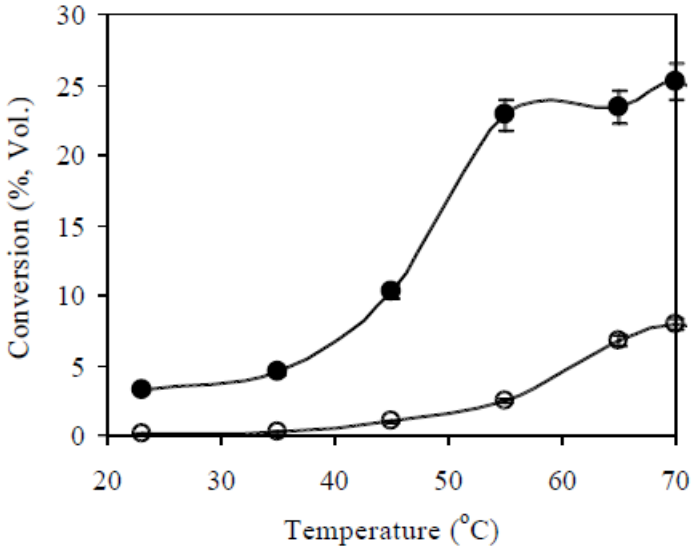

Figure 3.6 Effects of temperature on the transesterification activity of solubilized lipase (S-AK) in water-free reaction media. Reactions were executed in water bath for 1h.

Figure 3.7 shows the effect of reaction time on the transesterification using S-AK to catalyze ethanol in biodiesel transesterification at optimization condition. These reactions were sampled from 1 to 24 hours. After 24 hours reaction, the conversion of soybean oil reached 71%. Accounting the amount of enzyme applied (1 mg/ml), the catalytic reaction rate obtained with ethanol was 27.5 g-product/g-enzyme·h, which is more than 2 orders of magnitude higher than those observed for Novozym 435[213] and Lipozyme TL IM (0.245 g-product /g-enzyme·h) [214].

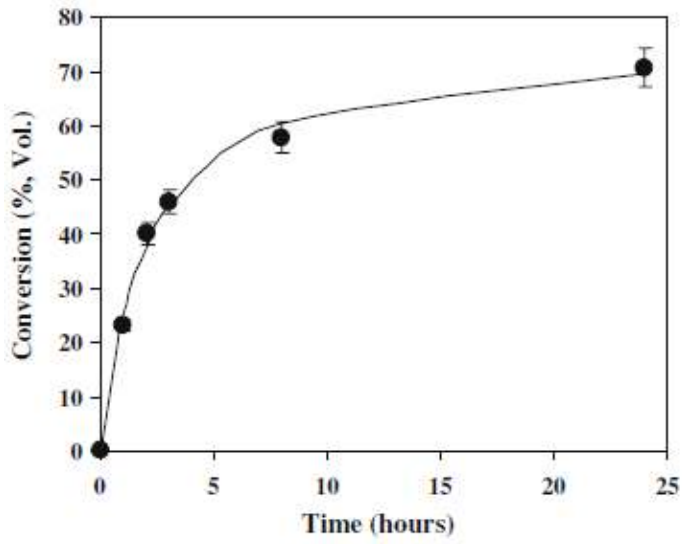

Figure 3.7 Time course of transesterification reaction catalyzed by solubilized lipase (S-AK) in water-free reaction media at 70ºC. Ethanol was examined in the reaction with soybean oil.

3.4 Conclusions

This work demonstrated that the solubilization of lipase significantly increased its activity for synthesis of biodiesel. The productivities of the solubilized enzyme in a water-free reaction system were over two orders of magnitude higher than other enzymes reported previously. This provides the potential to develop a one-pot and impurity-free synthesis of biodiesel, as all the components including the solubilized enzyme, substrates and products can all be part of the final biodiesel product. Interestingly, although the current industrial biodiesel products from chemical synthetic route are predominantly methyl esters, it appeared in our work that ethanol was actually a much more efficient substrate than methanol for the biosynthesis of biodiesel.

CHAPTER IV

PRODUCTION OF RECOMBINANT GLYCEROL DEHYDROGENASE

4.1 Introduction

Due to the growing demand for biodiesel, glycerol, the byproduct of biodiesel production, is becoming an over-whelming stream of biowaste. In the early years of biodiesel production, glycerol was considered as valuable/marketable byproduct, but the current annual output is surpassing the market volume by far. In the US, the biodiesel production could reach 650 million gallons annually by 2015[209], i.e. the glycerol generated from biodiesel industry will be around 2 million tons/year. However, the current global market for glycerol is only about 1.5 million tons/year. Scientists from various areas utilized their expertise to explore novel ways for the utilization of glycerol, e.g. converting glycerol into high value-added products[11]. Among the various approaches discussed in literature, the biotransformation of glycerol is one of the most promising approaches since it can be conducted at low cost with high specificity and is concomitantly environmental friendly.

Glycerol dehydrogenase (GDH) is capable to convert glycerol by oxidation into 1,3-dihydroxyacetone (DHA), which is a product of high value in the personal care and chemical synthesis industry. Although GDH is commercially available, the high price, insufficient stability and low activity hamper its application in industrial scale. A way out of this might be engineering of GDH to combine the catalytic property with other

features of recombinant proteins, such as high production yield and easy purification. In this chapter, a recombinant GDH conjugated with 6xhis-tag was overexpressed in *E. coli* BL21(DE3) strain. NAD^+-dependent glycerol dehydrogenase from *E. coli* MC 4100 has shown the highest activity in glycerol oxidation reaction as reported in literature [215], therefore, the glycerol dehydrogenase gene (*gld*A) amplified from wild type *E. coli* MC4100 was inserted into directional cloning vector (pET151/D-TOPO®) with T7 promoter. The successful transfection of *gld*A gene was characterized by several techniques including PCR, restriction digestion, and sequencing. The expression of the functional GDH was confirmed by SDS-PAGE electrophoresis, western blot and activity/structure studies. The recombinant GDH obtained in the study by homologous overexpress of *gld*A gene provided sufficient amounts for further experiments at a reasonable price. The presence of 6xHis tag also offers an easy immobilization of GDH on the supporting material in the bioreactor constructed.

4.2 Materials and Methods

4.2.1 Purification of Genomic DNA of from *E. coli* MC4100

E. coli strain MC4100 was obtained from American Type Culture Collection (ATCC), and cultivated in Luria-Bertani (LB) medium using G24 Environmental Incubator Shaker (New Brunswick Scientific Co. Inc, Edision, NJ). Genomic DNA from *E. coli* MC4100 was extracted by using Wizard® Genomic DNA Purification Kit (Promega: A1120). Typically, culture of *E. coli* MC4100 with 10^7 to 10^8 cells (1 ml) was added to a 1.5-ml microcentrifuge tube, and centrifuged at 13,000 rpm for 2 minutes to

pellet the cells. After removing the supernatant, Nuclei Lysis Solution (600 µl) was added to re-suspend the cells by gently pipetting, followed by incubation at 80^{o}C for 5 minutes to lyse the cells. The tube was then cooled to room temperature and 3 µl of RNase Solution were added. After inverting the tube 2-5 times to mix, the cell lysate was incubated at 37^{o}C for 30 minutes, and cooled to room temperature again. Protein Precipitation Solution (200 µl) was then added to the tube with RNase-treated cell lysate, and vortexed vigorously at high speed for 20 seconds. The sample was incubated on ice for 5 minutes, and centrifuged at 13,000 rpm for 3 minutes. The supernatant containing the genomic DNA of *E. coli* MC4100 was transferred to a clean 1.5-ml microcentrifuge tube containing 600 µl of isopropanol (100%) at room temperature. After gently mixing by inversion until the observation of thread-like strands of DNA, the tube was centrifuged at 13,000 rpm for 2 minutes. The supernatant was carefully removed, and with the remaining DNA pellet was then drained. Ethanol (600 µl, 70%) was added to the tube to wash the DNA pellet, and the tube was finally centrifuged at 13,000 rpm for 2 minutes. The supernatant was removed and the pellet was air-dried. Finally, DNA Rehydration Solution (100 µl) was added to rehydrate the DNA by incubating the solution overnight at 4^{o}C.

4.2.2 Production of Blunt-End PCR Product of *gld*A DNA

PCR primers were designed to introduce directional TOPO overhang of CACC upstream to allow the directional cloning into the pET151/D-TOPO vector. Primers had

a total length of 22 or 21 nucleotides respectively and the sequence was optimized by using the OligoPerfect^{TM} Designer. The designed primers are shown as below:

Forward Primer (5' to 3', Directional TOPO overhang underlined):

5'-CACCATGCCGCATTTGGCACTA

Reverse Primer (3' to 5'): AAGGACGTTCTCACCCTTATT-5'

Table 4.1 Composition of PCR reaction for the production of blunt-end *gldA* PCR product.

Reagents	reactions		
	gldA	Control	Blank
AccuPrime *Pfx* SuperMix (Invitrogen, 12344-040)	45 µl	45 µl	45 µl
Genomic DNA template from *E. coli* MC4100	1 µl	-	-
Forward Primer (100 ng/ml)	1 µl	-	1 µl
Reverse Primer (100 ng/ml)	1 µl	-	1 µl
Sterile water	2 µl	2 µl	2 µl
Control PCR template (750 bp)	-	1 µl	-
Control Forward Primer	-	1 µl	-
Control Reverse Primer	-	1 µl	-

PCR reactions for the production of blunt-end *gldA* and control products were prepared as described in Table 4.1. The PCR cycler (MiniCycler PTC-150, MJ Research, Waltham, MA) was programmed with an initial denaturing at 95 ^{o}C for 5 minutes, followed by 30 cycles of denaturing at 95 ^{o}C for 15 seconds, annealing at 55 ^{o}C for 30 seconds, and extension at 68 ^{o}C for 1.5 minutes. The reaction was concluded with a final

extension cycle at 68 ^{o}C for 30 minutes. A negative and positive control was carried along with water and Control PCR Template provided in the expression kit.

4.2.3 Agarose Gel Analysis of PCR Products

To visualize and confirm the amplification of *gld*A gene from *E. coli* genomic DNA on agarose gel electrophoresis, the samples from PCR reaction were mixed with 10x BlueJuice™ Gel Loading Buffer (Invitrogen, 10816-015) at a volume ratio of 1:1. Sterile water was added to reach a final volume to 10 µl. Agarose gel (0.6%) was prepared with UltraPure Agarose (Invitrogen, 15510-019) in TAE buffer. After the solidification of the gel, it was placed in the electrophoresis chamber, and samples were loaded and run at 200 V for about 30 minutes. Gel was stained in 5 µg/ml Ethidium Bromide solution for 20 min, and the image of gels were taken under UV on a BioDoc-It™ Imaging System (UVP, Upland, CA).

4.2.4 Purification of PCR Products

In order to deploy the PCR products in the TOPO cloning reaction, PCR products were purified by using the PureLink PCR Purification Kit (Invitrogen, K3100-01). Typically, 200 µl PureLink Binding Buffer HC with isopropanol was admixed to each PCR reaction mixture and carefully loaded to a PureLink Spin Column. After incubation for 1 min, the spin column was centrifuged at room temperature at 10,000 ×g for 1 minute. The flow through was discarded and 650 µl of Wash Buffer with ethanol were added into the column. First the column was centrifuged at 10,000 ×g for 1 minute to

wash DNA, and then centrifuged at maximum speed for 3 minutes to remove residual Wash Buffer. To elute the PCR products, the column was placed in a clean 1.7-ml Elution Tube and loaded with 50 µl of Elution Buffer (10 mM Tris-HCl, pH 8.5), and incubated at room temperature for 1 minute. The centrifugation was carried out at maximum speed for 2 minutes. Concentration and purity of the DNA was estimated by DNA gel electrophoresis. The purified PCR products were stored at -20 ^{o}C for TOPO Cloning Reaction.

4.2.5 TOPO Cloning Reaction and Transfection

The optimized TOPO cloning reaction condition is in Table 4.2. For TOPO cloning reaction, three microliters of each cloning batch were transformed into separate vials of competent cells (One Shot TOP 10), and gently mixed. Cells and DNA were incubated on ice for 30 minutes and heat-shocked for 30 seconds at 42 ^{o}C without shaking. Vials were immediately transferred on ice for a couple of minutes to cool down. To each vial, 250 µl S.O.C. medium were added and incubated by horizontal shaking (200 rpm) at 37 ^{o}C for 1 hour. To select transformed cells, 100 and 200 µl respectively of the cell culture were spread on two LB agar antibiotics selective plates containing 50 µg/ml of Ampicillin (Fluka, 10044) and incubated overnight at 37 ^{o}C.

Table 4.2 Optimized TOPO cloning reaction molar ratio

Reagent	Vector Only	Vector + Control	Vector + *gld*A
Sterile Water	4 µl	3 µl	0 µl
Salt Solution	1 µl	1 µl	1 µl
PCR Product	-	1 µl control PCR product	4 µl PCR *gld*A
pET TOPO Vector	1 µl	1 µl	1 µl

4.2.6 Purification of Plasmid DNA

Transformants were analyzed after picking around 10 colonies from each of the two LB agar selective plates and inoculating culture of 5 mL LB medium containing 50 mg/L Ampicillin. After incubating overnight at 37 ^{o}C while vigorously shaken, the cells were harvested by centrifugation at 10,000 rpm in a conventional, table-top microcentrifuge (Eppendolf 5415D) for 3 minutes. Plasmid DNA was extracted by using the QIAprep Spin Miniprep Kit (Qiagen, 27104). The pelleted bacterial cells were re-suspended in 250 µl of Buffer P1 (provided in the kit), followed by the admixture of250 µl of Buffer P2 and mixed thoroughly by inverting the tube 4-6 times. Since LyseBlue reagent was contained in buffer P1, the solution turned into blue. Buffer N3 of 350 µl was added and mixed thoroughly by inverting the tube 4-6 times. The solution turned into colorless upon the usage of LyseBlue reagent. The tubes were centrifuged for 10 min at 13,000 rpm in a table-top microcentrifuge, followed by carefully transferring the supernatant into the QIAprep spin column. QIAprep spin columns sitting on centrifuge tubes were centrifuged for 60 seconds, and the flow through fraction was discarded. The DNA absorbed in QIAprep spin columns was washed by sequentially adding 0.5 ml Buffer PB, and 0.75 ml of Buffer PE and centrifugation for another 60 seconds. The flow

through was discarded. The QIAprep spin columns were centrifuged for an additional 1 min to remove residual wash buffer. To elute DNA, each QIAprep column was placed in a clean 1.5 ml microcentrifuge tube with 50 µl Buffer EB added to the center of each QIAprep spin column. The QIAprep columns were allowed to stand for 1 min at room temperature, and centrifuged for 1min. Concentration and purity of plasmid DNA collected in the centrifuge tube was determined by spectroscopy and stored at -20 ^{o}C for future usage.

4.2.7 Analysis of Transformants by PCR and Sequencing

To confirm the appropriate N-terminal fusion tag of *gld*A gene in frame, the inserted fragment and the flanking DNA were sequenced by the BioMedical Genomics Center (BMGC) in University of Minnesota. For the sequencing reaction those forward and reverse primers that bind to the plasmid DNA flanking the insert and recommended by the manufacturer were used.

4.2.8 Expression *gld*A Gene in *E. coli*

To transform the vector construct or the positive control (10 ng each) into BL 21 Star (DE3) One Shot cells, one vial of competent cells was needed per transformation. As pET/D/*lacZ* was provided in the Cloning and Expression Kit it was used as positive control. One vial of BL21 Star (DE3) One Shot Cells was thawed for each transformation. Purified plasmid DNA (10 ng) (described in section 4.2.6) was added to each vial of BL21 Star (DE3) One Shot cells and gently mixed. Vials were incubated on

ice for 30 minutes, followed by heat-shocking the cells for 30 seconds at 42 ^{o}C followed by immediate cooling on ice before S.O.C. medium (250 µl) was added. The tubes were capped tightly and incubated at 37 ^{o}C for 30 minutes while shaken (200 rpm). The entire transformation batch was used for the inoculation of 10 ml of LB containing 50 mg/L Ampicillin and grown overnight at 37 ^{o}C with shaking.

The overnight culture (500 µl) was transferred into 10 ml of LB containing 50 mg/L Ampicillin and incubated at 37 ^{o}C under shaking till OD_{600} of around 0.8 was reached. The culture was split into two aliquots of 5 ml, from which one was induced by the addition of IPTG (β-D-thiogalactoside, Invitrogen 15529-019) at a final concentration of 1 mM, while the other aliquot served as control. The resulting cultures were incubated at 37 ^{o}C and 500 ul were sampled hourly for a total period of 6 hours. Withdrawn samples were centrifuged at maximum speed in a microcentrifuge for 30 seconds to recover the cells, while the supernatant was disregarded. The centrifuged cell pellets were stored at -20 ^{o}C.

Cell pellets were thawn and re-suspended in 500 µl of Lysis buffer for further analysis. Cell lysis was promoted by repetitive freezing and thawing cycles in liquid nitrogen and 42^{o}C water bath respectively for 3 times. Insoluble debris was pelleted by centrifugation at maximum speed in microcentrifuge for 5 minute at room temperature. The supernatant was transferred to a fresh tube and stored on ice.

4.2.9 Purification the Recombinant Protein

The presence of the N-terminal polyhistidine (6xHis) tag in pET151/D-TOPO vector allows purification of recombinant GDH with a metal-chelating resin such as ProBond or Ni-NTA. The purification was preformed by using ProBond™ Purification System (Invitrogen, K85001). ProBond™ Column was pre-treated as suggested by instructions. Recombinant protein was purified by using the native buffers, purification column and cell lysate. Typically, 8 ml of cell lysate were added under native conditions to a prepared Purification Column. The resin was reacted with the lysate solution for 60 minutes with gentle agitation. After the resin was settled by gravity, the supernatant was carefully aspirated out and analyzed by SDS-PAGE. The resin in the column was then washed with 8 ml Native Wash Buffer and settled by gravity. The supernatant of washing solution was carefully aspirated and subjected to SDS-PAGE analysis. The resin was washed for three more times. Bound recombinant protein was then eluted with 8 ml of Native Elution Buffer. Eluting fractions of 1 ml were collected and analyzed by SDS-PAGE.

4.2.10 SDS-PAGE

Samples of cell lysate, washing solutions and eluted fractions were analyzed by SDS-PAGE with NuPage 4-12% Bis-Tris Gel (Invitrogen, NP0323BOX). Samples were mixed 2×SDS-PAGE sample buffer and heated at 70 ^{o}C for 10 minutes. The samples were loaded at 10 µl to the gel slot as well as 5 µl of BenchMark Prestained Protein Ladder (Invitrogen, 10748010) was deployed as protein marker. Polyacrylamide gel was

stained with Coomassie Blue Stain Solution for ~6 hours, and destained for about 30min (Destain Solution I), and overnight (Destain Solution II).

4.2.11 GDH Activity Assay

The specific activity of GDH in the cell lysate and the purification fractions was determined with glycerol as substrate, and NAD^+ as cofactor [216]. The formation of NADH was measured spectrophotometrically at 340 nm. The protein content of each sample was measured using Bradford protein assay [217].

4.2.12 Purification of Recombinant GDH

Purified recombinant GDH was purified using an ultrafiltration cell (Amicon 8200, Millipore, MA, USA) with a membrane cut-off of 300 kDa (Amicon MW: 300,000 Millipore, MA, USA) by 0.05 M phosphate buffer (pH 7.0) to lower the salt concentration in the elute, since elevated salt amount might have adverse effects on the enzyme. Finally GDH was freeze-dried for further storage. The recombinant GDH was analyzed in Center for Mass Spectrometry and Proteomics in University of Minnesota to confirm the correct amino acid sequence. The protein structure prediction was done by submitting amino acid sequence to I-TASSER web server.

4.3 Results and Discussion

4.3.1 Amplification of *gld*A gene from *E. coli*

The genomic DNA was extracted from *E. coli* strain ATCC MC4100 and used as PCR template for the amplification of the *gld*A gene. Primers were designed based on the known *gld*A gene sequence as deposited in the EMBL data base as ECOUW89 under accession no. U00006 [218]. The successful amplification was confirmed via DNA gel electrophoresis and yielded a band of 1.1 kb, which complies with the known length of the gene (Figure 4.1).

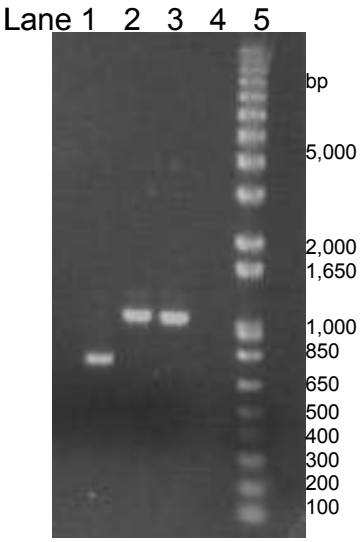

Figure 4.1 PCR products of *gld*A and control DNA template on 0.6% agarose gel. Lanes: 1: Control PCR product (750bp); 2: gldA sample 1; 3: gldA sample 2; 4: PCR reaction blank; 5: 1kb plus DNA ladder.

As shown in Figure 4.1, ~1,1 kb of PCR product of *gld*A was obtained in the extracted *gldA* samples in two different preparations (Lane 2 and 3), which is close to the expected size of *gld*A gene (1,143 bp). The PCR product of *gld*A gene was further

purified to remove the short DNA segment and primers for the use in clone reaction. The concentration of purified PCR product was estimated to be 10 ng/µl.

4.3.2 Analysis of Transformants by PCR and Sequencing

Transformants were analyzed by plasmid purification. The obtained plasmid DNA was used as PCR template T7 primers binding to the DNA sequences flanking the inserted *gld*A gene. As can be taken from Figure 4.2, the PCR product was slightly bigger (1.3 kb) than the *gld*A gene due to the presence of the 6xhis-tag and flanking DNA.

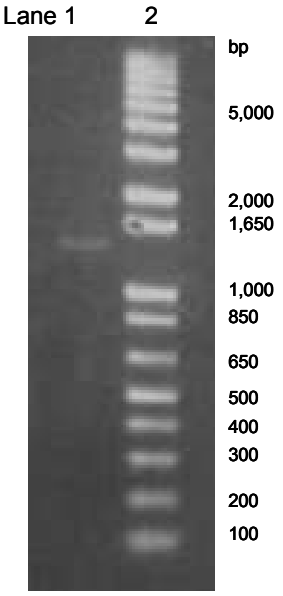

Figure 4.2 PCR amplification result using the plasmid DNA extracted from the transformants as template. Lane 1 clearly indicates that gldA was successfully inserted to the vector; lane2: 1kb plus DNA ladder.

The PCR products were purified and submitted to the BioMedical Genomics Center (BMGC) of the University of Minnesota for DNA sequencing. By that way it was

possible to confirm that the inserted gene is in frame and fully functional. The obtained sequence was aligned with the reference *gld*A gene sequence cloned from *E. coli* MC4100 [219] because the *gld*A gene sequence in MC4100 is not available in GenBank database. The alignment is shown in Figure 4.3 and indicates a 100% match.

Figure 4.3 Alignment of reference DNA sequence with DNA sequencing obtained by PCR amplification using the plasmid DNA extracted from the transformants as template. Sequences: top: reference gene sequence; bottom: gene sequence in this study.

4.3.3 Characterization of recombinant GDH

Recombinant GDH was purified by affinity bonding chromatography and resulting eluted fractions were analyzed by SDS-PAGE (Figure 4.4). The expected molecular weight of the recombinant GDH is about 44 kDa including the 6xHis tag and expression epitope (3 kDa). As shown in Figure 4.4, the culture cell lysate (lane 1) contained multiple proteins including recombinant GDH. Some recombinant GDH molecules were found in the flow-through samples from the ProBond® column (lane 9), which indicated the column capacity was reached. With four times of washing the column, unbound proteins were completely removed from the column (as shown from lane 10 to 14 by the absence of any protein). The GDH was eluted after using the 7-fold column volume of elution buffer and only one single band with a size of 44 kDa was observed (lane 2 to 8), indicating a high purity of recombinant GDH.

The optimized purification process yielded GDH with a specific activity > 80.6 U/mg, which outperforms the specific activity of 70 U/mg given for the commercial GDH. The highest yield obtained ranged to 10.2 mg of recombinant GDH per gram of wet cell paste, which is more than 3-fold higher than the previous reported yield of GDH from *Cellulomonas* sp. NT3060 [220] or even more than 8 times higher than that of GDH purified from *Klebsiella pneumoniae*[10].

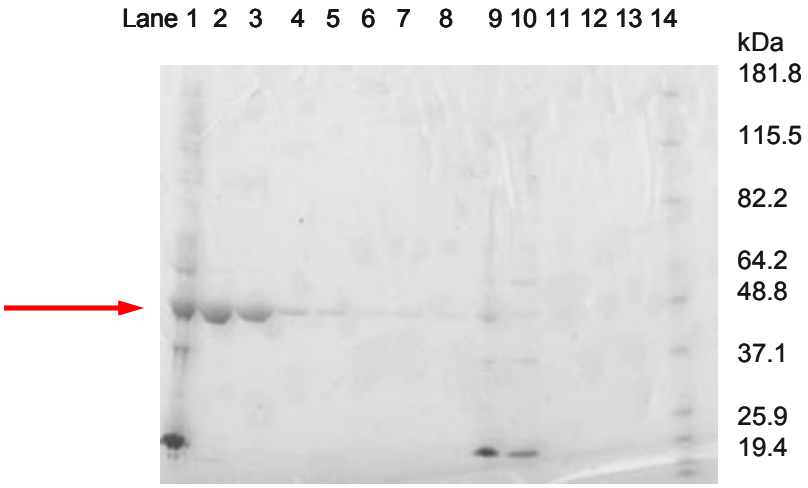

Figure 4.4 SDS-PAGE image of the purification of recombinant GDH from cell lysate. Lane 1: Culture induced by IPTG for 4 hours; lane 2 to 8: Elution Collection Fraction 1 to 7; lane 9: Binding residue sample; lane 10 to 13: Washing solution 1 to 4; lane 14: BenchMark Pre-Stained Protein Ladder.

4.3.4 Analysis of Purified Recombinant GDH

Purified recombinant GDH was analyzed in Center for Mass Spectrometry and Proteomics in University of Minnesota to confirm the correct amino acid sequence. The protein structure prediction was conformed by submitting amino acid sequence to I-TASSER web server for the homology modeling. The amino acid sequence obtained by In-gel Proteolytic Protein Digestion is shown in below, and analyzed by Scaffold 2 software to compare with the available amino acid sequence in Protein Data Bank. There is no exact match of amino acid sequence in Protein Data Bank. The probability of 95% was given by Scaffold 2 that this recombinant protein is glycerol dehydrogenase.

```
         10         20         30         40         50         60         70         80         90         100
....|....|....|....|....|....|....|....|....|....|....|....|....|....|....|....|....|....|....|....|
MPHLALLISKGAIMDRIIQSPGKYIQGADVINRLGEYLKPLAERWLVVGDKFVLGFAQSTVEKSFKDAGLVVEIAPFGGECSQNEIDRLRGIAETAQLGA

         110        120        130        140        150        160        170        180        190        200
....|....|....|....|....|....|....|....|....|....|....|....|....|....|....|....|....|....|....|....|
ILGIGGGKTLDTAKALAHFMGVPVAIAPTIASTDAPCSALSVIYTDEGEFDRYLLLPNNPNMVIVDTKIVAGAPARLLAAGIGDALATWFEARACSRSGA

         210        220        230        240        250        260        270        280        290        300
....|....|....|....|....|....|....|....|....|....|....|....|....|....|....|....|....|....|....|....|
TTMAGGKCTQAALALAELCYNTLLEEGEKAMLAAEQHVVTPALERVIEANTYLSGVGFESGGLAAAHAVHNGLTQLVLENAPVTAIPDAHHYYHGEKVAF

         310        320        330        340        350        360        370        380
....|....|....|....|....|....|....|....|....|....|....|....|....|....|....|....|....|
GTLEEIETVAALSHAVGLPITLAQLDIKEDVPAKMRIVAEAACAEGETIHNMPGGATPDQVYAALLVADQYGQRFLQEWE
```

However, compared the amino acid sequence of our recombinant GDH compared with the reference GDH sequence of *E. coli* O157:H7 (http://www.uniprot.org/uniprot/Q8X762) that has 380 amino acids, we found that both sequences are highly identical except that lysines at 11 positions (51, 63, 66, 108, 114, 168, 207, 229, 286, 328, and 334) in *E. coli* O157:H7 was replaced by leucines in our recombinant GDH, and one glycine was replaced by glutamine in position 236, and one alanine was replaced by serine in position 301. The comparison of amino acid sequence with the reference sequence was shown below, and 96.6% of the amino acid sequences are identical.

```
Comparison of:
(A) O157: H7 380 bp
(B) recombinant 380 bp
96.6% identity in 380 aa overlap (1-380:1-380); score: 2354 E(10000): 8.6e-230

               10        20        30        40        50        60
O157:  MPHLALLISKGAIMDRIIQSPGKYIQGADVINRLGEYLKPLAERWLVVGDKFVLGFAQST
       :::::::::::::::::::::::::::::::::::::::::::::::::: :::::::::
recomb MPHLALLISKGAIMDRIIQSPGKYIQGADVINRLGEYLKPLAERWLVVGDLFVLGFAQST
               10        20        30        40        50        60

               70        80        90       100       110       120
O157:  VEKSFKDAGLVVEIAPFGGECSQNEIDRLRGIAETAQCGAILGIGGGKTLDTAKALAHFM
       :: :: :::::::::::::::::::::::::::::::::::::::::: ::::: ::::::
recomb VELSFLDAGLVVEIAPFGGECSQNEIDRLRGIAETAQCGAILGIGGGLTLDTALALAHFM
               70        80        90       100       110       120

              130       140       150       160       170       180
O157:  GVPVAIAPTIASTDAPCSALSVIYTDEGEFDRYLLLPNNPNMVIVDTKIVAGAPARLLAA
       :::::::::::::::::::::::::::::::::::::::::::::::::: ::::::::::::
recomb GVPVAIAPTIASTDAPCSALSVIYTDEGEFDRYLLLPNNPNMVIVDTLIVAGAPARLLAA
              130       140       150       160       170       180

              190       200       210       220       230       240
O157:  GIGDALATWFEARACSRSGATTMAGGKCTQAALALAELCYNTLLEEGEKAMLAAEQHVVT
       :::::::::::::::::::::::::: :::::::::::::::::::: :::::: ::::
recomb GIGDALATWFEARACSRSGATTMAGGLCTQAALALAELCYNTLLEEGELAMLAAEGHVVT
              190       200       210       220       230       240

              250       260       270       280       290       300
O157:  PALERVIEANTYLSGVGFESGGLAAAHAVHNGLTAIPDAHHYYHGEKVAFGTLTQLVLEN
       :::::::::::::::::::::::::::::::::::::::::::::::::: ::::::::::::
recomb PALERVIEANTYLSGVGFESGGLAAAHAVHNGLTAIPDAHHYYHGELVAFGTLTQLVLEN
              250       260       270       280       290       300

              310       320       330       340       350       360
O157:  SPVEEIETVAALSHAVGLPITLAQLDIKEDVPAKMRIVAEAACAEGETIHNMPGGATPDQ
       .:::::::::::::::::::::::::: ::::: :::::::::::::::::::::::::::
recomb APVEEIETVAALSHAVGLPITLAQLDILEDVPALMRIVAEAACAEGETIHNMPGGATPDQ
              310       320       330       340       350       360

              370       380
O157:  VYAALLVADQYGQRFLQEWE
       ::::::::::::::::::::
recomb VYAALLVADQYGQRFLQEWE
              370       380
```

The major reason we choose *E. coli* MC4100 to extract the *gld*A gene for amplification is because a higher activity (18.2 micromoles of NAD^+ reduced per minute per milligram of total protein) of GDH was observed in one of its mutants [215]. Unfortunately, the underlying reason for this improved activity is not discussed by the authors. It was assumed that the observed mutations in its amino acid sequence might

contribute to the enhancement of activity. The fact which the specific activity of our purified recombinant GDH is higher than commercial GDH (80.6 vs. 70 U/mg) also indicated that the activity could benefit from those mutations.

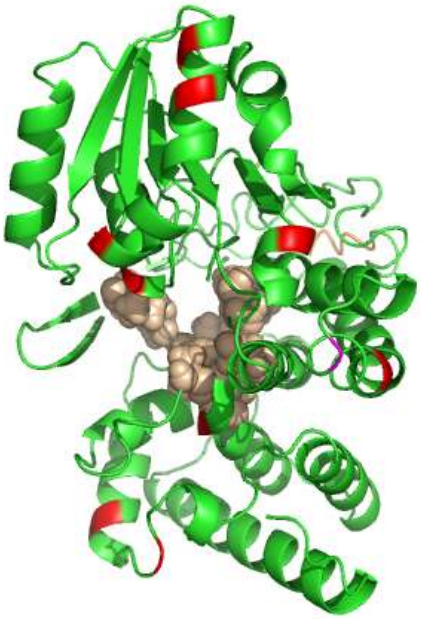

Figure 4.5 Protein structure animation of recombinant GDH. Orange: 6xHis; Red: Leucines in position 51, 63, 66, 108, 114, 168, 207, 229, 286, 328, and 334; Pink: Glycine in position 236; Yellow: Alanine in position 301. Spheres: predicted binding sites.

The amino acid sequence of recombinant GDH was used for the prediction of enzyme structure. The homology modeling of recombinant GDH was calculated by the I-TASSER web server, and the resulting protein structure was visualized via the Pymol software (Figure 4.5). In the function prediction of homology model, the homology model predicted over 94% that the Enzyme Commission number (EC) is EC 1.1.1.6, which represents NAD^+-dependent glycerol dehydrogenase. The results further confirmed that the recombinant enzyme obtained in this study is glycerol dehydrogenase.

4.4 Conclusions

The *gld*A gene from *E. coli* MC4100 was successfully transfected in *E. coli* BL 21 Star (DE3) One Shot cells with T7 promoters as proven by PCR, restriction digestion and sequencing. The recombinant GDH integrated with 6xHis tag was successfully expressed as confirmed by SDS-PAGE, western blot and sequence studies in which the recombinant enzyme showed the expected size and activity. The obtained yield of 10.2 mg·GDH/g·cell pastes is about 3 times higher than what has been reported in literature. The measured specific activity (80.6 U/mg) showed improvement of about 10-15% compared with the commercial source of GDH from *E. coli*. The recombinant GDH obtained in the study provided high active and sufficient amount of enzyme for further studies.

CHAPTER V

CARBON MATERIAL WITH BRANCHING CARBON NANOTUBES AND ITS APPLICATION IN A SINGLE CARBON FIBER MICROBIOSENSOR

5.1 Introduction

In this study the use of carbon-fiber and carbon nanotubes (CNT) hierarchical electrodes with the nanotubes branched out from the surface of the fibers was explored, and generated CNT structures with surfaces fully open for interactions with surrounding solutions. One additional goal of this research is to explore the use of renewable resources for the preparation of such carbon electrodes. Previous studies of carbon fiber electrode fabrication based on fossil-based polymers lack the potential of sustainability. A feasible approach could be carbonization of renewable materials from biomass. Cellulose, the most abundant polymeric constituent in biomass, is composed of β-D glucopyranose units which are linked together in linear chains by 1-4 glycosidic bonds. The pyranose units, upon pyrolysis, are dehydrated to a carbonaceous polymer intermediates which can be transformed into a polyaromatic structure [221], constituents characteristic of carbon materials. Indeed, many published studies have reported the production of carbon fibers from cellulose fibers in the form of native cellulose[222] and extruded regenerated cellulose fibers[223]. Hierarchical porous carbon structures have also been transformed through pyrolysis of cellulose acetate filters used in cigarettes[224].

These cellulose carbonization processes, however, were not aimed at electrochemical applications.

There have been so far no reported attempts in growing CNTs on surfaces of cellulose-derived carbon fibers to produce nanostructure materials. Metal-catalyzed growth of nanotubes has been applied widely in recent years for preparing a variety of nanostructured materials, such as the fiber-tube and fiber-fiber[225] hybrid carbon materials, for the purposes of increasing surface area, providing higher sensitivities and ease of preparation for many applications including field effect transistors[29]. The introduction of CNTs in this kind of nanostructured materials for electrochemical applications has resulted in a great improvement in electrochemical properties. All of these reported CNT growth are on fossil-based materials, and it is therefore necessary to investigate the use of renewable materials for sustainable production of CNT-based electrodes.

Single carbon fiber electrodes are greatly promising for microelectronic applications including high performance biosensor[30-32] and miniaturized energy devices such as fuel cells[33]. For sensor applications, single carbon fiber electrodes are especially appealing in that they require only a small amount of samples, but provide high signal/noise ratios and render short responding time[226-228]. Such sensors have found a variety of applications. For example, single carbon fiber electrodes have been applied for measurements of real time chemical release from single cells[229] and as neurotransmitters for *in vivo* monitoring of signal generation in brain cells[230, 231].

One drawback in using carbon fiber microelectrodes is that they provide only a limited surface area and thus very weak electronic signals which require very sensitive instrumental detection. This setback is a result of the small diameter of carbon fibers that ranges from several micrometers to tens of micrometers. One way to overcome this drawback is to deposit carbon nanotubes (CNTs) on the fiber surface to improve the overall surface area without substantially changing the size of the electrode. CNT deposition had been attempted on single carbon fiber microelectrode[34] and nanoelectrode [35] by dipping carbon fiber electrodes into CNT suspension with the aid of dispersing agents, such as surfactant (sodium dodecyl sulfate). Suspensions of CNTs in Nafion® solution were also used for CNT deposition on electrode by dip-coating[36] and by electrochemical deposition[37]. In addition to improving specific surface areas, CNTs also impart many favorable electronic properties desired for high performance biosensing and nano-electronic fabrication[38]. CNTs have also been found capable of promoting electron-transfer reactions, minimizing fouling of electrode surfaces[39], enhancing electrocatalytic activity, and facilitating the immobilization of enzymes and antibodies on the surface of electrodes[40, 232]. As such, CNT-fabricated carbon fiber microelectrodes have been examined for biosensors[233], micro-column separation[234], and biofuel cells[235].

Advances were made on preparing and using CNT-containing electrodes for oxidation of NADH but the advantages of CNTs have yet to be more fully tapped. Viry et al. reported a method for producing CNT fibers by co-electrospinning CNT with poly (vinyl alcohol) polymer, followed by a heat-treatment procedure to remove the polymer,

producing fibers in the form of CNT bundles[236]. Such CNT fibers were used as micro disk electrodes and examined for glucose assay, and were found able to offer improved activities for the oxidation of NADH as compared to single carbon fiber electrodes. In another effort, similar CNT fibers were prepared by a simple particle-coagulation spinning process, involving the injection of a homogeneous CNT dispersion in a polymer solution, and the produced fibers have an interconnected CNT/polymer-chain network[237]. Such CNT-containing fiber microelectrodes exhibited good electrocatalytic activities and effectively reduced the NADH oxidation potential by ~0.2 V[238]. To our opinion, the abovementioned preparation of CNT-containing electrodes does not promise to fully capitalize the potentials of CNTs, as the fabrications generally led to CNTs that are bundled together or embedded inside other supports such as polymers, exposing only a portion of CNTs for reactions.

This work explores the use of cellulose materials for preparation of hierarchical carbon materials. A new and facile fabrication production method of CNT-carbon fibers is developed through carbonization of cellulosic fibers and growth of CNT in the presence of Fe. A single CNT-modified carbon fiber was then used as a microelectrode, and tested for the efficiency of oxidation reaction of NADH generated from the glycerol oxidation reaction to explore its potential in large scale electrochemical applications involving NADH reuse and regeneration. It is expected that the single CNT-modified carbon fiber from cellulose will provide sensitive detection corresponding to the concentrations changes of NADH in glycerol oxidation reaction, lower the overpotential of NADH oxidation on carbon electrode and reduce the electrode fouling.

5.2 Materials and Methods

5.2.1 Production of CNT-modified carbon microfiber

Cellulose fiber, acquired as medical grade cotton wool from Malaysia (Weng Thye Heng SDN BHD, Penang, Malaysia) and U.S. (U.S.P. Sterile Absorbent Cotton Roll, U.S. Cotton (CANADA) Co. Canada) were pre-treated before modifying with CNT. For easy discussion in the following sections, the fiber samples are named as Malaysia- and US- accordingly. The pre-treatment involved dipping of a cotton wool pad ($2 \times 2''$) into 50 ml of well suspended dimethylformamide solution containing 3.3 wt% of Fe (III) acetylacetonate ($Fe(C_5H_7O_2)_3$, (>99.9%, Aldrich, St. Louis, MO, USA) for 2 hours at room temperature. The pre-treated sample was dried at room temperature in a convection-flow fume hood for overnight before carbonization. Carbonization and CNT modification were performed in a high temperature tubular furnace (Sentro Tech., Model STT-1200-3.5-12, Cleveland, OH, USA) with a procedure adopted from reference[219] with modification. The furnace has a max power of 7 kW, max temperature of 1200^{o}C. The schematic illustration of the setup was depicted in Figure 5.1.

The chamber of furnace was first purged with argon at a flow rate of 450 ml/min for 30 min. After loading of the pre-treated cotton wool pad, the sample was annealed at 250^{o}C for 3 hours. The Fe^{3+} ions loaded on cellulosic fibers were reduced to Fe by introducing hydrogen into the furnace chamber at a flow rate of 150 ml/min for 4 hours after the temperature stabilized at 500^{o}C in the argon atmosphere. The cellulosic sample was carbonized at 850^{o}C for 30 min, and then cooled to 700^{o}C. For the carbonization of cellulosic sample without modification of CNT, the sample was cooled down further to

room temperature with all other steps remain the same except that the pre-treatment step was omitted. The growth of CNT on carbon fibers, conducted at 700°C, was initialized by adding hexane vapor as the carbon source carried by argon at the flow rate of 600 ml/min. The desired length of CNT was controlled by the feeding time of hexane, which is in the range of 3~20 min.

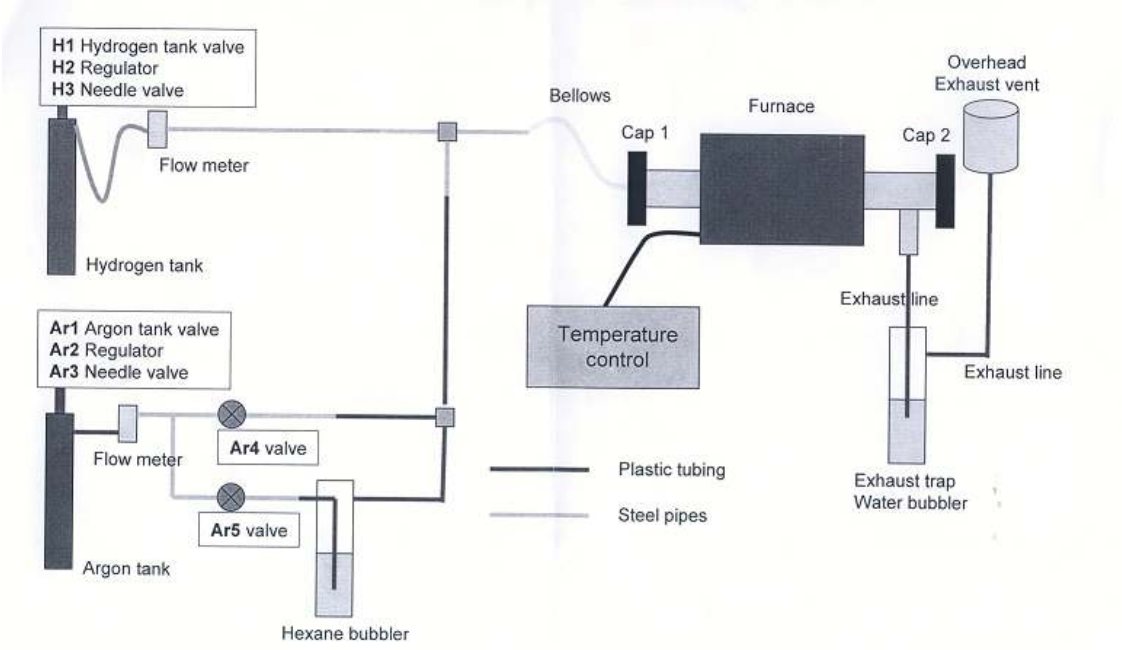

Figure 5.1 Schematic illustration of the setup of carbonization process.

The morphology of carbonized samples was studied by using scanning electron microscopy (Hitachi S3500N Variable Pressure SEM) and transmission electron microscopy (Philips CM12 Transmission Electron Microscope). The surface areas of samples were determined by using gas sorptometer (ASAP 2000, Micromeritics, Norcross, GA, USA) based on physical adsorption of nitrogen gas molecules. The adsorption isotherm was analyzed using the BET method[239] to calculate for the

quantity of gas involved in the monolayer coverage of material surfaces, thereby allowing estimation of specific surface area. All measurements above were preformed in accordance with standard sample preparation protocols.

5.2.2 Fabrication of carbon fiber microelectrode

One single carbon fiber (modified with or without CNT) was pulled out from respective carbonized sample pads, and glued with conductive carbon paint (SPI supplies, West Chester, PA, USA) on a segment of copper wire (L = 85 mm) inserted through a capillary (Drummond Scientific Company, Broomall, PA, USA). Both ends of the capillary tube were sealed with epoxy glue (Armstrong Products Company, Easton, MA, USA). The exposed fiber length was measured under an optical microscope, and controlled by trimming to 3 mm. The resulting microelectrodes are named as carbon fiber microelectrode (CFME) and CNT-carbon fiber microelectrode (CNT-CFME). The schematic illustration of fabrication is shown in Figure 5.2. After drying at room temperature for overnight, the fabricated carbon fiber microelectrode was used in the following electrocatalytic measurements.

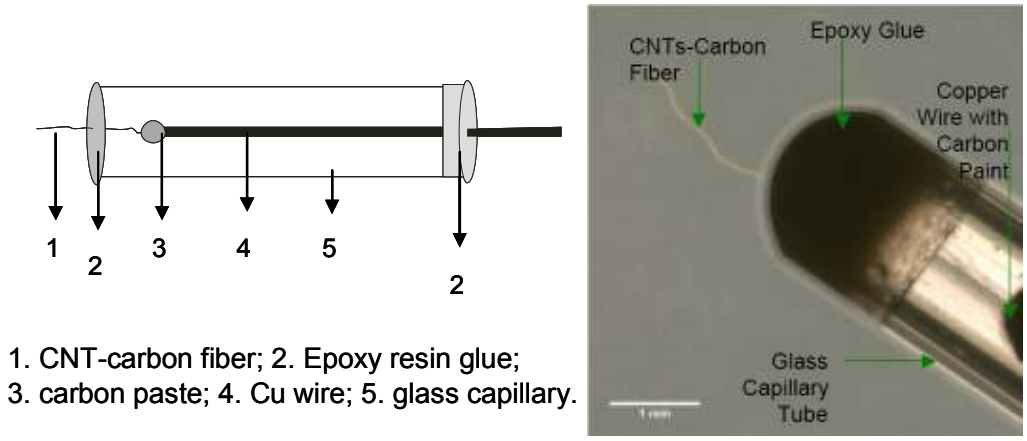

Figure 5.2 Scheme of illustration and image of fabricated CNT-CFME electrode.

5.2.3 Electrocatalytic studies of carbon fiber microelectrodes

The electrochemical properties of microelectrodes were tested with the CHI 760C electrochemical workstation (CH Instruments, Inc. Austin, TX, USA) with a three-electrode system. CFME or CNT-CFME was used as the working electrode. The Ag/AgCl electrode and Pt wire electrode were used as reference and counter electrodes, respectively. The effective electrocatalytic surface area of each microelectrode was measured by using cyclic voltammetry at different scan rates (0.01 to 0.3 V/s) with $K_3Fe(CN)_6$ as electrolyte in 0.1 M KCl. The oxidation of NADH on CFME and CNT-CFME was investigated by cyclic voltammetry of 0.5 mM NADH (Sigma, St. Louis, MO, USA) in 0.05 M NH_4Cl-NH_4OH buffer (pH 9.0). When CFME or CNT-CFME was applied in the regeneration of NAD^+ in glycerol oxidation reaction, 4 ml of total reaction system containing 25 mM of glycerol (Sigma, St. Louis, MO, USA), 0.24 U/ml of

glycerol dehydrogenase (Sigma, St. Louis, MO, USA), and various concentrations of NAD^+ ranging from 0 to 2 mM were used.

5.3 Results and Discussion

5.3.1 Effects of Fiber Source on Morphology of Carbonized Material

Cellulosic fibers from different regions of growth were examined in this study. One kind of cellulosic fiber was from Malaysia with tropical climate, and another kind of cellulosic fiber was grown in USA. The cellulosic fibers were selected for testing the universality of the method developed in this study. The growth and morphology of CNT on carbon fibers are evidenced with SEM. The images of carbonized cellulosic fibers are shown in Figure 5.3. The Malaysia- cellulosic fiber tends to yield straight fiber after carbonization, and the US- cellulosic fiber showed curly and spiral in morphology. As shown in Figure 5.3A, the surface of cellulosic fibers showed some uniform roughness patterns along the fiber length. After the cellulosic fiber was loaded with Fe precursor, a continuous thin film is uniformly coated onto the surface (data not shown). During the reduction of Fe^{3+} to Fe with H_2, different sizes of iron particles were formed on the surface of carbonized fiber surface (Figure 5.4). Since the surface of cellulosic fiber is not smooth, the Fe particles are not uniformly formed. Individual cellulosic fibers have an average diameter of ~20 μm (Figure 5.3A), which was reduced to ~15 μm after carbonization, suggesting a loss of material as reported in another study on cellulose carbonization [222]. Other than the differences in morphology, carbonized Malaysia-cellulosic fibers is less hydrophobic during applications.

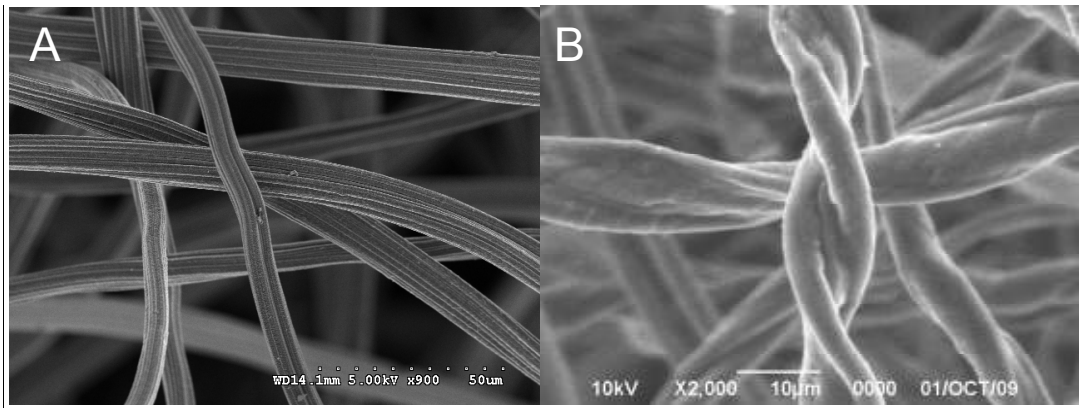

Figure 5.3 Comparison of carbonized fiber from different sources. (A) Carbonized Malaysia-fiber; (B) Carbonized US-fiber.

This study examined the growth of CNT on the surface of carbonized cellulosic fibers. Controlled growth of carbon nanotubes on fiber surfaces was realized via deposition of metal particles without addition of dispersing aids. When cotton pad was deposited with Fe^{3+} salt (pre-treatment) followed by carbonization and reduction, the Fe salts were successfully reduced to Fe nanoparticles. Using Malaysia-fiber as an example, the Fe catalyst formed a layer of nanoparticles (~500 nm in diameter) on the surface of carbonized Malaysia-fiber before the initiation of CNT growth (Figure 5.4).

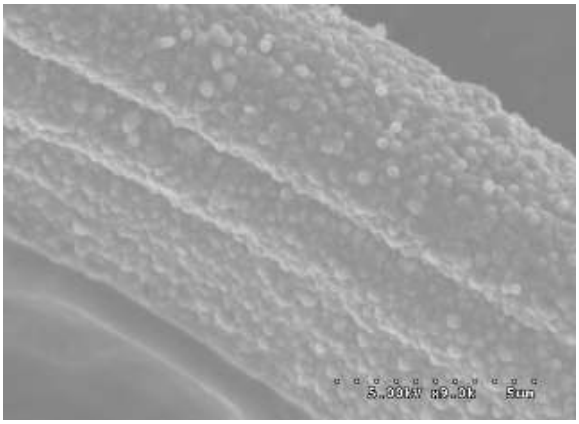

Figure 5.4 Carbonized Malaysia-fiber with metal catalyst on the surface of carbon fiber. Catalyst: Fe 3% in DMF solution; Hexane feeding: 0 min; (A) Carbonized; (B) Carbonized US-fiber.

When hexane was provided as carbon source for 5 min in order to grow CNT on the surface of carbonized fiber, uniformly grown CNT were observed on both samples, as shown in Figure 5.5.

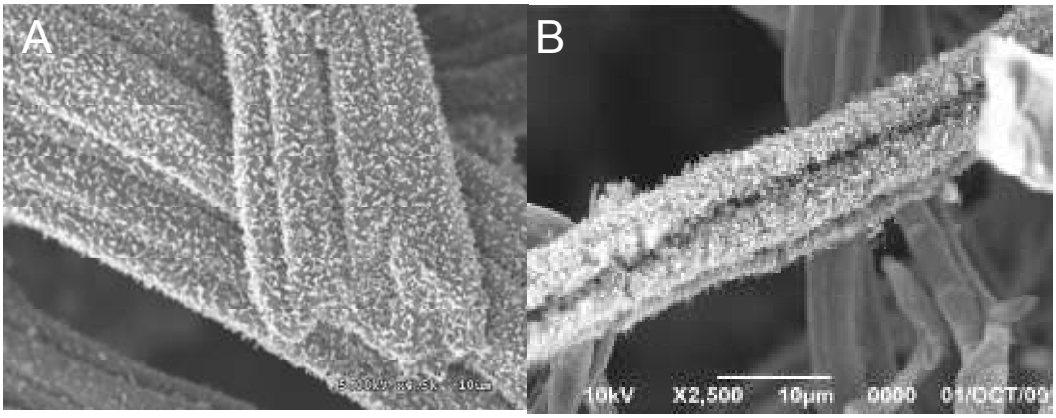

Figure 5.5 Comparison of carbonized fiber with CNT grown on the surface from different sources. Catalyst: Fe 3% in DMF solution; Hexane feeding: 5 min; (A) Carbonized Malaysia-fiber; (B) Carbonized US-fiber.

5.3.2 Effect of Feeding Time of Hexane on the Growth of CNT

Hexane works as carbon source for CNT growth on the surface of carbonized cellulosic fiber. It is obvious that the longer of supplying time of hexane, the longer CNT can grow. Upon CNT growth, however, the diameter of individual fibers was reduced to a range of 10 to 15 μm. This diameter decrease could be attributed to the prolonged heat exposure during the CNT growing stage, causing a diameter shrinkage that prevailed over the diameter gain from the grown (protruded) CNTs. The hexane supply time influenced the length of CNT grown on the carbonized fiber surfaces. As shown in Figure 5.6, two different batches of preparation with 5 min and 20 min of hexane feeding are compared. In Figure 5.6B, CNT with length of couple of microns have been produced on the surface of carbonized fiber with 20 min of hexane feeding. A longer hexane exposure time resulted in longer CNT.

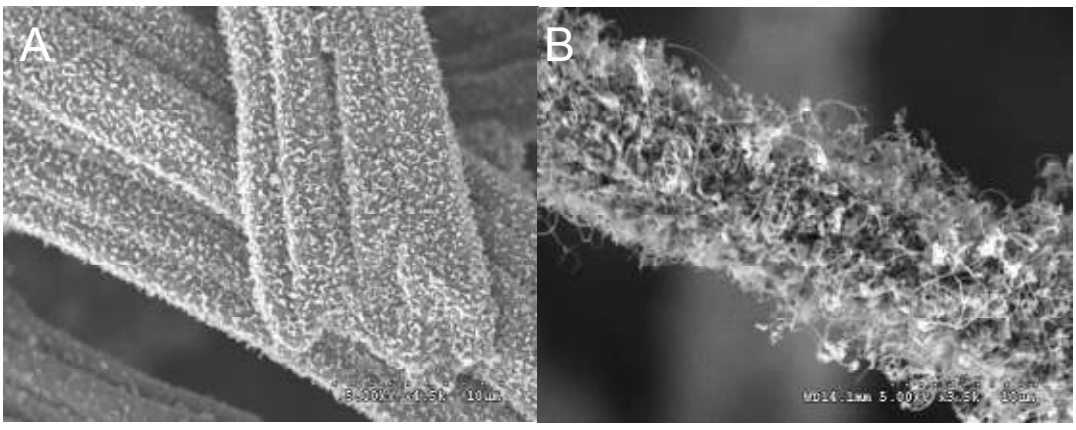

Figure 5.6 Effect of hexane feeding on the length of CNT grown on the surface of carbonized fiber. Cellulose fiber used: Malaysia-fiber; catalyst: Fe 3% in DMF solution; (A) hexane feeding for 5 min; (B) hexane feeding for 20 min.

The carbonized fibers prior to CNT growth maintained 30.3% of the original weight. On the other hand, the cotton pad without loading of Fe salt weighed 26.5% of the original weight after undergoing the same procedure of carbonization, thus the deposited metal particle amounted to 3.8% of the fiber weight. The CNT-grown carbon fibers exhibited a weight gain that corresponds to the increased CNT length. The weight of (CNT-enabled) carbon fibers, as a percentage of the starting cellulose fibers, increased linearly (from 30.3% to 42.2%) at the first 10 min of hexane exposure. The weight gain slowed down after 10 minutes, with a weight ratio of 45.4% at 20 min. This observation could be attributed to the limited space adjacent to the fiber surface for CNTs at high growth density.

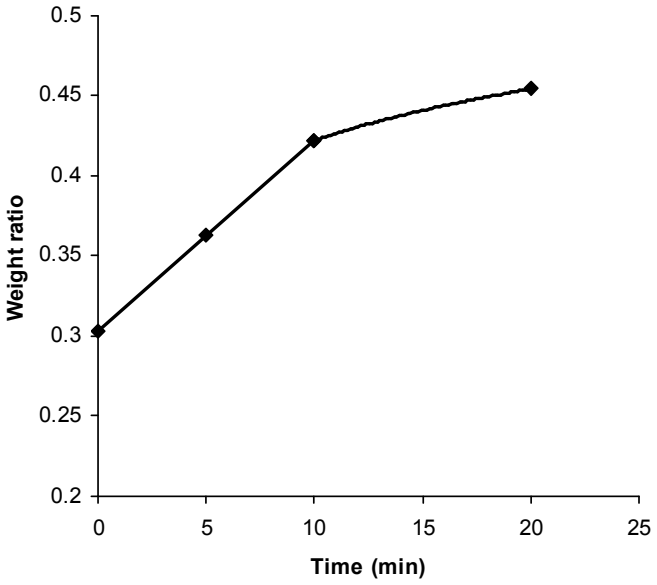

Figure 5.7 Weight ratio of carbonized fiber with different supplying time of hexane.

5.3.3 Effect of Catalyst on CNT Growth on Carbon Fiber

Catalyst plays an important role in the carbonization process of cellulosic fiber. In this study, Fe and Ni salts were introduced in the pretreatment of cellulosic fiber, and were reduced to metal nanoparticles to initiate the growth of CNT. No observable difference was found by using two solvents and metal catalysts. However, the electrochemical properties of carbonized materials with different metal catalyst were different on the desired applications, which will be discussed in the following chapters.

5.3.4 Surface Area of CNT-Carbon Fiber

The CNT-carbon fibers prepared was further investigated, and monitored with TEM. Samples of these fibers were first suspended in an ethanol/H_2O mixture and sonicated for 2 minutes. In TEM images, coiled and branched CNT were observed on the surface of carbon fibers, with the iron particle core on the tip of CNT (Figure 5.8), verifying that CNT growth was enabled at the catalysts locations. This observation is in agreement with previously reported CNT growth on synthetic electrospun polyacrylonitrile (PAN) fibers[219] in which CNT were grown at the location where catalysts exist. Two different diameters of CNT were found (~100 nm and ~10 nm), and the thinner CNT was not observable in SEM images. These TEM results also indicated that the Fe precursor formed different sizes of particles during reduction, but only the large Fe particles could be observed with SEM. The TEM images also revealed that thinner CNT (~10 nm) are hollow and branched, while thicker (~100 nm) CNT are on the surface of carbon fiber. A similar anchorage of carbon nanofibers on structured carbon

microfibers has also been reported[28]. However, this previous study reported growth of nanofibers on the surface of carbon microfibers, while our present study clearly demonstrates the growth of carbon nanotubes.

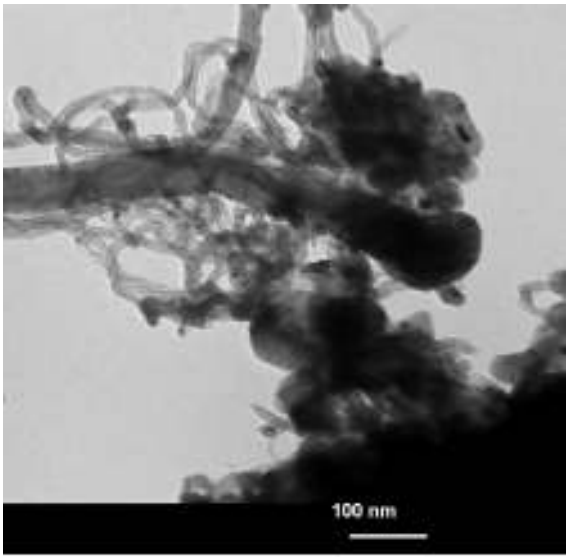

Figure 5.8 TEM image of CNTs on carbon fiber. Two different sizes of CNT (~100nm and ~10nm) are shown.

In a bigger dimensional scale, the CNT-modified carbon fibers produced in this study are a 3-D structured material (Figure 5.9). Our success in producing such materials from renewable fibers strongly contrasts other research with CNT growth, which was conducted on fossil-based fibers [219]. In addition to the size shown in Figure 5.9, different geometries of materials can also be produced with the same protocol.

Figure 5.9 Image of 3-D CNT coated carbon fiber material.

To investigate surface areas of the carbonized samples, two samples were selected (carbonized fibers and CNT-carbon fibers) for the BET measurement. The BET surface area of blank carbon fibers was below the measurement limit (10 m^2/g). The BET result for CNT carbon fiber was 36.4 ± 0.2 m^2/g, thus showing a dramatic increase in the surface area with the growth of CNTs on carbonized fibers. This surface area is comparable to the reported data (23 m^2/g) for CNT grown on carbon felt[28] for 1 to 9 hours. Moreover, after optimization of operational parameters, BET surface area of CNT-carbon fiber reached up to 291 m^2/g.

In addition to BET surface area of bulk samples, the effective surface area of single fiber available for electrochemical reaction was measured using cyclic voltammetry. Carbon fiber (Figure 5.3A) and CNT-carbon fiber (Figure 5.6B) were made into microelectrodes, and named as the carbon fiber microelectrode (CFME) and CNT-carbon fiber microelectrode (CNT-CFME) consequently. Both microelectrodes were tested at different scan rates in 4 mM of $K_3Fe(CN)_6$ in 0.1 M of KCl solution. Results are shown in Figure 5.10.

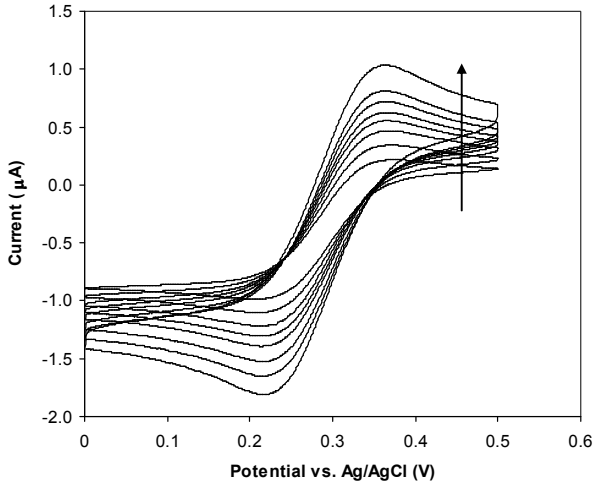

Figure 5.10 Cyclic Voltammograms of CNT-Carbon Fiber Microelectrode. The electrolyte used is 4 mM $K_3Fe(CN)_6$ in 0.1 M KCl solution, and the scan rate varies as 0.01, 0.025, 0.05, 0.075, 0.1, 0.15, 0.2 and 0.3 V/s. Arrow in the figure indicates the increasing of scan rate.

The effective surface area of CFME and CNT-CFME were calculated based on the Randles Sevich equation[240]:

$$I_p = 2.69 \times 10^5 n^{3/2} ACD^{1/2} v^{1/2} \qquad (1)$$

where, n is the electron numbers transferred, in this case n=1 for $K_3Fe(CN)_6$;

A is the electrode surface area;

C is the concentration of $K_3Fe(CN)_6$;

D is the diffusion coefficient of $K_3Fe(CN)_6$, which is 7.62×10^{-6} cm^2/s in 0.1 M KCl solution[241];

v is the scan rate in cyclic voltammetry.

Values of the effective surface area of single CFME and CNT-CFME were, respectively, 2.0×10^{-4} and 2.6×10^{-4} cm^2/mm. The fiber surface area/volume could be estimated from the length (1 mm) of the exposed fiber and the fiber diameter (11.2

micron for CFME, and 14.4 micron for CNT-CFME) determined from SEM. Results showed that the surface area of CFME and CNT-CFME were 1.2×10^5 and 2.7×10^5 m^2/m^3, respectively, suggesting an over two-fold increase in the effective electrode surface area. Such an increase is less compared to the BET measurement which revealed more than 3-fold enhancement in specific surface area. The disparity can be explained by the difference in diffusion patterns between the $K_3Fe(CN)_6$ used in cyclic voltammetric measurements and the nitrogen gas used in BET adsorption measurements. Since smaller molecules such as nitrogen can diffuse into smaller pores, more surface area is detected in BET measurements. Indeed, the BET measurement gave an average pore size of 9.67 nm in the presence of thinner CNT, and this pore size is large enough for the diffusion of small molecules.

Since carbonized fibers in this study will be used in electrochemical applications, electrical conductivity is a very important factor to study. Conductivity results of the carbonized cellulosic fiber and CNT grown carbonized cellulosic fiber were, respectively, calculated to be 3030 ± 550 S/m and 4592 ± 828 S/m by measuring the current passing through a single fiber when a known voltage was applied. The electrical conductivity of polyacrylonitrile (PAN) based electrospun fiber and the CNT-PAN nanofiber have been reported, respectively, to be 480 S/m [242] and 1315 S/m [219]. The conductivity of our carbonized cellulosic fiber is over six folds higher than that of the electrospun PAN fiber, indicating that carbonized cellulosic fibers have the potential to be widely used in electrocatalytic area. When branched CNT were grown on the surface of the carbonized cellulose fiber, the conductivity increased another 1.5 times.

5.3.5 Electrochemical Oxidation of NADH on Single Fiber Microelectrode

CFME and CNT-CFME electrodes were used as working electrodes in a three-electrode electrochemical setup for detecting the oxidation of NADH. NADH is the reduced form of nicotinamide adenine dinucleotide (NAD^+), an important electroactive biomolecules. The NAD^+/NADH is shared by over 300 dehydrogenase enzymes as cofactor[39]. In bioelectrochemical applications, the recycle of NADH to NAD^+ is important for the purpose of sustainability. The direct oxidation of NADH to NAD^+ was hardly realized on traditional electrodes, such as gold, platinum, and glassy carbon electrode, due to the high overpotential (>1.0 V) caused by sluggish charge transfer kinetics[55, 56] and electrode fouling by the adsorption of NADH and the produced NAD^+[243]. The CNT-based electrode illustrated the possibility of reducing the overpotential of NADH. It has been reported that the catalytic ability on the oxidation of NADH was improved by modifying the electrodes with CNT[244].

In the present work the different oxidation properties of NADH on CFME and CNT-CFME were first investigated by cyclic voltammetry in the presence/absence of 0.5 mM NADH in 0.05 M NH_4Cl-NH_4OH buffer (pH 9.0). As shown in Figure 5.11, both electrodes showed catalytic ability for the oxidation of NADH without the presence of any mediator. However, the oxidation current of NADH started to increase after the potential reached 0.45 V on CFME, while it started right after the potential reached 0.2 V on CNT-CFME. The result for CNT-CFME is comparable to the previously published oxidation potential (+0.4 V) of heat treated multi-walled carbon nanotubes fiber microelectrode[238]. The higher surface area and the presence of CNT served to

facilitate the oxidation of NADH on carbon fiber electrode and to lower the overpotential. When the potential of both electrodes stays at 0.6V, the oxidation current of NADH on CNT-CFME is 0.28 μA, which is over 10 times higher than that on CFME. From the cyclic voltammograms, we also observe that the current became stabilized at the potential range of 0.55V to 0.78V, thus allowing us to conclude that within this potential range, the oxidation rate of NADH on the surface of CNT-CFME reached equilibrium with the diffusion rate of NADH to the electrode surface.

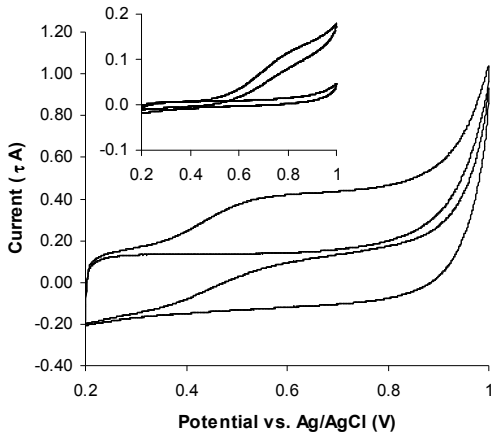

Figure 5.11 Cyclic Voltammograms of CNT-CFME and CFME (insert). The electrolyte used is 0.5mM NADH solution (pH=9.0) in 50 mM NH_4Cl-NH_4OH buffer (pH 9.0); scan rate 100 mV/s.

The oxidation of NADH on CNT-CFME was investigated by examining currents generated in cyclic voltammetry and amperometry, respectively. As shown in Figure 5.12A the oxidation currents of NADH in both measurements were closely agreeable, and the linear range for NADH detection is up to 2.5 mM. The detection limit of CNT-CFME electrode was 0.008 mM for NADH, which is slightly lower than the 0.01 mM

reported in the literature on a polymer-modified carbon fiber electrode [245]. A typical current response to changes of NADH concentrations is shown in Figure 5.12B. From the amperometry experiment, the current response time was ~14 seconds, i.e. it took about 14 second for the current to reach 95% of the stable reading.

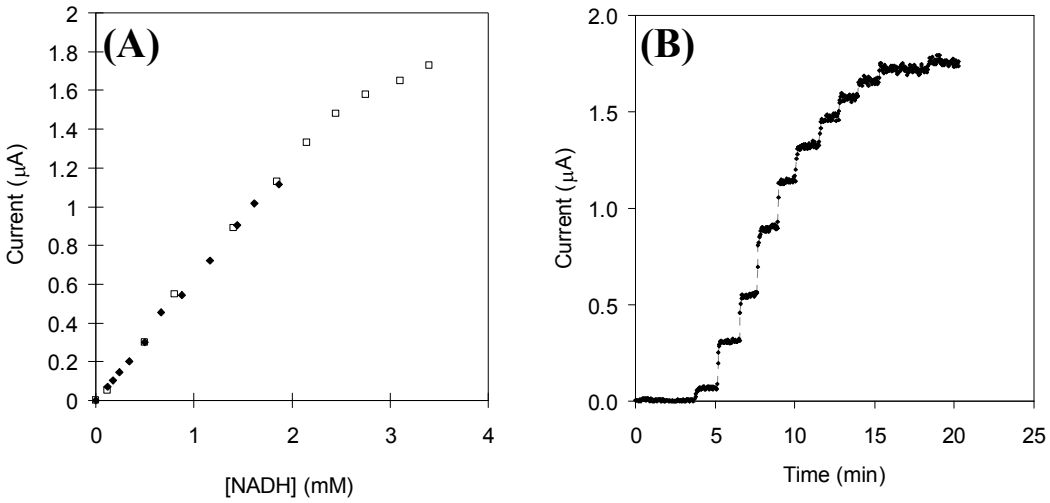

Figure 5.12. Current Responses in Detecting NADH. (A) Current of NADH oxidation to the change of NADH concentration on cyclic voltammogram and Amperometry. Filled diamond (♦): current reading from CV; Open square (□): current reading from I-t; (B) Typical current response to NADH concentration in amperometry without stirring. Aliquot of NADH solution was injected to the electrochemical cell, with [NADH] = 0.15 mM in the first injection, and an increase of 0.35 mM each time thereafter.

5.3.6 Single Fiber Microbiosensor

The highly sensitive and efficiency redox reaction of NADH can therefore be applied to many bioassays that involve the activity of NADH. We explore in this work the reaction of glycerol oxidation catalyzed by GDH. The glycerol oxidation reaction was carried out in a 4-ml 3-electrode electrochemical cell, with CNT-CFME electrode as the working electrode and Ag/AgCl and Pt wire electrodes as the reference and counter

electrodes. The reaction was conducted at initial concentrations of 50 mM of glycerol, 2 mM of NAD^+, and 26.7 U/ml of GDH.

The time course of NADH concentrations (Figure 5.13) in the reaction system was recorded from the increasing peak current at 0.55 V in cyclic voltammograms in a non-stirring system. The potential was selected to be 0.55 V based on the high oxidation current of NADH in the range of 0.55V to 0.78V from cyclic voltammogram.

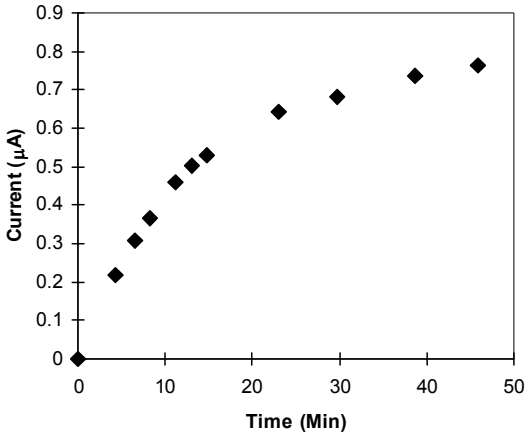

Figure 5.13 Signal response of NADH oxidation current in cyclic voltammetric measurement in a non-stirring system. Reaction conditions: [Glycerol] = 50 mM; [NAD^+] = 2 mM; [GDH] = 26.7 U/ml in 50 mM NH_4Cl-NH_4OH buffer (pH 9.0).

Figure 5.13 shows that the current increased with time linearly for the first 10 minutes, thus exhibiting the concentration of product-time relationship at the initial reaction of Michaelis-Menten kinetic model. When a longer reaction time was allowed, the oxidation current tends to reach a stationary stage. Therefore, data at the point of 20 min were used in the following studies, since the measurements were more stable.

To examine current efficiency of NADH oxidation on the CNT-CFE electrode, the stabilized current readings at 0.55 V on cyclic voltammogram was compared to the currents calculated from NADH oxidation. The NADH generation at various NAD^+ concentrations can be respectively measured by monitoring NADH absorbance at 340 nm using a UV-Vis spectrometer. From the absorbance of NADH at 340 nm, the concentration of NADH generated in the reaction can be calculated. The current of oxidation for such an amount of NADH can be determined from the NADH generation rate, with the assumption that one NADH provides one electron to the electrode at the oxidation potential. Comparisons of current readings on cyclic voltammograms and theoretical currents calculated are presented in Figure 5.14. The current efficiency could be calculated by dividing current measurements from cyclic voltammograms with the theoretical current at each NAD^+ concentration. The oxidation current at different initial NAD^+ concentrations reached different efficiency levels, ranging from 65% at 0.5 mM of NAD^+ to 93% at 1.0 mM of NAD^+, indicating that the NADH generated from glycerol oxidation reaction can be nearly completely oxidized on CNT-CFME electrode at an NAD^+ concentration larger than 1.0 mM. This indication signifies the promise for large scale bioelectrochemical applications by using our CNT-modified cellulose-based carbon fibers as the electrode.

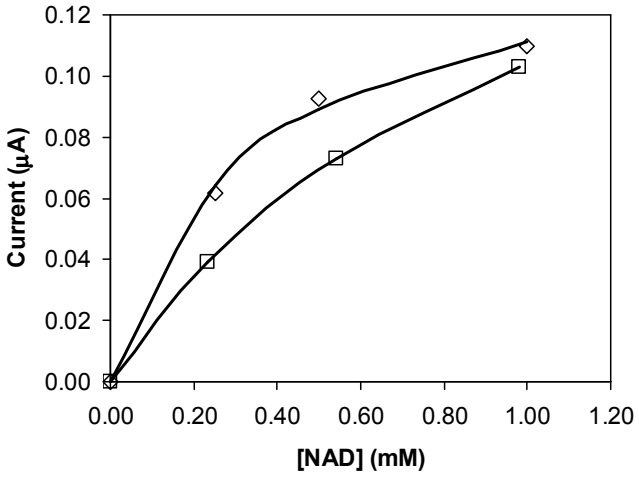

Figure 5.14 Comparison of kinetics of glycerol oxidation reactions in microelectrode system measurement and traditional UV-Vis readings. [Glycerol]=25 mM, [GDH]=0.24 U/ml, and [NAD^+] varies from 0 to 2 mM. Empty squares (□): stabilized I-t current reading; full circles (●): current calculated from NADH absorbance at 340nm in UV-Vis reading.

Other than regenerating NADH in large-scale bioelectrochemical applications, the single carbon fiber microelectrode presented in this chapter can also be used in biosensors involving enzyme reactions with NAD^+/NADH as a cofactor. Using glycerol oxidation reactions catalyzed by glycerol dehydrogenase as an example, all three components (glycerol, NAD^+, and glycerol dehydrogenase) can be measured electrochemically based on the principle of NADH oxidation on CNT modified carbon fiber microelectrodes. Based on equations 2 and 3, the measured current from the oxidation of NADH on the electrode would indicate the concentration of a component (glycerol, NAD^+, or glycerol dehydrogenase) if the other two components were provided in excess.

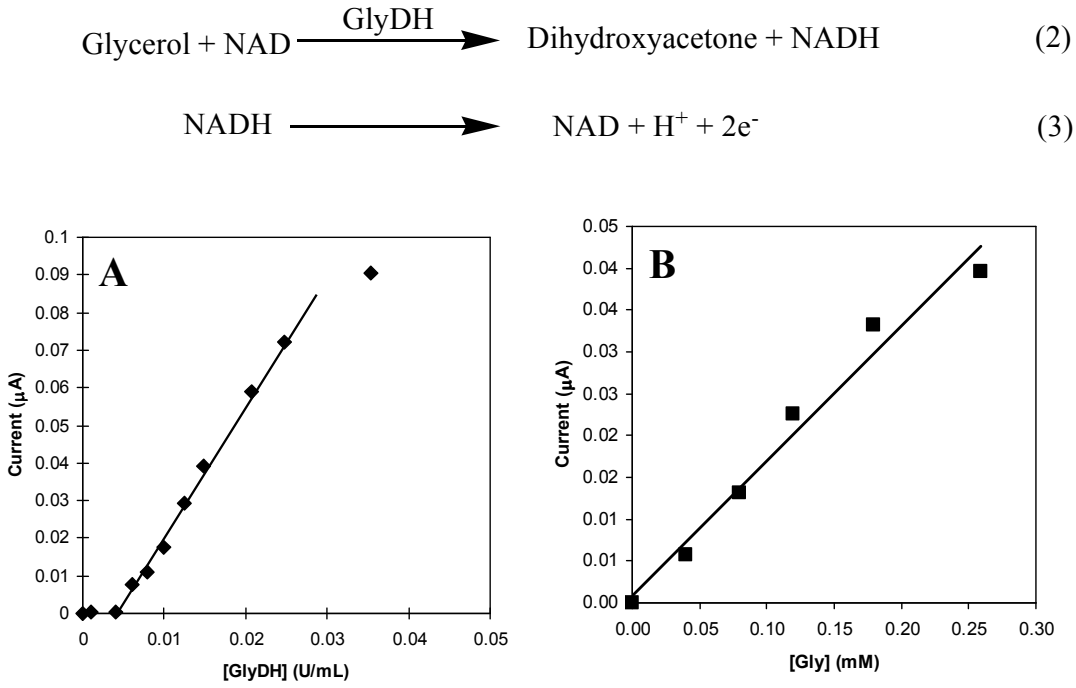

Figure 5.15 Linear detection ranges of glycerol dehydrogenase and glycerol with constant NAD^+ concentration (2 mM). (A) Current response by detecting NADH generation in glycerol oxidation reaction to the changes of glycerol concentration, [GDH] =0.4 U/ml; (B) Current response by detecting NADH generation in glycerol oxidation reaction to the changes of glycerol dehydrogenase concentration, [Glycerol] = 20 mM.

Calibration curves of glycerol and glycerol dehydrogenase at 0.6 V in amperommetry with a constant NAD^+ concentration (2 mM) are shown in Figure 5.15. For detecting glycerol, the linear detection range was from 0 to 0.25 mM (Figure 5.15A), and the detection limit was 0.04 mM (data not shown). The detection limit of glycerol on this CNT-CFME is the same as the detection limit reported on a NAD^+ modified carbon paste electrode[246]. For the measurements of glycerol dehydrogenase activity, the linear range of glycerol dehydrogenase measurement (Figure 5.15B) is from 0.004 to 0.05 U/ml, and the detection limit is 0.004 U/ml. These figures demonstrate the multiple

applications that this kind of CNT-carbon fiber electrodes can be used for. Moreover, for other dehydrogenase enzymes that work with NAD^+, a broad range of substrate can also be detected with methods similar to the approach in this paper. The benefits of lower cost of electrode materials, less amount of samples used and smaller system setup can also be realized.

5.4 Conclusions

A new method of fabricating carbon microfiber electrodes is reported in this chapter by growing carbon nanotubes with carbonization of a cellulosic material (cotton wool) in the presence of metal ions as the catalyst in a high temperature furnace. Process was optimized in the factors of cellulosic fiber sources, pretreatment catalyst, pretreatment solvent, and supplying time of carbon source. The process provides a fast approach in the manufacturing of carbon materials for electrochemical applications. The resulting carbon materials were fabricated into carbon microelectrodes and tested in the detection of NADH oxidation. The overpotential of NADH decreased from over 0.8 V to 0.6 V for CNT modified carbon fiber electrode, indicating that the presence of CNT could lower the overpotential of NADH oxidation on carbon electrode and thus reduce possibilities of electrode fouling. The single fiber microelectrode is promising for applications such as enzyme, glycerol, and NADH biosensors. Combining with a wide range of dehydrogenase that can be selected to work with NADH, the applications of such a microelectrode can be expanded to include biomedical devices, bioenergy processes, and production of many enzyme-catalyzed products. The carbonization

method of cellulosic fibers reported is also expected to be an appealing approach for the production of large geometry electrodes suitable for industrial scale electrochemical processes.

CHAPTER VI

ELECTROCHEMICAL REGENERATION OF COFACTOR ON CARBON ELECTRODE AND PRODUCTION OF DHA FROM GLYCEROL

6.1 Introduction

It has been reported in many literatures that oxidation of NADH on bare electrodes tends to involve high overpotentials, for example, direct electrochemical oxidation of NADH at pH 7.0 was observed at 1.1 V on carbon electrode[22] and 1.3 V on the platinum electrode[23]. In the case of NAD(H), such high potentials tend to denature cofactor and cause the fouling of electrode. Therefore, highly active mediators are favorite in reducing the overpotentials on electrodes[24]. A number of mediators were tested in NADH oxidation at lower potentials, but they are generally associated with high toxicity, poor stability and reusability due to the leaching problem. The use of mediator also complicates the purification and recovery of product, which makes the utilization of mediators a daunting task for large-scale bioprocessing applications. As another approach, and reported in many previous studies and the results presented in this study, NADH can be directly oxidized on electrode of gold, platinum and carbon, however, a large overpotential (>1 V) is usually required due to the sluggish charge transfer kinetics[55, 56]. With the surging development of new materials and nanotechnology, carbon nanotube (CNT) material was applied on the surface of electrode

to reduce the oxidation potential of NADH [204, 207, 238, 247-251]. Oxidation peaks of NADH were observed at 0.33 and 0.36 V on single- and multi-walled carbon nanotubes coated electrodes, respectively[248]. It was also reported that carefully arranged CNT on electrode were able to oxidize NADH at ~0 V[207]. However, the overpotential decrements varied greatly in different coating schemes of electrode or various approaches of CNT-assembly[249, 252-255]. Other than that, the electrochemical activities of CNT are very dependent on the approaches of synthesis and pretreatment because the different functional groups generated are responsible for catalytic performances in some cases. Higher density of such oxygen-related groups e.g. hydroxyl, carboxyl, and quinone[248, 256] on CNT might result in better electrochemical catalytic performance. One drawback is that CNT displayed remarkable nonselective catalytic properties towards the oxidation of biological substances that other than the targeted cofactor, such as ascorbate, acetaminophen, dopamine and urate, etc.[257]. That made it difficult to use CNT electrodes to oxidize NADH selectively in the presence of those impurities. The reaction system concerned in this study, however, lacks such common biological impurities and CNT electrode is therefore a handy choice.

The electrochemical method of NADH oxidation as described in Chapter V has been developed for biosensor applications in detecting glycerol, glycerol dehydrogenase (GDH), NADH, and other compounds and enzymes where reaction involves NAD(H) as a cofactor. The same method can also be applied for regeneration of NAD^+, facilitating the production of 1,3-dihydroxyacetone (DHA). It has also been demonstrated by others that electrochemical regeneration of NAD^+ could be realized more efficiently through the

use of redox additives as mediator to the reaction system. For example, Meldola's blue (8-dimethylamino-2,3-benzophenoxzine, abbreviated as MB), one of phenoxazine dyes containing naphthaline group, was used as an electron relay for NADH oxidation by adsorbing MB onto glassy carbon electrodes (GCE)[258], and methylene green (MG) immobilized on CNT electrode[259] was applied as a mediator for NADH oxidation to accelerate the electron transfer rate between NADH and the electrode.

Recombinant GDH produced in Chapter IV was also characterized for the catalysis of glycerol oxidation reaction in this chapter. The reaction mechanism and product inhibition kinetics were studied. Immobilized recombinant GDH was used in the catalysis reaction of glycerol oxidation to test stability and reusability of such enzyme in large scale applications. Electrochemical regeneration unit of NADH was able to couple with immobilized GDH reaction unit in the constructed production system. The operational parameters were studied as well.

6.2 Methods

6.2.1 Preparation of MB-CNT Electrode

Carbon nanotubes (length: 1~5μm, diameter: 30±15 nm) were purchased from Nanolabs, and sulfuric acid (95~98%), nitric acid, and Meldola's blue were purchased from Sigma-Aldrich. Typically, 100mg of Carbon nanotubes were first pretreated by a mixture of 7.5 ml of sulfuric acid and 2.5 ml of nitric acid in a 20ml vial. The vial was sealed and shaken at 200 rpm for overnight. After overnight shaking, the CNT suspension was diluted with 100 ml DI water and vacuum filtered using glass fiber filters

(S&S Biopath, Riviera Beach, FL), and dried at 80 ^{o}C in an oven for overnight. Before coating, the GCE was polished with 0.05 μm aluminum slurry followed by sonication in DI water and ethanol for 5 min each. The treated electrode was applied for continuous cyclic sweeping from -0.5V to +1.0V *vs.* Ag/AgCl reference electrode at a scan rate of 50 mV/s in phosphate buffer (pH 7.0) for 20 cycles to make sure that electrode was properly cleaned. CNT suspension in 0.5% of Nafion® solution (20 μL) was added on the surface of GCE, and dried at room temperature until uniform film of CNT was formed on glassy carbon electrode. The MB-CNT electrode was prepared by immersing the CNT-GCE electrode in 1 mM MB solution (pH 7.0 PBS) for 10 min, as described in reference[258]. The prepared electrode (denoted as MB-CNT-GCE henceforth) was washed with DI water and then dried at room temperature.

6.2.2 Preparation of MG-CNT Electrode

Glassy carbon electrode was pretreated as described in section 6.2.1, and methylene green was polymerized on CNT-GCE by electrochemical polymerization. The resultant electrode is hereafter named as MG-CNT-GCE. For DHA synthesis system, carbon cloth (2 cm×2 cm) was used. Poly(methylene green) modified electrode was prepared by cyclic sweeping at a CNT-carbon electrode from -0.5 to +1.2 V at 50 mV/s in phosphate buffer containing 1.5 mM methylene green. The sweeping lasted for 20 cycles. The modified electrodes were then rinsed with phosphate buffer and stored at 4 ^{o}C in the same solution for further use.

6.2.3 Electrochemical Property of Electrodes for NADH Oxidation

The cyclic voltammetry of modified CNT-GCE electrode was performed in a 3-electrode electrochemical cell with 10 ml of 0.1 M phosphate buffer solution (pH 7) by using Ag/AgCl electrode as reference, and Pt wire electrode as counter electrode. The amperometry of NADH oxidation reaction was examined at 0.1 V *vs.* Ag/AgCl in the buffer system as mentioned above under various NADH concentrations. The whole electrochemical system was purged with nitrogen for at least 20 minutes to remove oxygen from the solution. Another effort for electrochemical regeneration of cofactor is that the CNT-carbon fiber material prepared in Chapter V was used directly as electrode in DHA synthesis system.

6.2.4 Kinetics Study of Recombinant GDH

The kinetic parameters of glycerol oxidation reaction catalyzed by recombinant GDH were studied by varying the concentrations of glycerol and NAD^+. The reaction velocity was measured by recording the absorbance of NADH at 340 nm, and the initial velocity on glycerol oxidation was calculated with respect to the concentration of NAD^+ at fixed concentrations of glycerol.

6.2.5 DHA Synthesis with Immobilized GDH and in situ Cofactor Regeneration System

Enzyme and cofactor were immobilized on microparticles (Polybead Carboxylate Microspheres, 5.68×10^9 particles/ml, Polysciences Inc., Warrington, PA, USA), with the average diameter of 2 μm. The typical procedure of immobilization was conducted by

using PolyLink Protein Coupling Kit for carboxyl Microspheres (PL01N, Bangs Laboratory Inc., Fishers, IN, USA)[260]. In a typical preparation of immobilization, 0.5 ml of microparticles suspension was immobilized with 0.5 mg of enzyme (GDH or laccase). For immobilization of cofactor on microparticles, 1.5 mg of β-NAD^+ was used in the immobilization procedure versus 0.5 ml of microparticles suspension.

The glycerol oxidation reaction was conducted in a 50-ml ultrafiltration cell (Millipore, Billerica, MA, USA) equipped with ultrafiltration membrane (pore size 1.2 μm). Immobilized enzyme and cofactor on microparticles were stirred at 200 rpm and the reaction solution was circulated by a peristaltic pump (ColeParmer, Vernon Hills, IL) at the rate of 2 ml/min.

6.2.6 DHA Synthesis with Immobilized GDH and Stand-alone Cofactor Regeneration System

Recombinant GDH was immobilized on the ProBond® resin by attaching 6xHis tag with Ni^{2+} ion on the resin. A fixed bed chromatography column loaded with such resin was used in DHA synthesis system as a bioreactor. In a separated unit of mediator-free cofactor regeneration, direct oxidation of NADH was realized in a 3-electrode electrochemical cell with 3-D CNT-carbon fiber electrode (developed in Chapter V) as working electrode, Ag/AgCl electrode as reference electrode; and carbon paper electrode as counter electrode. The potential was applied with an electrochemical workstation (CHI 760C, CH Instruments, Inc. Austin, TX, USA).

6.2.7 Analysis of DHA

DHA generated from glycerol oxidation reaction was analyzed on HPLC after modified with pentafluorobenzyloxime[261] (PFBHA, O-(2,3,4,5,6-Pentafluorobenzyl)hydroxylamine hydrochloride, 76735 Fluka, St. Louis, MO). Typically, 150 μL of sample or DHA standard solution was mixed with 50 μL of saturated NaCl solution prepared in DI water. PFBHA solution (10 mg/ml) of 150 μL was added to the mixture, and shaken at 200 rpm for 10 minutes. The reaction solution was then mixed with 150 μL of saturated NaCl solution and 1 ml of acetonitrile for extraction. The solution was shaken at 1000 rpm for 15 minutes. Samples from acetonitrile phase was taken (150 μL) and analyzed in HPLC equipped with a C18 column and UV detector. The program was designed as 50% of acetonitrile in water for the first 9 minutes, followed by increasing acetonitrile percentage to 90% at 10 minutes, and the percentage was maintained until 13 minutes and returned to 50% at 14 minutes.

DHA concentration was also determined by florescence spectrometry as reported by Sawieki et al.[262]. Typically, 2 ml of reaction flow-through solution in a 20-ml vial on ice was mixed with 3 ml of 0.1% anthrone (A1631 Sigma, St. Louis, MO) in concentrated sulfuric acid. After cooling down the mixture to room temperature, 3 ml of glacial acetic acid was added to the vial. The excitation and emission of the sample were measured on a fluorescence spectrophotometer (Cary Eclipse Fluorescence spectrophotometer, Varian, Palo Alto, CA, USA).

6.3 Results and Discussion

6.3.1 Cofactor Regeneration of Modified CNT-GCE Electrode

The prepared MB-CNT-GCE electrode was first scanned in the reaction buffer system (0.1 M phosphate, pH 7) to determine the oxidation potential of NADH. The cyclic voltammetry was executed in a three-electrode electrochemical cell with MB-CNT-GCE electrode as working electrode, Ag/AgCl electrode as reference, and Pt wire electrode as counter electrode. The electrolyte used was 50 mM phosphate buffer (pH 7) with various concentrations of NADH. As NADH concentration increased in the electrochemical cell, the oxidation current increased as shown in Figure 6.1. From the cyclic voltammogram, NADH oxidation peaks can be identified at the potential of 0.1 V.

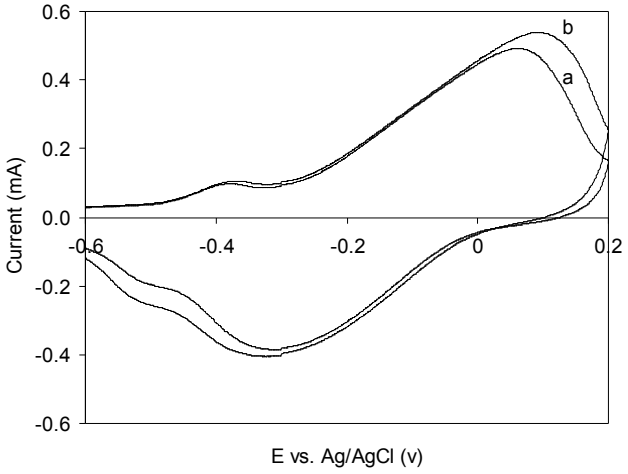

Figure 6.1 Cyclic voltammograms of Meldola's Blue modified CNT-GCE electrode in (a) 50 mM phosphate buffer (pH 7), (b) a + 25 μM NADH; Scan rate, 50 mV/s.

With the NADH oxidation potential of 0.1 V on MB-CNT-GCE electrode, the oxidation current was measured by amperometry (I-t) with the increase of NADH

concentration to test the response time of the electrode to the substrate. The I-t curve is shown in Figure 6.2. The results of both cyclic voltammetry and amperometry techniques indicated that the MB-CNT-GCE electrode can oxidize NADH successfully at the potential of 0.1 V. However, the adsorption of Meldola's blue on electrode can not prevent the mediator from leaching, which caused many other problems including difficulties in product purification and reusability of electrode.

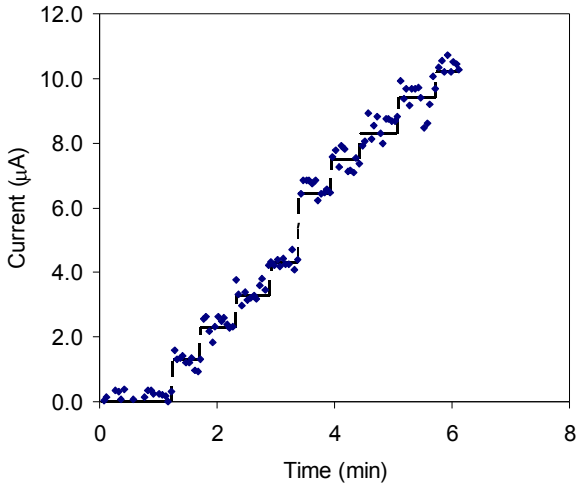

Figure 6.2 Amperometric response of the Meldola's Blue-CNT electrode for successive additions of 10 μM NADH (except 20 μM NADH at time of 3.5 min). Applied potential, l00 mV; Stirring rate, 200rpm.

Other than Meldola's blue, several other mediators have been reported in oxidizing NADH[246, 263-266], such as methylene green. Methylene green can be electrochemically polymerized on the surface of electrode, which is regarded as immobilized mediator with minimum leaching problem. In this study, poly(methylene green) was immobilized on CNT-GCE electrode for the study of electrode property, and also applied on carbon cloth electrode for the oxidation of cofactor (NADH) in reaction

system. The cyclic voltammogram with/without the presence of NADH using CNT-GCE electrode is shown in Figure 6.3. The oxidation current of NADH began to increase when the potential is higher than 0.1 V, which is similar to the oxidation potential of NADH on MB-CNT-GCE electrode. The MG-CNT-GCE electrode was tested for reusability study, and no significant leaching phenomenon was observed during oxidization reactions, which is desired in the following study.

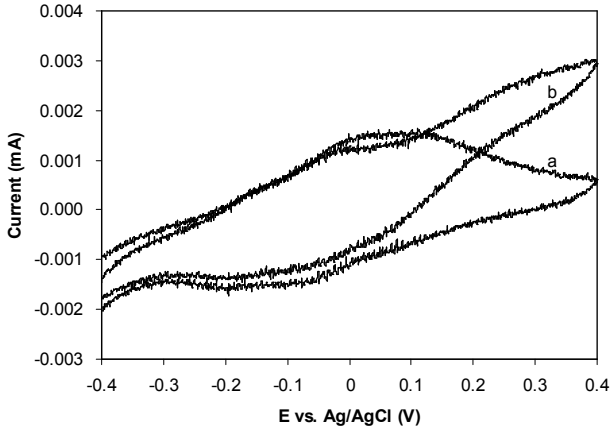

Figure 6.3 Cyclic voltammogram of poly(methylene green) modified CNT-GCE electrode in (a) 50 mM phosphate buffer (pH 7), (b) a + 2 mM NADH; Scan rate, 10 mV/s.

6.3.2 Buffer Selection for Glycerol Oxidation Reaction

The MB-CNT-GCE electrode demonstrated a good catalytic activity on the oxidation of NADH in neutral buffer system. However, basic buffer system was usually selected in reality because of the high reaction rate of glycerol oxidation reaction. The reaction rate (NADH generation rate) was used as an indicator for the selection of buffer system suitable for glycerol oxidation reaction. K^+ and NH_4^+ ions are known as activating compound to GDH from *E. coli*[122]. A series of buffer containing such ions

were used to measure the reaction rate of glycerol oxidation in the presence of NAD^+ as cofactor. Reaction was carried out in a 20ml-vial, with total reaction volume of 1.5 ml containing 0.1 M glycerol, 20 mM NAD^+ and 3μg/ml recombinant GDH in buffer solution. At each time point, 20 μL of reaction solution was pipetted out and diluted with 980 μL of desired buffer solution in a 1.5 mL disposable cuvette. Absorbance of NADH at 340 nm was recorded.

It has been seen in Figure 6.4 that the reaction rates are very high in buffer systems of NH_4OH-NH_4Cl buffer (pH 10), NH_4OH-NH_4Cl buffer (pH 10) with additive of KCl, and K_2HPO_4-KOH buffer (pH10) with additive of NH_4Cl, which is corresponding to the previous report that K^+ and NH_4^+ ions are activating compounds for GDH activity. Figure 6.4 also indicated that NH_4^+ has a better activation effect on glycerol dehydrogenase activity than K^+, since the reaction rate in K_2HPO_4-KOH buffer is very low, but increased dramatically after adding NH_4Cl. The above three buffers have also been used to test the stability of mediator (Meldola's blue). Meldola's blue has two peaks on its UV scan chromatogram at 320 nm and 570 nm, which is responsible for the electrochemical activity of NADH oxidation. The stability of Meldola's blue was monitored by the peak at 570 nm. The results showed that the mediator stability in K_2HPO_4-KOH buffer system was very poor, thus, it was eliminated from the candidate buffer systems of reaction. Therefore, NH_4OH-NH_4Cl buffer system was used in the following study.

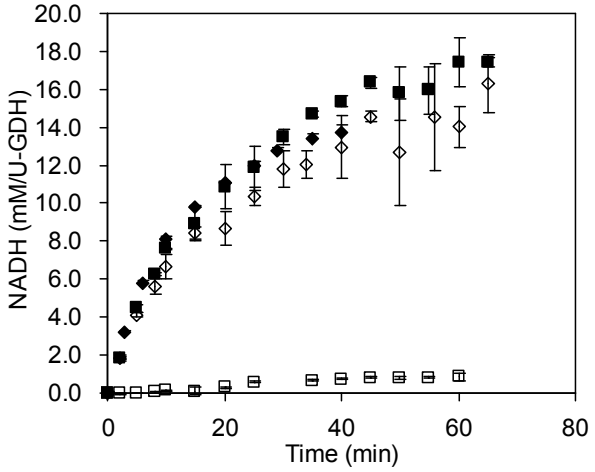

Figure 6.4 Reaction rate of glycerol oxidation in different buffer system. Buffers: 0.1 M NH_4Cl-NH_4OH (pH 10) (♦); 0.1 M K_2HPO_4-KOH (pH 10) with 0.1 M NH_4Cl (■); 0.1 M NH_4Cl-NH_4OH (pH 10) + 0.1 M KCl (◊); 0.1 M K_2HPO_4-KOH (pH 10) (□).

6.3.3 The Kinetics and Inhibition of Recombinant Glycerol Dehydrogenase

The kinetic parameters of GDH in glycerol oxidation reaction were studied by varying the glycerol and NAD^+ concentrations. Intersecting lines in the double reciprocal plots indicate a sequential mechanism for the enzyme reaction (Figure 6.5). As reported[124], glycerol oxidation reaction to DHA follows a ordered Bi-Bi mechanism, thus, the K_m and V_{max} values of recombinant GDH were calculated based on this mechanism. From the experimental data, the K_m was calculated to be 25.7 mM while V_{max} value was estimated to be 69.9 μM/min. The K_m value obtained from our recombinant GDH was slightly lower than the reported K_m value of GDH produced in wild strain of MC4100 (38 mM), while the V_{max} value is about 3-fold higher than that in MC4100 wild strain[215]. Comparing to other GDH from enzyme database[122], the K_m

value of the GDH is this study is in the lower end of the K_m values of GDH across different strains. The K_{cat} value calculated from V_{max} is 121.2 s^{-1}.

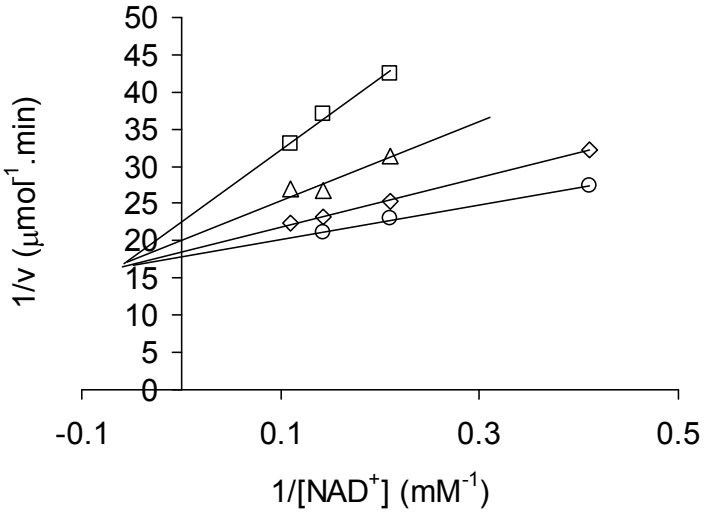

Figure 6.5 Lineweaver-Burk plots for glycerol oxidation reaction catalyzed by recombinant GDH. Glycerol concentrations: 25 mM (□); 50 mM (Δ); 75 mM (◊); and 100mM (○).

The inhibition kinetics was studied by varying NADH and DHA concentration presented in the reaction system. Product inhibition studies indicated that NADH is a competitive inhibitor with respect to NAD^+ at the saturated level of glycerol (Figure 6.6A) according to the Dixon plot, thus, the K_i value of NADH was calculated to be 0.028 mM. It was seen from Figure 6.6B that DHA is a noncompetitive inhibitor with respect to glycerol at the almost saturated concentration of NAD^+, thus, the K_i value of DHA is 0.064 mM.

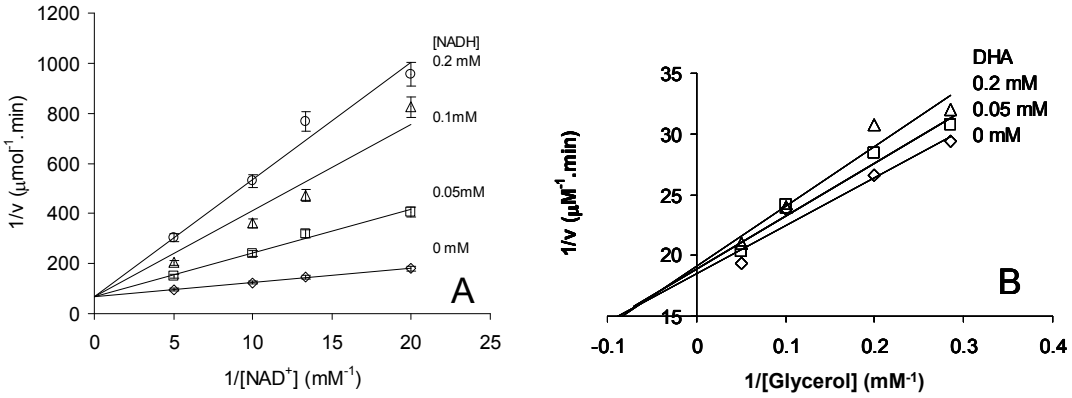

Figure 6.6 Product inhibitions by NADH and DHA for glycerol oxidation.

6.3.4 DHA Synthesis with Immobilized GDH and *in situ* Cofactor Regeneration System

To transform glycerol into high value-added DHA, an integrated *in situ* cofactor regeneration system was studied. GDH was immobilized on microparticles as described in section 6.2.5. The reaction setup with *in situ* cofactor regeneration is shown in Figure 6.7.

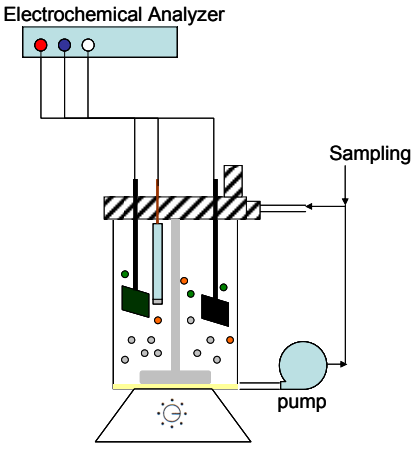

Figure 6.7 Experiment setup for DHA synthesis with *in situ* cofactor regeneration. The regeneration potential of NADH was controlled at 0.1 V *vs.* Ag/AgCl electrode. Enzymes and cofactor were immobilized on microparticles.

Briefly, glycerol oxidation reaction was catalyzed by immobilized GDH and produced NADH, which is oxidized on poly(methylene green) modified carbon electrode (2 cm×2 cm). The proton released from NADH oxidation reaction was converted to water by immobilized laccase on another electrode. The reaction system was constructed by an ultrafiltration cell equipped with a membrane with pore size of 1.2 μm to retain the microparticles inside of the reactor, and the microparticles with immobilized enzymes (GDH and laccase) was suspended by stirring at 200 rpm by magnetic stirring.

The DHA generated from the reaction was monitored by HPLC to calculate the total turnover number (TTN) of NAD^+. A typical chromatogram of HPLC operation is shown in Figure 6.8. With the reaction time of 2 h and 5 h, the TTN number of NAD^+ calculated based on initial NAD^+ concentration applied is 2,512 at 2 hours and 3,547 at 5 hours. The TTN number of cofactor regeneration in this reaction system reached scale up requirement for the DHA production.

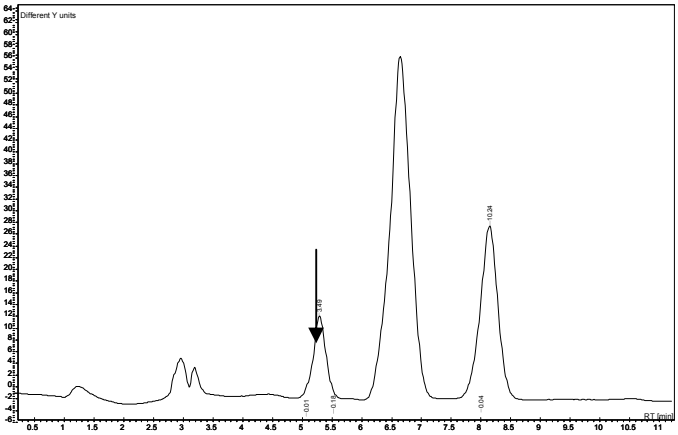

Figure 6.8 Typical HPLC chromatogram of DHA analysis in glycerol oxidation reaction. The arrow indicates DHA peak, retention time around 5 min. The peak around 6.5 min is the peak for excess PFBHA, and the peak at 8 min is internal standard (hydroxyacetone).

6.3.5 DHA Synthesis with Immobilized GDH and Stand-alone Cofactor Regeneration System

To eliminate the usage of mediator in DHA synthesis, a stand-alone electrochemical regeneration process of NADH without involvement of mediator was conducted for the production of DHA from glycerol. The reactor includes two units: reaction unit and regeneration unit, as shown in Figure 6.9. The reaction unit was constituted by a fixed bed reactor packed with ProBond® resin immobilized with recombinant GDH purified from *E. coli* culture. The 6xHis tagged enzyme has affinity bonding with Ni^{2+} ion on the resin, which prevents the leaking of enzyme from the reactor. Glycerol solution in desired buffer with NAD^{+} was fed to the reactor, and unreacted glycerol and generated NADH were collected from the flow-through of the column.

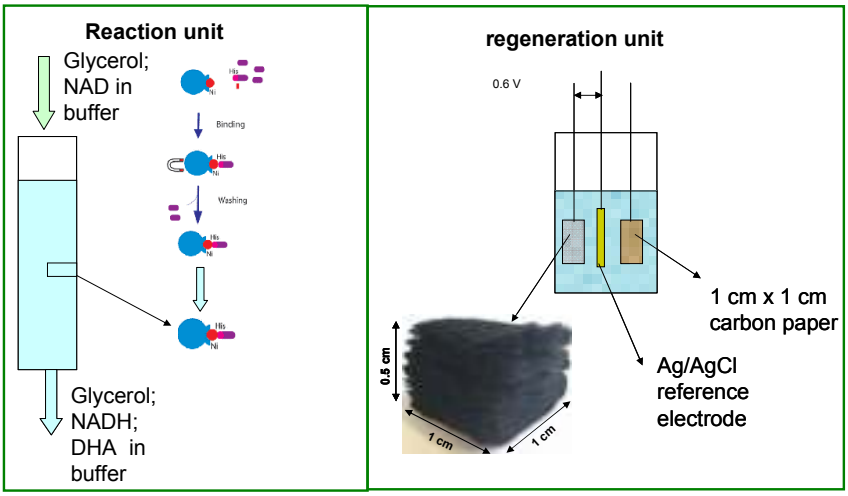

Figure 6.9 Schematic illustration of reaction process of DHA production.

The direct oxidation of NADH on a 3-D CNT-carbon fiber electrode was used in the mediator-free regeneration unit. The NADH in flow-through fraction from reaction unit was regenerated in a separated electrochemical cell equipped with three electrodes: Ni-CNT-carbon fiber electrode as working electrode; Ag/AgCl electrode as reference electrode; and carbon paper electrode as counter electrode. The applied regeneration potential is 0.6 V. The solution regenerated was fed back to the fixed bed reactor for the second cycle of reaction.

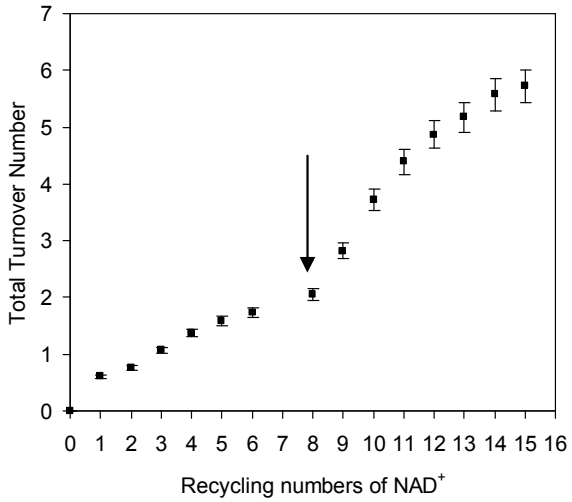

Figure 6.10 Total turnover numbers of NADH in DHA synthesis reaction system with stand-alone cofactor regeneration. The arrow indicates the adding of additional glycerol in reaction reagent.

A typical operation with reaction and regeneration cycles is shown in Figure 6.10, the amount of DHA accumulated with the increase of NAD^+ reuse cycles. The TTN of NAD^+ tends to reach platform (~2) at the cycle 8 due to the depletion of glycerol in reaction reagent. When fresh glycerol was added in reaction reagent, the yield and

concentration of DHA increased further. After 15 cycles of recycling in 5 hours, the TTN of NAD^+ reached more than 5.

6.4 Conclusions

The use of mediators immobilized on carbon electrode successfully reduced the overpotential of NADH oxidation from over 0.8 V on carbon electrode to 0.1 V. Especially the carbon electrode modified with poly(methylene green) tends to show improved stability and better reusability, which the electrode was continuously operated in DHA synthesis system for 5 hours. Cofactor regeneration was examined through two reaction routes, i.e., enzymatic reaction separated from electrochemical cofactor regeneration and integrated reaction-regeneration. For the integrated *in situ* cofactor regeneration system, the TTN number of NAD^+ was as high as ~3,500 in a 5-h operation. Results in the stand-alone regeneration system with mediator-free condition indicated that direct oxidation of NADH was realized on 3-D CNT-carbon fiber electrode with relatively low overpotential (0.6 V). With NAD^+ regeneration in a separate electrochemical unit, the TTN number of DHA produced from glycerol oxidation reaction reached over 5 after 15 cycles. Although the TTN number of NAD^+ in this stand-alone regeneration system is relatively low due to the limitation of apparatus, the advantages of this setup includes easy enzyme immobilization, direct oxidization and environment friendly.

CHAPTER VII

KINETIC LIMITATIONS OF A BIOELECTROCHEMICAL ELECTRODE USING CARBON NANOTUBE-ATTACHED GLUCOSE OXIDASE FOR BIOFUEL CELLS

7.1 Introduction

Nanotechnology has expanded rapidly over the past decades into a broad range of areas such as electronic, sensing, smart materials, and biomedical technologies. In the case of biocatalysis, nanoscale materials provide the upper limits in balancing the contradictory factors including surface area, mass-transfer resistance, and effective enzyme loading for maximum efficiency[267]. Nanomaterials of various configurations such as nanofibers, nanotubes, nanoparticles, and nanoporous materials have been examined as supports for enzymes[268-270]. Many of this type of ‘‘nanobiocatalysts’’ displayed enhanced performance in terms of catalytic efficiency and durability in comparison with their native parent enzymes. The emergence of nanobiocatalysts also brought about chances for high-performance bio-electrodes for biosensors and biofuel cells. For electrochemical applications, supports of biocatalysts have to possess a good electronic conductivity. For that, glucose oxidase (GOx) has been attached to gold nanoparticles[54, 55, 271]. However, the use of noble metal catalysts may not be suitable for large-scale devices. On the contrary, carbon nanotubes (CNT) are preferred as a supporting material in bioelectronic applications, as CNT could afford both a good

conductivity and a low price ($0.4–1.75/g) at the same time. Therefore, CNT-enzyme hybrid materials that integrate the structural and electronic features of CNT with the bioactivity of enzymes have manifested great potentials for bioelectrochemical applications[7-9]. Enzyme-polymer single-walled CNT composites have been prepared and examined for biocatalytic performance in a previous study[190]. Improved enzyme activity was observed in comparison with enzyme-containing composites without using single-walled CNT. CNT have also been intensively studied for biosensing, and many CNT-based biosensors showed better selectivity and/or improved sensitivity[272-276].

Driven by the increasing demand in clean and efficient power generation, fuel cells, as an alternative technology to thermo-mechanical power generation processes, can directly convert chemical energy of non-nuclear fuels into electricity with a theoretical efficiency approaching 100% and zero pollution emission. Biofuel cells with microbial or enzymatic biocatalysts can effectively catalyze redox reactions under ambient conditions and neutral pH values. In contrast to noble metals, biocatalysts are renewable and the cost of production can be very low, as microorganisms and enzymes such as detergent enzymes can be economically produced from large-scale fermentation processes once their market is developed. In addition, because of the unique catalytic activity of biocatalysts, biofuel cells can utilize biomass such as carbohydrates and organic pollutants in wastewater whereas metal catalysts need pure and simple structure fuels such as pure hydrogen and methanol[158-160]. Exciting advances in this area have been made since the first enzyme-based biofuel cell was reported in 1964[158, 175, 277, 278]. For example, GOx and microperoxidase-11 have been monolayer assembled on a gold

electrode (0.4-cm-diameter disk) and applied in a glucose/cumene peroxide biofuel cell. A power output corresponding to 4.1mW/cm^2 based on the projected electrode area was observed[279]. Much improved power density per volume (1.7mW/mm^3) was achieved with miniaturized glucose/O_2 biofuel cells[176]. In another study, a cell lifetime of up to 45 days was reported with enzymes entrapped in a modified Nafion membrane[182, 280]. More studies using CNT-based enzyme catalysis have been published with different approaches to improve the electron transfer or power output in biofuel cells[8, 29, 30]. Still, the performance of biofuel cells, in terms of power density, lifetime, and operational stability, falls far behind those of traditional fuel cells. It is widely accepted that the low power density of biofuel cells is a result of the slow reactions associated with the immobilized biocatalysts. However, hitherto there are no systematic studies on the role of reaction kinetics in determining the performance of biofuel cells. Since glucose oxidase-catalyzed reaction has been well studied in the applications of biosensors and biofuel cells[273, 274, 281], in this study, we present the kinetic analysis of CNT-attached glucose oxidase on electrode, and the correlation of that to the performance of biofuel cell. The results are expected to be of interests as well to other areas such as biosensors where enzyme-based electrodes are involved.

7.2 Materials and Methods

7.2.1 Materials

Glucose oxidase (Type X-S, from *Aspergillus niger*, 157,500 U/g), β-D(+)-glucose, Nafion1 perfluorinated ion-exchange resin (5 wt%), and 1,4-benzoquinone (98%)

were purchased from Sigma–Aldrich (St. Louis, MO). Hydroquinone (HQ) was purchased from EMD Chemicals (Gibbstwon, NJ). N-ethyl-N'-(3-dimethylaminopropyl)-carbodiimide (EDC), N-hydroxysuccinimide (NHS, 98+%), and carbon felt (3.18mm thick, 99.0%) were purchased from Alfa Aesar (Ward Hill, MA). Customized membrane cathodes were purchased from FuelCellStore.Com, Inc. (Boulder, CO). Multi-wall CNT (CNT, OD: 30±15 nm; length: 1~5 mm) was provided by NanoLabs, Inc. (Newton, MA). Glassy carbon electrode (GCE, D¼3mm), platinum wire electrode and Ag/AgCl reference electrode were purchased from CH instruments, Inc. (Austin, TX). Graphite rod (1/16″×6″) was ordered from Poco Graphite, Inc. (Decatur, TX). MES buffer salt was obtained from Pierce (Rockford, IL) and prepared as manual suggested. Unless specially mentioned otherwise, all other reagents were of ACS grade or higher.

7.2.2 Covalent Attachment of Enzyme on Carbon Nanotubes

CNT were treated with strong acids prior to the immobilization of enzyme. Typically, 20 mg of CNT was added into an acid solution consisting of H_2SO_4 (98%, 150mL) and HNO_3 (70%, 50 mL), followed by overnight shaking (200 rpm) at room temperature. The resulting CNT were washed with deionized water and dried at 80 ^oC in a vacuum oven. For the surface functionalization, the acid treated CNT (2 mg/mL) were re-suspended and stirred for 1 h in 250mM MES buffer containing 87mM of NHS and 5.3mM of EDC. After stirring, the suspension was washed with 100mM MES buffer (pH 6.5). The covalent attachment of GOx to the CNT surface was achieved by mixing the functionalized CNT (1 mg/mL) and GOx (10 mg/mL) by the volume ratio of

2:1. The mixture was allowed to react for 1 h under shaking at room temperature. The final preparations were washed with 100mM sodium phosphate buffer (pH 7.0) until no GOx were detected in the washing solution. The GOx loading on CNT was determined by using reverse biuret protein assay, and the procedure is described as following: the analytical reagent A was prepared by dissolving 15 mg $CuSO_4 \cdot 5H_2O$, 45 mg of potassium sodium tartrate, and 2.4 g of NaOH into 100 mL DI water, while reagent B was prepared by dissolving 25 mg ascorbic acid and 37 mg of bathocuproinedisulfonic acid disodium salt in 100 mL DI water. Typically, 0.05 mL of CNT–GOx suspension was added to 0.2 mL of reagent A, and incubated at 37 ^{o}C for 5 min. Then 1.0mL of reagent B was added and incubated for an additional 0.5 min. The solution was filtrated through 0.2 mm syringe filter and the absorbance at 485nm was measured on UV–Vis spectrophotometer (UV-1601, Shimadzu, Kyoto, Japan). The protein content was calculated using BSA determined through the same procedure except CNT–GOx sample was replaced with the same volume of BSA solution.

7.2.3 Bioanode Preparation

To prepare the enzyme electrodes, a final concentration of 3 mg-CNT/mL of CNT–GOx was dispersed in 0.5 wt% Nafion® solution in phosphate buffer (100 mM, pH 7.0). Nafion solution was prepared by mixing 5 wt% of Nafion® perfluorinated ion-exchange resin with of phosphate buffer (100 mM, pH 7.0) in the volume ratio of 1:9. Aliquot (20 mL) of suspension was dropped on the polished surface of electrode while using GCE. When carbon felt was used as electrode supporting material, the electrode

(0.33 cm^2) was immersed directly into the solution of CNT–GOx. The electrodes coated with CNT–GOx were allowed to dry under ambient condition for 2 h, followed by washing with fresh phosphate buffer. The electrode was stored at 4 ^oC prior to any using.

7.2.4 Kinetic Study of Biocatalysis with Native, CNT–GOx, and Bioanode

The kinetic studies of native GOx and CNT–GOx were performed by using benzoquinone (BQ) as the electron acceptor and monitoring the absorbance of HQ at 290nm without applying potential and current on the working electrode. The working solution consisted of varying concentration of glucose and BQ in 100mM phosphate buffer (pH 7.0). In each measurement, working solution and a small aliquot of GOx or CNT–GOx were mixed in a 3-mL cuvette. The absorbance of HQ at 290 nm was recorded in UV–Vis spectrophotometer. For electrode coated with CNT–GOx, the working solution consisted of 100mM of glucose and 10mM of BQ. The electrode was incubated in the working solution, and reaction time course was obtained by sampling periodically 1mL of working solution. Kinetic measurements at each glucose/BQ concentration have been repeated three times, and the model calculation was based on the average of three measured values.

7.2.5 Amperometric Study of Bioanode

Amperometry analysis was performed with an Electrochemistry Workstation 760B (CH instruments, Inc.). A three-electrode testing cell was used with glassy carbon bioanode as the working electrodes, Ag/AgCl electrode and a Pt wire as the reference and

counter electrode separately. Before each test, the electrolyte (100mM phosphate buffer contained 10mM of BQ) was purged with nitrogen for 20 min with stirring to remove oxygen from solution, and all electrodes were allowed to equilibrate. The working electrode was hold at 0.6 V versus reference electrode. Small aliquots of glucose stock solution were added, and the current response to the glucose concentration was recorded.

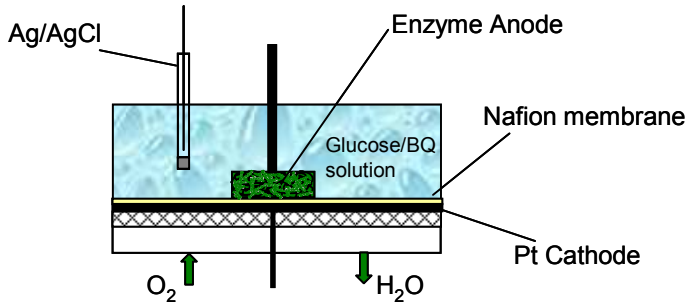

Figure 7.1 Scheme of glucose biofuel cell system.

7.2.6 Glucose Biofuel Cell with Bioanode

The carbon electrode coated with CNT–GOx composites was applied as an anode in a model glucose/O_2 biofuel cell as shown in Figure 7.1. The bioanode was pressed against the customized proton diffusion membrane-cathode with a graphite rod. Typically, the anodic electrolyte containing 100 mM glucose and BQ (10mM) as the redox mediator was used as fuel. Oxygen was supplied to the cathodic chamber at a flow rate of 100 mL/min as oxidant. The capacity of anodic chamber was 7mL. Voltage, current and the anodic and cathodic potentials were monitored using Keithley 2700 digital multimeter (Keithley Instruments, Inc., Cleveland, OH). The current and power densities were calculated based on the projected surface area of bioanode.

7.3 Results and Discussions

7.3.1 The Attachment of GOx to CNT

GOx was attached onto multi-wall CNT, which were preactivated with strong acids as reported previously[282]. We evaluated the efficiency of acid activation of CNT via conductance titration[283], which showed the content of carboxylic group (–COOH) reached 0.19±0.02mmol/g-CNT, indicating ~2% activation of all the carbon content of CNT. The enzyme loading was determined to be 40 ± 2 mg-GOx/g-CNT through reverse biuret method[275]. According to the estimation of specific surface area of CNT ($125m^2/g$) following the method reported by others[276], it implies that ~15% of the external surface area of CNT was covered by GOx. A bioanode was constructed by coating the CNT–GOx composite to carbon felt along with Nafion® (0.5 wt%) through a doping–drying process. A good distribution of CNT–GOx on the surface of fibers of carbon felt was achieved (Figure 7.2). Assuming CNT contact directly with the carbon felt which serves as the electrode; such an electrode configuration promises immediate access of conductive surface in the vicinity of the enzyme molecules, thus, shortening the distance for the mediator, the electron carrier, to shuttle between them.

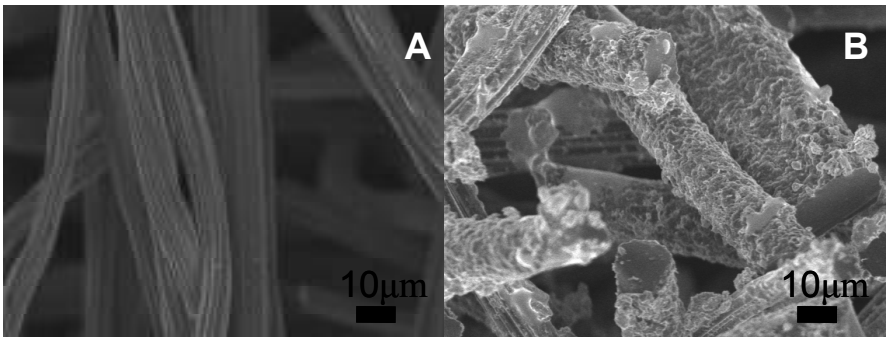

Figure 7.2 Microscopic images of carbon felt electrodes. (A) SEM image of blank carbon felt; (B) SEM image of carbon felt coated with CNT-attached GOx.

7.3.2 Model Development

It is generally believed that the mediated glucose oxidation reaction takes place through several transformation steps. Using BQ as mediator, the reactions can be expressed as:

$$\text{GOx(FAD)} + \text{Gluc.} \underset{k_{-1}}{\overset{k_1}{\rightleftharpoons}} \text{GOx(FAD)-Gluc.} \quad (1)$$

$$\text{GOx(FAD)-Gluc.} \xrightarrow{k_2} \text{GOx(FADH}_2\text{)} + \text{Gluconolactone} \quad (2)$$

$$\text{GOx(FADH}_2\text{)} + \text{BQ} \underset{k_{-3}}{\overset{k_3}{\rightleftharpoons}} \text{GOx(FADH}_2\text{)-BQ} \quad (3)$$

$$\text{GOx(FADH}_2\text{)-BQ} \xrightarrow{k_4} \text{GOx(FAD)} + \text{HQ} \quad (4)$$

BQ has been a widely applied mediator for enzymatic redox reactions[284]. BQ has a redox potential of 0.1 V versus SHE electrode[285], which is similar to that of methylene green; its reaction rate constant, however, can be over 100-fold higher than the latter[286]. The reaction kinetics for the BQ mediated oxidation of glucose has been generally regarded as a Ping-Pong Bi Bi model[287] . With the replacement of glucose oxidase with the other enzyme catalyzed oxidation reactions and BQ with the other mediators, the proposed model in this study can be applied to the other biofuel cell systems with the same principal shown here. To analyze the enzymatic reaction (glucose oxidation reaction) and electron transfer rates, kinetic studies were carried out with BQ as an electron acceptor. The process was monitored by measuring the absorbance of HQ at 290nm. The working solution consisted of varying concentrations of glucose and BQ dissolved in phosphate buffer (pH 7.0, 100 mM). The kinetic study of carbon felt

electrode coated with CNT–GOx was performed with 100 mM of glucose and 10mM of BQ. The electrode was immersed in the working solution, time course of the reaction was obtained by sampling 1 mL of the reaction solution periodically. At each given concentration of BQ, the dependence of reaction velocity (v) on the concentration of the glucose ([S]) can be described in the following equation (Eq. 5):

$$\frac{v}{V'_{\max}} = \frac{[S]}{K'_m + [S]} \tag{5}$$

where, v is the reaction velocity (mM/s); V'_{max} and K'_m is apparent Michaelis–Menten parameters, unit as mM/s and mM; [S] is glucose concentration (mM).

Similarly, the dependence of v on the concentration of BQ at a given glucose concentration can also be expressed in the same way. When concentrations of both substrates, benzoquinone ([BQ]) and glucose ([G]), are considered as variables, reaction rate will be[288]:

$$\frac{v}{V_{\max}} = \frac{[G][BQ]}{\alpha K_m^G [BQ] + K_m^{BQ}[G] + [G][BQ]} \tag{6}$$

V_{max}: the limiting rate of the enzymatic reaction (mM/s);

[BQ], [G]: the concentration of benzoquinone and glucose;

$\alpha K_m^G = (k_{-1}+k_2)/k_1$: the limiting Michaelis constant for glucose when BQ is saturating, and

$\alpha = k_4/k_2$; $K_m^{BQ} = (k_{-3} + k_4)/k_3$: the limiting Michaelis constant for BQ when glucose is saturating.

7.3.3 The Reaction Kinetics of CNT–GOx

The above model was first applied to evaluate the impact of immobilization on the activity of GOx. The intrinsic kinetic parameters of GOx and the corresponding apparent parameters of CNT–GOx and the CNT–GOx on carbon felt electrode were obtained by best fitting the model to time courses of reactions. Experimental data were obtained for different formats of GOx by varying the concentration of the substrates (with [*G*] controlled as 10, 25, 45, 90, and 150 mM; [*BQ*] as 0.1, 0.5, 1.0, 2.0, and 5.0 mM). Example fittings (same fitting effect was observed for all other sets of experimental data) with determined kinetic parameters are shown in Figure 7.3A and B.

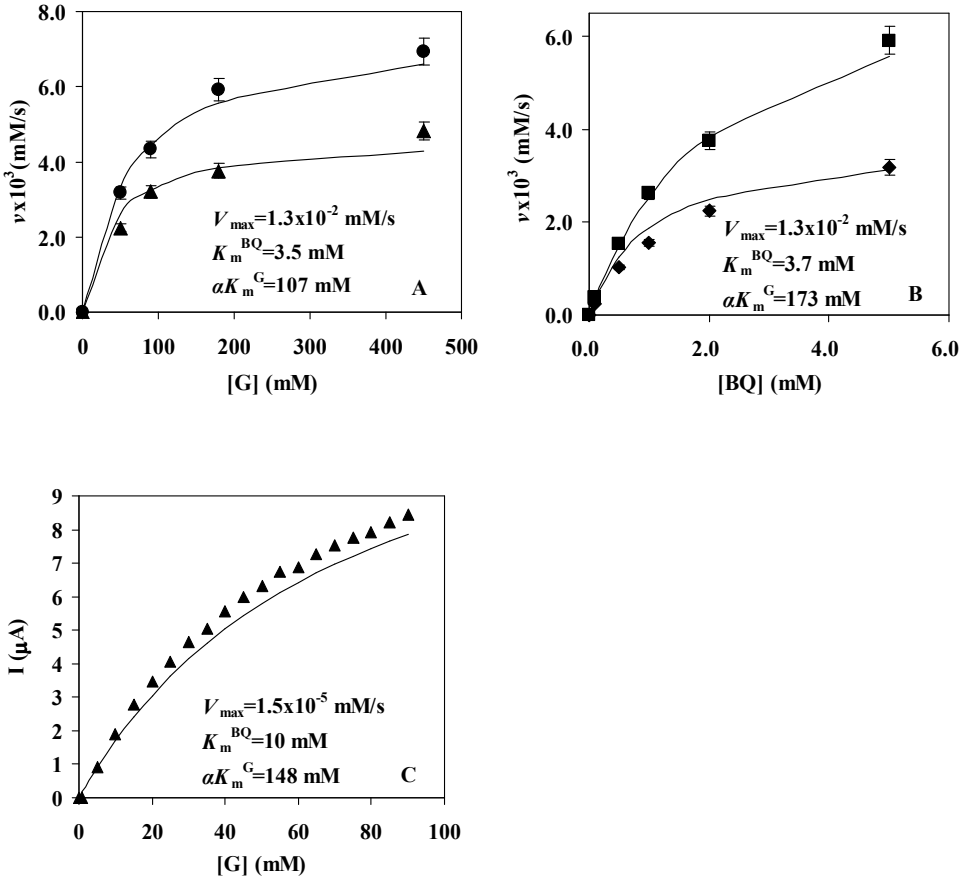

Figure 7.3 Model predictions of reaction rate and current density. The reactions were controlled to the same amount of enzyme, 1 μg. (A) Best fitting with reaction rate (v) as a function of glucose and BQ for native GOx: BQ concentrations were kept at 2.0 mM (▲) and 5 mM (●); (B) Best fitting with reaction rate (v) as a function of glucose and BQ for CNT-attached GOx: glucose concentrations were kept at 25 mM (♦) and 90 mM (■); (C) Comparison of the predicted current generation with amperometric measurement of CNT-GOx electrode: amperometric readings at 0.6 V (▲) with [BQ] = 10 mM. Solid lines (—): model prediction. Electrode has a projected surface area of 0.33 cm^2.

7.3.4 The Efficiency of CNT-Based Biofuel Cells

A biofuel cell was constructed by coupling the bioanode with a Pt cathode. The Pt cathode was chosen with intent to minimize the limitation of cathode reaction. The

potential-current (*V–I*) and power density-current (*P–I*) curves of such a biofuel cell are shown in Figure 7.4. The biofuel cell result in Figure 7.4 represents a typical measurement with bioanode, even though here experimental result of a single run is reported. The open-circuit potential of the biofuel cell was measured as 0.57 V, and a maximum power density of 77 mW/cm^2 was reached at 0.51 V. The observed power density is about eight times higher than that of a similar glucose/O_2 biofuel cell but with laccase as the cathode catalyst[289] . We may assume that such a difference between the two types of biofuel cells essentially reflected the limitation of the laccase-based cathode. The potential of the biofuel cell maintained unchanged when the current was low; but started dropping sharply when the current density reached 150 μA/cm^2 and eventually reached short-circuit current at ~206 μA/cm^2, a point at which the power generation of the system was limited by concentration polarization of the mediator on the surface of the bioanode. When performing repeating experiments of biofuel cells with bioanode from same preparation, the current and power densities results were very consistent.

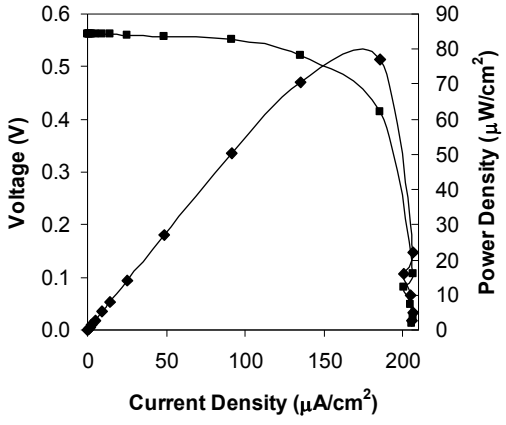

Figure 7.4 Characteristic curves of glucose/O_2 biofuel cell with CNT-GOx bioanode. Electrode has a projected surface area of 0.33 cm^2. (■) *V-I*; (♦) *P-I*.

It appeared, however, that the maximum power density observed for the biofuel cell was much lower than what implied by the catalytic capability of GOx on the electrode. According to the model prediction, the GOx applied to the electrode should be able to catalyze the reaction at the rate of 1.3×10^{-4} mmol/h·μg-GOx. Albeit being much slower than that of free GOx, that reaction rate, which has included the effects of reduced enzyme accessibility and additional mass transfer resistance (both glucose and the mediator BQ), points to a current density of 22 μA/cm^2·μg-GOx or 528 μA/cm^2. When accounted for power density at 0.51 V, the CNT–GOx anode should be able to produce ~270 mW/cm^2. The projected current density is about 2.6 times the value of the short-circuit current density, indicating that the fuel cell reaction only reached 39% of the catalytic power of the CNT–GOx-based electrode. Accordingly, major loss of power generation should attribute to factors such as internal electron and proton transfer resistances inherent in the fuel cell system.

One may argue that whether enzyme immobilization is necessary as in most cases there is no direct electron transfer between the enzyme active site and electrode. To address this question, we tested power generation using free GOx at the anode compartment. Despite the fact that free GOx can afford much faster reactions, the maximum current density obtained was 2.3 μA/cm^2·μg-GOx, 10 times lower than that observed with CNT–GOx electrode, representing only 0.007% of the catalytic capability of free GOx. Apparently, immobilization of enzyme on the electrode helped to improve the performance of the fuel cell. Even though the apparent reaction rate of the electrode-immobilized enzyme was low because of the limited enzyme accessibility and additional

substrate diffusion resistance, the shortened distance for the mediator to shuttle between the enzyme active sites and the surface of the electrode overweighed the accessibility and diffusion limitations. Enzyme immobilization is desired for better performance.

7.4 Conclusions

In summary, the kinetic model with parameters determined in this study successfully predicted the current generation from an enzyme-based bioanode when it was examined as a single electrode. We also observed that the biofuel cell employing the CNT–GOx anode was only able to generate a power density equivalent to <40% of reaction capability of the enzyme immobilized on the electrode. It appeared to us that factors such as electron and proton transfer resistances rather than catalytic reaction rate are overwhelming in limiting the power generation of the biofuel cell.

CHAPTER VIII

APPLICATION OF TIN-MODIFIED CARBON FIBER ELECTRODE FOR ELECTROCHEMICAL REDUCTION OF CARBON DIOXIDE

8.1 Introduction

Carbon dioxide (CO_2) is one of main green house gases concerned for global warming. With the rising public awareness about this issue, the lowering the CO_2 content in the atmosphere has been identified as one of the key challenges faced in today's world[42, 43]. In developing new technologies toward carbon sequestration, people favor concepts that promise production of valuable chemical or fuel products from CO_2, beyond the simple CO_2-fixation are favored that yield a valuable product in form of chemicals or fuels. The reduction of CO_2 has been realized through several approaches including chemical[44], photochemical[45], enzymatic[46] and electrochemical[47] methods. For example, reduction of CO_2 to syngas, which can be subsequently used for synthesis of fuels, was realized by using chemical catalysts under high temperature and pressure [44]. Photochemical and enzymatic methods have been proven to reduce CO_2 at ambient conditions, though the concentration of the product is generally too low to be applied for large scale applications. Among the above mentioned techniques, the electrochemical reduction of CO_2 appears to be more promising because as electricity is a relatively cheap and can be generated from renewable resources, such as wind and solar energy. As widely reported, formate[61], methanol[290], methane[291] and other long

chain hydrocarbon[292] can be produced by electrochemical reduction of CO_2. The final products of electrochemical reduction of CO_2 are usually a mixture of carbon monoxide, formate, methanol and hydrogen due to similar standard electrode potentials (E^0). Furthermore, reaction parameters such as temperature, pressure, electrolyte and electrode properties are also critical[293] for the composition of the final reduction products. Thus, as shown in previous studies [47, 60, 61], certain products can be promoted at specific electrodes and conditions in electrochemical reduction of CO_2. For example, formate was favorably produced on sp-group metal electrodes[47], whereas hydrocarbons were selectively generated on a Cu electrode[60]. Hence, the electrochemical properties of the electrode will determine the product species obtained from electrochemical reduction of CO_2.

Formate is not only the direct reduction product of CO_2, in fact it is a useful chemical to be converted into fuel or used in fuel cells. The standard electrode potential of CO_2 conversion to formate is -0.2 V *vs.* NHE (normal hydrogen electrode)[61]. Production of formate by CO_2 reduction can be achieved with simple equipment and at high efficiency and have been the matter of ongoing research. For example, Chaplin[60] reviewed the effects of reaction conditions and electrode material on electrochemical reduction of CO_2 pathways, especially the formation of formate. Other studies showed that formate can be produced on Hg, In, Pb, Cd and Sn electrode with high selectivity[47]. Hori[62] revealed that formate was the predominant product of CO_2 reduction on Sn-electrode. The utilization of Sn electrode offered high current and good selectivity, which are the critical prerequisites for large scale operations. The production of formate

by CO_2 reduction using Sn based electrodes has been investigated by several other researchers. Mahmood[294] used a gas diffusion electrode based on Sn for the reduction of CO_2 to formate and reached a yield of about 50% in current efficiency (CE). Li and Oloman[61] also reported the development of mesh tinned-copper[295, 296] and pure Sn granules electrodes[296] for the continuous production of formate by electrochemical reduction of CO_2. However, metal based electrodes have some drawbacks since they are expensive and easily susceptible to fouling. Therefore, metal catalysts incorporated into carbon based electrode materials were favorite in CO_2 reduction reaction to formate because of low price of carbon material and its sustainability. A carbon fiber based electrode[297] was used as cathode in reducing CO_2 at ambient condition.

Carbon dioxide is a highly stable molecule and difficult to be reduced because of the double bonds between carbon and oxygen molecules. Excess energy input, effective reaction conditions, active catalysts are required for the electrochemical reduction of CO_2. The electrochemical reduction of CO_2 occurs on the cathode and is enabled by the supplied electrical energy. Reaction equations (1-5) represent the possible reduction route of CO_2 conversion into formate [291].

$$CO_2 \longrightarrow CO_{2\,ads} \quad (1)$$

$$CO_{2\,ads} + e^- \longrightarrow CO_{2\,ads}^{\bullet -} \quad (2)$$

$$CO_{2\,ads}^{\bullet -} + H_2O + e^- \longrightarrow COOH_{ads} + OH^- \quad (3)$$

$$COOH_{ads} + e^- \longrightarrow COOH^-_{\,ads} \quad (4)$$

$$COOH^-_{\,ads} \longrightarrow COOH^-_{\,aq} \quad (5)$$

Where, $CO_{2\,ads}$ represents adsorbed CO_2 molecules on cathode electrode; $CO_2^{\cdot -}{}_{ads}$ is $CO_{2\,ads}$ radical; $COOH_{ads}$ is adsorbed formate produced from the reaction; $COOH^-_{ads}$ is formate radical; and $COOH^-_{aq}$ is the formate radical in solution.

The mechanism of formate production can be summarized as below. Firstly, hydrated CO_2 is adsorbed on the electrode, accepts one electron to form CO_2^- radial, which reacted with water or H molecule adsorbed on catalytic activity site forming adsorbed HCO_2^- radical and OH^- ion. The HCO_2^- radial is adsorbed on electrode and accepted one electron to be reduced to formate ion; finally, formate ion broke away from electrode surface to solution. According to the mechanism of electrochemical reduction of CO_2, the adsorption of CO_2 anion radical on the surface of electrode and the quantity of active site available for catalytic reaction determine the productivity of reduction reaction. The selection of appropriate electrode materials and the fabrication of electrode are crucial for effective CO_2 reduction. Comparing to conventional materials, nanostructure materials, such as carbon nanotubes (CNT) have been proven to possess more active sites and higher specific surface area to realize CO_2 reduction[63]. Combining the porous structure and unique catalytic ability of CNT, fabricated carbon

electrode deployed with CNT with metal catalyst could result in higher reaction activity for electrochemical production of formate from CO_2.

In this study, as described in Chapter V, a 3-D carbon based material which composed by carbonized cellulosic fiber (CF) with CNT was developed. Cellulosic fibers were first deposited with Fe or Ni catalyst, and carbonized in a high temperature tubular furnace followed by the growth of CNT. The resultant material was denoted as carbon nanotubes-carbon fiber (CNT-CF). Sn plating on CNT-CF material was designed to further improve the electrode selectivity of formate. This Sn-CNT-CF electrode was developed and tested in the realization of CO_2 reduction to formate.

8.2 Methods

The carbonization of cellulosic fiber materials and the growth of CNT were performed as described in Chapter V.

The 3-D carbonized electrode material was immersed in DI water for three times to remove adsorbed amorphous carbon, and the resultant material was dried at room temperature. After drying, the CNT-CF material surface was first sensitized in a solution of 0.1 M HCl with 20 g/L $SnCl_2$ (dehydrate, 98+%, Acros Organics) for 30 min and then activated in 0.25 M HCl with 0.8 g/L $PdCl_2$ for 3 hours. After rinsing with DI water, a Sn film was formed on the surface of CNT-CF by electroless Sn plating at room temperature within 5 hours, and the composition of electroless plating solution is showed in Table 8.1. Finally, CNT-CF material with Sn film was rinsed with DI water, and dried

at room temperature. The resultant material was fabricated into an electrode and used for electrochemical reduction of CO_2.

Table 8.1 Composition of electroless plating solution

Ingredient	Concentration
$SnCl_2 \cdot 2H_2O$	30 g/L
HCl	50 ml/L
$CO(NH_2)_2$	80 g/L
$Na_3C_6H_5O_7 \cdot 2H_2O$	60 g/L
$NaH_2PO_2 \cdot H_2O$	80 g/L

Firstly, the dried Sn-CNT-CF material was cut into cubes with an edge length of 1 cm and connected to a carbon rod by carbon paint (SPI supplies, West Chester, PA, USA). Then, the electrode was wrapped with one piece of thin plastic film. The film was punctured to allow the diffusion of substrate, as shown in Figure 8.1. The electrochemical characterization of the electrode was performed on an electrochemical workstation (CHI 760C, CH Instruments, Inc. Austin, TX, USA) with a three electrodes system. Carbon dioxide was supplied by bubbling through a water container continuously into the sealed electrochemical cell, and the tail gas was collected into a 0.5 mL sealed H_2O bottle on ice. Ag/AgCl electrode and Pt wire electrode were used as reference and counter electrode respectively. The electrolysis were conducted under controlled potentials at room temperature (25 ^oC) with CO_2 bubbled into 4 mL electrolyte solution. The electrolyte solution containing the formed formate was analyzed by gas chromatography (GC430, Varian, Palo Alto, CA, USA) [298].

Figure 8.1 Image of Sn-CNT-CF electrode.

8.3 Results and Discussion

8.3.1 Electrode Material for the Electrochemical Reduction of CO_2 to Formate

Carbon materials were modified with Sn plating to assist the formate production, as discussed previously. The SEM-images of CF, CF with Sn plating, CNT-CF, and CNT-CF with Sn plating materials are presented in Figure 8.2. In Figure 8.2B, the surface of carbon fiber was covered by a uniform layer of tin coating, comparing to the bare surface of carbon fiber presented in Figure 8.2A. After growing of CNT on the surface of cellulosic carbon fiber, the SEM images without and with Sn plating are shown in Figure 8.2C and Figure 8.2D. From Figure 8.2D, the Sn plating smoothly covered the surface of both CNT and carbon fiber as well.

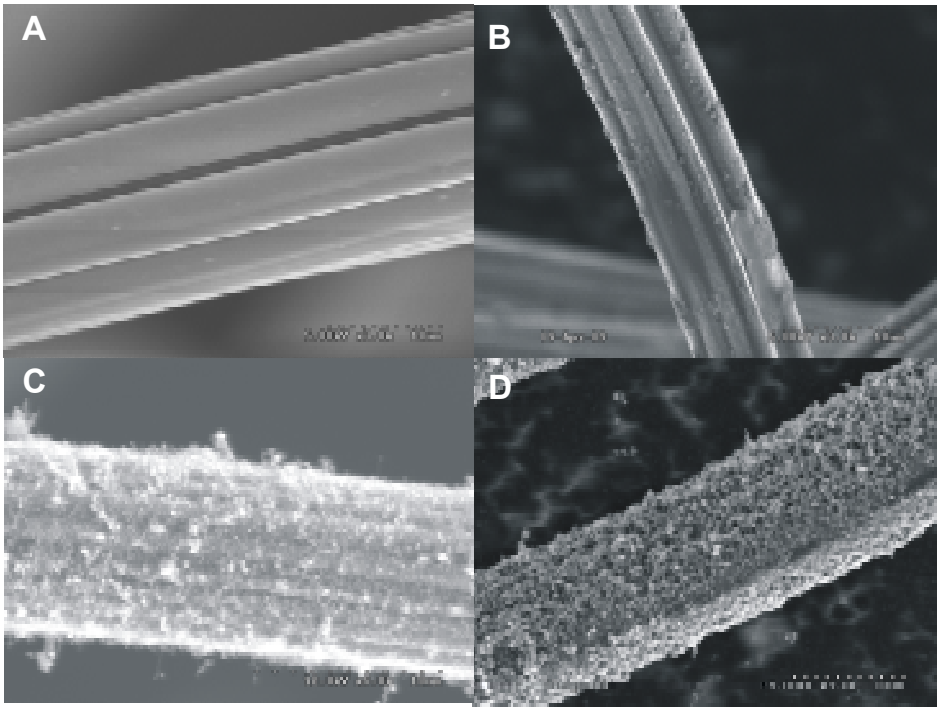

Figure 8.2 SEM images of (A): carbonized cellulosic fiber; (B): carbonized cellulosic fiber with Sn film; (C): carbonized cellulosic fiber with CNT, and (D): carbonized cellulosic fiber with CNT and Sn film.

As formate is the desired product of this study, the usage of a novel composite electrode material might be applied and help to leverage this technology towards the production of formate based on literatures discussed previously. The performance of novel carbon composite electrode material produced in this study was evaluated by the determination of formate concentration and current efficiency. The results were used to judge the feasibility of large scale production. To compare the performance of Sn-CNT-CF material in the electrochemical reduction of CO_2 with other commercial available carbon materials, electrodes made of carbon paper, CF, CNT-CF and CNT-CF with Sn plating were used as cathode in electrochemical reduction of CO_2. The comparison of

results using carbon paper (1 cm^2), cubic CF and CNT-CF electrodes as cathode are listed in Table 8.2.

Table 8.2 Formate productivity using different materials

Materials	Concentration (mM)	Current Efficiency (%)
Carbon paper	<0.0173	0
CF	0.112	6.0
CNT-CF (Fe)	0.0953	3.0
CNT-CF (Ni)	0.353	7.1
CNT-CF (Fe) with Sn	9	10.0
CNT-CF (Ni) with Sn	30	29.0

No or only negligible amounts of formate were produced on either carbon paper or carbon fiber electrode as shown in Table 8.2. Carbon fiber with branched CNT produced in the presence of Fe and Ni catalysts only showed a moderate catalytic activity with a current efficiency below 10%. Yamamota et al[297] studied the electrochemical reduction of CO_2 in the micropores of carbon fiber activated with Fe and Ni catalysts. In the same element group, Fe and Ni have similar catalytic properties concerning the hydrogenation and the hydrogen evolution in course of the electrolysis of water. Yamamota et al. showed the activation of carbon fiber with Ni is superior over Fe regarding the formate production, which is same as we observed in this study. The reason of higher formate yield was explained by Yamamota et al. with a steric factor of the catalytic Ni which enables of the efficient production of formate. Steric configuration of Ni particles is beneficial to adsorb the CO_2-$CO_2^{\cdot-}$ adduct. In this study, CNT were grown by incorporation Fe and Ni catalysts on the surface of carbon fiber, and Fe and Ni

particles stayed on the tip of CNT after growth, as shown in Figure 5.8 (Chapter V). In this context Ni particles on CNT might supply a hydrogen-enriched surface by bonding more H and consequently facilitating the formate production[299]. The experimental data of formate production from CNT-CF electrode agree with the above theory

In order to further improve the selectivity and current efficiency of electrochemical reduction of CO_2 to formate, some other catalysts need to be introduced. Sn, In and Pb electrodes have been proven to be favorable in producing formate [62]. For this investigation Sn was selected because the toxicity of In and Pb make them environmental unfriendly. In this study, in addition to the increased surface area enabled by Ni particle and growth of CNT on the carbon fiber, the Sn film was deposited on CNT in order to provide as many reaction sites as possible for the catalysis reaction. The deposition of the Sn film can be realized by plating[63], chemical vapor deposition[300] and e-beam deposition [301]. Electroless plating was selected in this study for the deposition of Sn film, since the drastic stirring or acid treatment involved in other methods would peel off CNT from carbon fibers. The resulting Sn-CNT-CF electrode allowed the formation of 30 mM formate with a current efficiency of around 30%, as shown in Table 8.2.

8.3.2 Reduction Potential of CO_2 to Formate

The potential of CO_2 reduction is affected by many factors, including catalyst type and electrolyte species. In this study, the electrochemical reduction occurred in a 15-mL reactor containing 4 mL of electrolyte (typically 0.5 M $NaHCO_3$ is used).

Electrodes made of Sn-CNT-CF material were used as cathode, while a Pt wire was used as counter electrode. In the so assembled electrolysis cell, the following electrochemical reactions occur on the electrodes:

Cathode reactions

$$H_2O + 2\,e^- \longrightarrow 2OH^- + H_2\,(gas) \qquad (6)$$

$$CO_2 + 2\,e^- + H_2O \longrightarrow COOH^- + OH^- \qquad (7)$$

Anode reaction

$$H_2O \longrightarrow \frac{1}{2}O_2\,(gas) + 2H^+ + 2\,e^- \qquad (8)$$

Different redox potentials were applied on cathode in order to maximize formate concentration and current efficiency. Formate concentration and current efficiency are explored against the applied redox potentials in range of -0.8 V to -2.3 V. Apparently the minimum threshold of the redox potential is -1.6 V since values below do not account for the detection of significant amounts of formate. Raising the redox potential from -1.6 to -1.9 V was responded by a steadily increasing formate concentration up to 35 mM, and remained on this level when the voltage was further increased up to -2.3 V. Current efficiency showed a maximum value of 53% at -1.9 V. Therefore, the optimum redox potential of -1.9 V is selected because both formate concentration and current efficiency reached the maximum. The formate concentration did not improved much with further increasing redox potential of operation to -2.3 V, but the current efficiency dramatically decreased from 53% to about 35%. It indicates that more side products were produced at a higher potential. As optimum potential a voltage of -1.9 V was identified, which is the same as reported standard potential of $CO_2^{\cdot -}$ formation (-1.9 V *vs.* N.H.E) [302]. This

high negative potential is needed for the formation of $CO_2^{\cdot -}$ due to a large reorganizational energy between the linear molecule and bent radical anion. Based on the mechanism of CO_2 reduction, the negatively charged $CO_2^{\cdot -}$ radical is usually presumed to be an intermediate upon the acceptance of one electron after the adsorption of CO_2 to the electrode. The subsequent protonation of $CO_2^{\cdot -}$ completes the conversion to formate. When the applied potential was far below the potential of $CO_2/CO_2^{\cdot -}$ redox couple, only low amounts of formate were produced. This indicates that the $CO_2^{\cdot -}$ formation is the limiting step in the whole reaction.

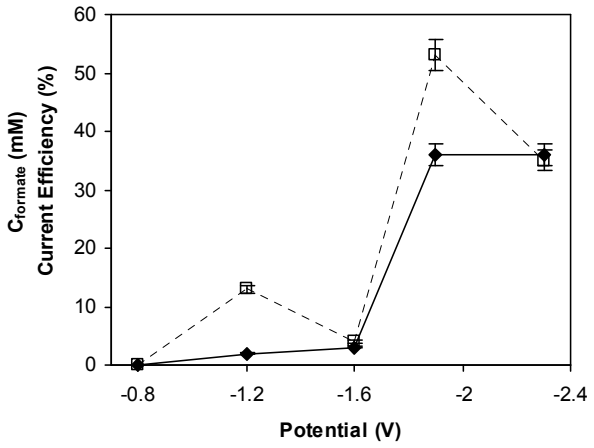

Figure 8.3 Effect of redox potential on the production of formate from CO_2 reduction. Concentration of formate: solid diamonds; current efficiency: open squares.

8.3.3 Effect of Electrolytes on CO_2 Reduction to Formate

Because the $CO_2^{\cdot -}$ radical is only formed at high overpotential, the reaction mechanism involves not only the electron transfer on the electrode interface, but also the characteristics of used electrolyte might have an influence on the productivity of formate. Therefore, various electrolytes were investigated in order to maximize the production of

formate and current efficiency. Firstly, pure water, Na_2SO_4 and $KHCO_3$ were used as electrolyte in CO_2 reduction. Figure 8.4 shows that the obtained redox current efficiency of CO_2 in Na_2SO_4 and $KHCO_3$ solutions is much higher than that observed with pure water. It might be explainable by the fact that pure water is not as easy ionizable as Na_2SO_4 and $KHCO_3$.

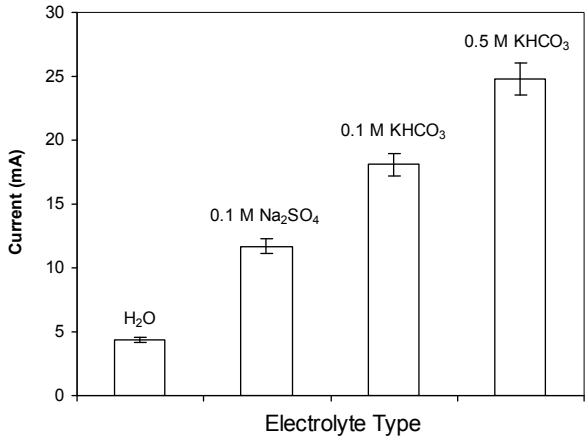

Figure 8.4 Redox current efficiency observed with different electrolytes.

The effect of electrolyte on formate productivity was also studied in two conditions: with and without bubbling CO_2 into the electrolyte solution. The results show that bubbling CO_2 can dramatically increase the formate productivity. These results suggest that a great number of bubbled gaseous CO_2 gets adsorbed on the surface of the electrode to undergo a reduction reaction. It was also observed, that the formate productivity in 0.1 M $KHCO_3$ solution was higher than in 0.1 M Na_2SO_4 because the bicarbonates equilibrium in $KHCO_3$ might promote more CO_2 hydrate molecule to react on the electrode. In addition to that, the concentration of electrolyte also had effects on

the productivity. Higher concentrations of electrolyte are beneficial in producing more formate with a higher current, since more salt molecules result in higher conductivity in electrolyte.

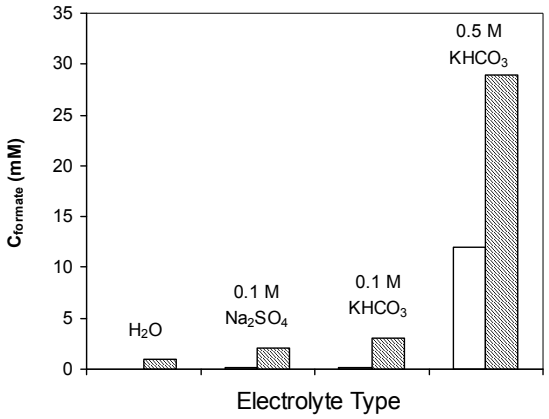

Figure 8.5 Formate concentration in different electrolyte solutions with/without CO_2 bubbling. Blank bar: without CO_2 bubbling; Shadowed bar: with CO_2 bubbling.

8.3.4 Effects of Electrolysis Temperature of CO_2 Reduction to Formate

Theoretically, increasing reactor temperature will favor reactions with higher activation energy. Increasing temperature in this study may elevate reaction rates and reduce overpotential, but it may also reduce the amount of adsorbed species on an electrode and CO_2 solubility in electrolyte. In this section, Sn-CNT-CF electrode was used as working electrode to reduce CO_2 to formate with CO_2 gas continually bubbled into $KHCO_3$ solution. The large surface area of CNT-CF material was expected to adsorb CO_2 molecules easily, and Sn film could improve the selectivity towards formate production.

Solubility of CO_2 in water is 3.36 g/L at 0 ^oC and 1.449 g/L at 25 ^oC, respectively. Carbon dioxide molecules exist in aqueous solution as equilibrium between H_2CO_3 and HCO_3^-. The more CO_2 molecules are present in the electrolyte, the more CO_2 molecules can be adsorbed on the cathode to get reduced, enhancing the yield for formate. Therefore, formate concentration and current efficiency were tested at 0 and 25^oC, and the results showed formate production at 0 ^oC was lower than 25 ^oC (Table 8.3). The results indicate that the solubility of carbon dioxide in electrolyte is not the limiting factor in the reduction of CO_2 to formate. With the elevation of the temperature, even though the solubility of CO_2 in electrolyte decreased, the temperature effect on the facilitation of reaction rate is more dominant.

Table 8.3 Impact of temperature on formate productivity

Temperature (^oC)	Concentration (mM)	Current Efficiency (%)
0	9.1	10.9
25	24	27.7

8.4 Conclusion

In most of the previous studies the electrochemical reduction of CO_2 has been tackled by using metal electrodes, and only a few recent reports discussed the selectivity of CO_2 reduction products on carbon electrodes. Carbon based electrodes have the advantages of low cost, high specific surface area, and of being renewable. In this study, 3-D carbon fiber material was prepared by the growth of CNT on the surface of carbon fiber in the presence of Fe or Ni catalyst. Different catalysts (Ni and Fe) were studied regarding their performance in formate production. Moreover, this material was

modified with Sn by electroless plating to improve the catalytic selectivity towards formate production. The resulting new Sn-CNT-CF electrode combined the porous structure of CNT-carbon fiber, the ability for hydrogen enrichment of Ni, and Sn's unique catalytic behavior beneficial toward the formate production. With this Sn-CNT-CF composite material a formate concentration of 30 mM was reached corresponding to a current efficiency higher than 50%. This result complies with the previously reported redox current efficiencies at some metal electrodes. Compared with regular CF electrode, the current efficiency of Sn-CNT-CF electrode was 5 times higher. The increased productivity of formate was because of the improvement of hydrogen adsorption and the introduction of Sn catalytic on electrode. Even though more systematic studies will be needed for the optimization of reaction conditions, based on the results in this chapter, it becomes obvious that this new material has the potential to outrange the traditional metal electrode material in the electrochemical application of CO_2 reduction.

CHAPTER IX

CONCLUSIONS AND PATH AHEAD

9.1 Conclusions

This research focused on utilization of natural resources (soybean oil, carbon dioxide and glycerol) for the production of value-added products (dihydroxyacetone and formate), and explored novel biocatalysis for high efficiency bioprocessing, bioenergy generation and cofactor regeneration. Major biotransformation reaction processes concerned in this study included biodiesel synthesis and DHA production. The major approaches were to manipulate microenvironment of enzyme catalysts and incorporation of enzymes with nanostructured materials. This study combined the concepts of biocatalysis and electrochemistry to generate unique enzymatic catalysis systems for potential industrial biotransformation. Toward that, recombinant glycerol dehydrogenase with 6xHis tag was produced via the transfection of *gld*A in *E. coli* BL21(DE3). For electrochemical regeneration of cofactor, a novel carbon fibrous electrode was developed and its catalytic capability, stability and efficiency were investigated and enhanced by employing concepts of nanotechnology, electrochemistry, and chemistry. In other efforts, the potential applications of the carbon electrode were also examined for micro-biosensor and CO_2 reduction. The specific conclusions are:

(I) This project demonstrated for the first time the biosynthesis of biodiesel in a water-free biocatalytic reaction system using an organic soluble lipase, and proved that

the organic soluble enzyme afforded much improved catalytic efficiency through homogenous reaction kinetics. The organic soluble lipase showed the best catalytic activity towards the synthesis of biodiesel at 55 ^{o}C. The productivity of such a solubilized enzyme (in terms of g-product/g-enzyme·h) was over two orders of magnitude higher than other enzymes reported previously. It can be concluded that highly efficient biocatalysis can be greatly promising for biodiesel synthesis.

(II) In this study, the transfection of *gld*A in *E. coli* BL21(DE3) with a T7 promoter was used to produce histag glycerol dehydrogenase. The yield of enzyme reached 10 mg·GDH/g·cell paste, which is about 3 times higher than that previously reported with *Cellulomonas* sp. NT3060. The specific activity and stability of the recombinant enzyme were also found improved in comparison with commercially available products.

(III) A novel approach of utilizing cellulosic material for biochemical processes was developed. The process provided a fast approach in the manufacturing of carbon materials with high specific surface area for electrochemical applications. We demonstrated that the development of 3-D carbon electrode materials by using carbonized cellulosic fibers with branched CNT. The specific surface area of the electrode was increased substantially, reached 291 m^2/g, which is about 30-fold higher than that of carbon fibers without CNT. Such material was applied successfully in the subsequent development of large-size 3-D electrode, and appeared to be highly efficient in realizing NAD^+ regeneration, biosensing and CO_2 reduction.

(IV) Electrochemical cofactor regeneration for continuous production of DHA from glycerol using immobilized GDH was examined. The effect of mediators, including Meldola's blue and poly(methylene green) were investigated for NAD^+ regeneration. Both mediator modified electrodes reduced the oxidation potential of NADH to ~0.1 V. On the other hand, the use of mediators is generally expected to shorten the lifetimes of electrodes. Two DHA production processes, namely *in situ* and stand-alone cofactor regeneration, were therefore developed with one approach examines the use of mediators for higher reactivity, while the other probes better stability without the use of mediator. It was shown that when cofactor regeneration was achieved through a separated unit without the use of mediators, 15 regeneration cycles was realized with no observable activity loss for both the enzyme and electrode. The separated operation was also designed to protect the enzyme from product inhibition. It appeared that for such a reactor design, the electrochemical regeneration of NAD^+ is the limiting step, presumably due to the slow reaction on the surface of electrode. When cofactor regeneration was achieved *in situ* in the presence of mediators, the total turnover number (TTN) of NAD^+ reached over 3,000 in a 5-h operation, driven by the improved activity of the electrode for cofactor regeneration. In addition, immobilized laccase also showed efficient conversion of protons to water along with the enzymatic production of DHA. Although further extensive studies are needed to further optimize the overall process, the current research achieved better understanding on the use of the 3-D carbon electrode for cofactor regeneration toward enzymatic production of DHA.

(V) The growth of branched CNT on surface of carbon fiber electrode reduced the overpotential for direct oxidation of NADH from originally over 0.8 V to lower than 0.6 V. Lower overpotentials are desired for the electrochemical processes not only for the consideration of energy consumption, but also for the reduction of electrode fouling. Taking advantages of the improved electrochemical activity and specific surface area of the hierarchical structure, a highly sensitive and stable micro biosensor was developed using a single CNT-carbon fiber. The biosensor was applied successfully for detection of glycerol and GDH, with detection limits of 40 μM and 0.004 U/ml achieved for glycerol and GDH, respectively. It is expected that the applications of such a miniaturized biosensor can be expanded to many fields including biomedical devices, bioenergy processes, and biocatalytic synthesis.

(VI) The direct reduction of carbon dioxide to formate was realized by applying the modified CNT-CF material as the working electrode. It was observed that the catalyst composition on the carbon electrode determines the current efficiency of the process, and the introduction of Sn by electroless plating to the 3-D carbon electrode significantly improved the current efficiency. While the use of Ni achieved a current efficiency that was 2 times higher than that with Fe reduction of CO_2, the use of the Sn-CNT-CF electrode afforded a current efficiency 5-fold higher than that of CF electrode. Integrating with solar panels, we expect that the findings from the current research can eventually contribute toward economic and sustainable carbon capture.

(VII) To explore the feasibility of applying biofuel cell technology for biochemical production, biocatalysis fundamentals especially reaction kinetics of a model biofuel cell system was examined. A model glucose-oxygen biofuel cell with the application of immobilized glucose oxidase as anode catalyst was studied to determine the kinetic limitations of enzymatic biofuel cells. The kinetic parameters were used successfully in the prediction of current generation from an enzyme-based bioanode when it was examined as a single electrode. The biofuel cell employing the CNT–GOx anode was only able to generate a power density equivalent to <40% of reaction capability of the enzyme immobilized on the electrode. It appeared to us that factors such as electron and proton transfer resistances rather than catalytic reaction rate are overwhelming in limiting the power generation of the biofuel cell. This study will facilitate future development of electro-biocatalytic production of DHA using a biofuel cell process.

9.2 Path ahead

Enzymes offer precise molecule control in producing chemicals from renewable raw materials possessing multiple functional groups such as glycerol concerned in this study. The application of biofuel cell technology for DHA production is greatly attractive as it produces energy and value-added product simultaneously. This research has set a solid basis toward technology development down that direction, and future research regarding application of the 3-D carbon electrode for glycerol-based biofuel cells should be conducted.

The current research promises economic production of DHA. That will not only facilitate the traditional applications of DHA, but will also trigger exploration of a broader range of new applications. For example, the market price of DHA is set at ~$240/kg as a result of the inefficiency of the currently available technologies, eliminating the possibility of using DHA for general-purpose materials. Full capitalization on the potentials of the technologies revealed through this research, it is possible to reduce the production cost of DHA substantially to be lower than that of lactic acid, therefore making it affordable to be used as a renewable building block for plastics and polymers. Enzymatic conversion of DHA into acids and alcohols has also been proven feasible, in addition to many chemical conversion routes. That can be expected to expand the scope of glycerol-base products even more dramatically.

BIBLIOGRAPHY

1. Brasaemle, D.L., *The perilipin family of structural lipid droplet proteins: stabilization of lipid droplets and control of lipolysis.* Journal of Lipid Research, 2007. **48**: p. 2547-2559.

2. Al-Zuhair, S., *Production of Biodiesel by Lipase-Catalyzed Transesterification of Vegetable Oils: A Kinetics Study.* Biotechnology Progress, 2005. **21**: p. 1442-1448.

3. Du, W., Y. Xu, and D. Liu, *Lipase-catalysed transesterification of soya bean oil for biodiesel production during continuous batch operation.* Biotechnology and Applied Biochemistry, 2003. **38**: p. 103-106.

4. Salis, A., M. Pinna, M. Monduzzi, and V. Solinas, *Biodiesel production from triolein and short chain alcohols through biocatalysis.* Journal of Biotechnology, 2005. **119**: p. 291-299.

5. Noureddini, H., X. Gao, and R.S. Philkana, *Immobilized Pseudomonas cepacia lipase for biodiesel fuel production from soybean oil.* Bioresource Technology, 2005. **96**: p. 769-777.

6. Samukawa, T., M. Kaieda, T. Matsumoto, K. Ban, et al., *Pretreatment of Immobilized Candida antarctica Lipase for Biodiesel Fuel Production from Plant Oil* Journal of Bioscience and Bioengineering, 2000. **90**: p. 180-183.

7. Bonnardeaux, J. *Glycerin Overview*. Report for the Western Austrialia Department of Agriculture and Food 2006; Available from: http://www.agric.wa.gov.au/content/sust/biofuel/glycerinoverview.pdf.

8. Pagliaro, M. and M. Rossi, *The future of glycerol New uses of a Versatile Raw Material*. RSC Green Chemistry Book Series, ed. J.H. Clark and G.A. Kraus. 2008, Cambridge: The Royal Society of Chemistry. 127.

9. Wang, L., J. Qian, Z. Hu, Y. Zheng, et al., *Determination of dihydroxyacetone and glycerol in fermentation broth by pyrolytic methylation/gas chromatography.* Analytica Chimica Acta, 2006. **557**: p. 262-266.

10. Chen, H., Y.-h. Wu, Z.-h. Wu, B.-s. Fang, et al., *Purification and Characterization of Glycerol Dehydrogenase from Klebsiella pneumoniae.* Journal of Wuxi University of Light Industry, 2005. **24**(1): p. 1-5.

11. Pagliaro, M., R. Ciriminna, H. Kimura, M. Rossi, et al., *From Glycerol to Value-Added Products.* Angew. Chem. Int. Ed., 2007. **46**: p. 4434-4440.

12. Ciriminna, R., G. Palmisano, C.D. Pina, M. Rossi, et al., *One-pot electrocatalytic oxidation of glycerol to DHA.* Tetrahedron Letters, 2006. **47**: p. 6993-6995.

13. Dimitratos, N., F. Porta, and L. Prati, *Au, Pd (mono and bimetallic) catalysts supported on graphite using the immobilisation method: Synthesis and catalytic testing for liquid phase oxidation of glycerol.* Applied Catalysis A: General, 2005. **291**(1-2).

14. Bianchi, C.L., P. Canton, N. Dimitratos, F. Porta, et al., *Selective oxidation of glycerol with oxygen using mono and bimetallic catalysts based on Au, Pd and Pt metals* Catalysis Today, 2005. **102-103**: p. 203-212

15. Besson, M., R. Garcia, and P. Gallezot, *Chemoselective catalytic oxidation of glycerol with air on platinum metals* Applied Catalysis A: General, 1995. **127**(1): p. 165-176.

16. Marshall, J.H., J.W. May, and J. Sloan, *Purification and Properties of Glycerol: NAD^+ 2-Oxidoreductase（Glycerol Dehydrogenase）from Schizosaccharomyces pombe.* Journal of General Microbiology, 1985. **131**: p. 1581-1588.

17. Burton, R.M. and N.O. Kaplan, *A DPN Specific Glycerol Dehydrogenase from Aerobacter Aerogenes* J. Am. Chem. Soc., 1953. **75**(4): p. 1005-1006.

18. Asnis, R.E. and A.F. Brodie, *A Glycerol Dehydrogenase from Escherichia Coli.* The Journal of Biological Chemistry, 1953: p. 153-159.

19. Lapenaite, I., A. Ramanaviciene, and A. Ramanavicius, *Current Trends in Enzymatic Determination of Glycerol.* Critical Reviews in Analytical Chemistry, 2006. **36**: p. 13–25.

20. Liu, W. and P. Wang, *Cofactor Regeneration for Sustainable Enzymatic Biosynthesis.* Biotechnol. Adv., 2007. **25**: p. 369-384.

21. Chenault, H.K. and G.M. Whitesides, *Regeneration of nicotinamide cofactors for use in enzymatic synthesis.* Appl. Biochem. Biotechnol., 1987. **14**(2): p. 147-197.

22. Moiroux, J. and P.J. Elving, *Effects of Adsorption, Electrode Material, and Operational Variables on the Oxidation of Dihydronicotinamide Adenine Dinucleotide at Carbon Electrodes.* Anal. Chem., 1978. **50**: p. 1056-1062.

23. Haegfeldt, H., *Adsorption and Electrochemical Oxidation Behaviour of NADH at a Clean Platinum Electrode.* J. Electroanal. Chem., 1980. **110**: p. 295-302.

24. Gorton, L. and E. Domínguez, *Electrocatalytic oxidation of NAD(P)/H at mediator-modified electrodes* Reviews in Molecular Biotechnology, 2002. **82**: p. 371-392.

25. Song, H.K., S.H. Lee, K. Won, J.H. Park, et al., *Electrochemical regeneration of NADH enhanced by platinum nanoparticles.* Angew Chem Int Ed Engl, 2008. **47**(9): p. 1749-52.

26. Viry, L., A. Derre, P. Garrigue, N. Sojic, et al., *Optimized carbon nanotube fiber microelectrodes as potential analytical tools.* Anal Bioanal Chem, 2007. **389**(2): p. 499-505.

27. Yoon, S.K., E.R. Choban, C. Kane, T. Tzedakis, et al., *Laminar Flow-Based Electrochemical Microreactor for Efficient Regeneration of Nicotinamide Cofactors for Biocatalysis.* Journal of the American Chemical Society, 2005. **127**(30): p. 10466-10467.

28. Li, P., Q. Zhao, X. Zhou, W. Yuan, et al., *Enhanced Distribution and Anchorage of Carbon Nanofibers Grown on Structured Carbon Microfibers.* . J. Phys. Chem. C., 2009. **113**(4): p. 1301-1307.

29. Qu, L., F. Du, and L. Dai, *Preferential Syntheses of Semiconducting Vertically Aligned Single-Walled Carbon Nanotubes for Direct Use in FETs.* Nano Letters, 2008. **8**(9): p. 2682-2687.

30. Endo, M., M.S. Strano, and P.M. Ajayan, *Potential applications of carbon nanotubes*, in *Carbon Nanotubes*. 2008, Springer/Heidelberg: Berlin. p. 13-61.

31. Wang, J. and Y. Lin, *Functionalized carbon nanotubes and nanofibers for biosensing applications.* Trends in Analytical Chemistry, 2008. **27**(7): p. 619-626.

32. Nakano, K., K. Nakamura, K. Iwamoto, N. Soh, et al., *Positive-feedback-mode scanning electrochemical microscopy imaging of redox-active DNA-poly(1,4-benzoquinone) conjugate film deposited on carbon fiber electrode for micrometer-sized hybridization biosensor applications.* Journal of Electroanalytical Chemistry, 2009. **628**: p. 113-118.

33. Mano, N., F. Mao, and A. Heller, *Characteristics of a Miniature Compartment-less Glucose-O_2 Biofuel Cell and Its Operation in a Living Plant.* Journal of the American Chemical Society, 2003. **125**: p. 6588-6594.

34. Wang, Y., Q. Li, and S. Hu, *A multiwall carbon nanotubes film-modified carbon fiber ultramicroelectrode for the determination of nitric oxide radical in liver mitochondria.* Bioelectrochemistry, 2005. **65**: p. 135-142.

35. Chen, R., W. Huang, H. Tong, Z. Wang, et al., *Carbon Fiber Nanoelectrodes Modified by Single-Walled Carbon Nanotubes.* Anal. Chem., 2003. **75**: p. 6341-6345.

36. Swamy, B.E.K. and B.J. Venton, *Carbon nanotube-modified microelectrodes for simultaneous detection of dopamine and serotonin in vivo.* Analyst, 2007. **132**: p. 876 - 884.

37. Du, F., W. Huang, Y. Shi, Z. Wang, et al., *Real-time monitoring of NO release from single cells using carbon fiber micro-disk electrodes modified with single-walled carbon nanotubes.* Biosensors & Bioelectronics, 2008. **24**(3): p. 415-421.

38. Sgobba, V. and D.M. Guldi, *Carbon nanotubes-electronic/electrochemical properties and application for nanoelectronics and photonics.* Chem. Soc. Rev., 2009. **38**: p. 165-184.

39. Nowall, W.B. and W.G. Kuhr, *Electrocatalytic Surface for the Oxidation of NADH and Other Anionic Molecules of Biological Significance.* Analytical Chemistry, 1995. **67**(19): p. 3583-3588.

40. Wang, J., M. Gu, J. Di, Y. Gao, et al., *A carbon nanotube/silica sol-gel architecture for immobilization of horseradish peroxidase for electrochemical biosensor.* Bioprocess and Biosystems Engineering, 2007. **30**(4): p. 289-296.

41. Valcrcel, M., S. Crdenas, and B.M. Simonet, *Role of Carbon Nanotubes in Analytical Science.* Anal. Chem., 2007. **79**(13): p. 4788-4797.

42. Johnson, J., *Dealing with Carbon Dioxide from Coal.* C&E News, 2007. **85**(14): p. 48-51.

43. Ritter, S.K., *What Can We Do With Carbon Dioxide?* C&E News, 2007. **85**(18): p. 11-17

44. Song, C., A.M. Gaffney, and K. Fujimoto, eds. *CO_2 Conversion and Utilization* Acs Symposium Series 809. 2001, American Chemical Society, Washington, DC.

45. Kočí, K., L. Obalová, and Z. Lancy, *Photocatalytic reduction of CO_2 over TiO_2 based catalysts.* Chemical Paper, 2008. **61**(1): p. 1-9.

46. Lu, Y., Z.-y. Jiang, S.-w. Xu, and H. Wu, *Efficient conversion of CO_2 to formic acid by formate dehydrogenase immobilized in a novel alginate–silica hybrid gel.* Catalysis Today, 2006. **115**(1-4): p. 263-268.

47. Jitaru, M., D.A. Lowy, M. Toma, B.C. Toma, et al., *Electrochemical reduction of carbon dioxide on flat metallic cathodes.* Journal of Applied Electrochemistry, 1997. **27**: p. 875-889.

48. Ghindilis, A.L., P. Atanasov, and E. Wilkins, *Enzyme-catalyzed direct electron transfer: Fundamentals and analytical applications.* Electroanalysis, 1997. **9**(9): p. 661-674.

49. Varfolomeev, S.D., I.N. Kurochkin, and A.I. Yaropolov, *Direct electron transfer effect biosensors.* Biosensors and Bioelectronics, 1996. **11**(9): p. 863-871.

50. Freire, R.S., C.A. Pessoa, L.D. Mello, and L.T. Kubota, *Direct electron transfer: An approach for electrochemical biosensors with higher selectivity and sensitivity.* Journal of the Brazilian Chemical Society, 2003. **14**(2): p. 230-243.

51. Schuhmann, W., *Amperometric enzyme biosensors based on optimized electron-transfer pathways and non-manual immobilization procedures.* Reviews in Molecular Biotechnology, 2002. **82**(4): p. 425-441.

52. Board, N.B., *Specification for Biodiesel (B100)*.

53. Klibanov, A.M., *Improving enzymes by using them in organic solvents.* Nature, 2001. **409**: p. 241-246.

54. Clark, W.M., *Oxidation-reduction potentials of organic systems*. 1960, Baltimore: Williams & Wilkins.

55. Moiroux, J. and P.J. Elving, *Effects of adsorption, electrode material, and operational variables on the oxidation of dihydronicotinamide adenine dinucleotide at carbon electrodes.* Analytical Chemistry, 1978. **50**(8): p. 1056-1062.

56. Jaegfeldt, H., *Adsorption and electrochemical oxidation behavior of NADH at a clean platinum electrode.* Journal of Electroanalytical Chemistry and Interfacial Electrochemistry, 1980. **110**(1-3): p. 295-302.

57. Moiroux, J. and P.J. Elving, *Mechanistic aspects of the electrochemical oxidation of dihydronicotinamide adenine dinucleotide (NADH).* Journal of the American Chemical Society, 1980. **102**(21): p. 6533-6538.

58. Jaegfeldt, H., *A study of the products formed in the electrochemical reduction of nicotinamide adenine dinucleotide.* Bioelectrochemistry and Bioenergetics, 1981. **8**(3): p. 355-370.

59. Chenault, H.K. and G.M. Whitesides, *Nicotinamide Cofactor Regeneration.* Appl. Biochem.Biotechnol., 1987. **14**: p. 147-196.

60. Chaplin, R.P.S. and A.A. Wragg, *Effects of process conditions and electrode material on reaction pathways for carbon dioxide electroreduction with particular reference to formate formation* Journal of Applied Electrochemistry, 2003. **33**(12): p. 1107-1123.

61. Oloman, C. and H. Li, *Electrochemical Processing of Carbon Dioxide.* Chem. Sus. Chem., 2008. **1**(385-391).

62. Hori, Y., K. Kikuchi, and S. Suzuki, *Production of CO and CH_4 in Electrochemical Reduction of CO_2 at Metal Electrodes in Aqueous Hydrogencarbonate Solution* Chemistry Letters, 1985. **14**(11): p. 1695-1698.

63. Liu, W.L., S.H. Heieh, and W.J. Chen, *Preparation of Sn films deposited on carbon nanotubes.* Applied Surface Science, 2007. **253**: p. 8356-8359.

64. Faber, K., *Biotransfermations in Organic Chemistry*. 4th Edition ed. 2000, Berlin: Springer-Verlag.

65. Schmid, A., J.S. Dordick, B. Hauser, A. Kiener, et al., *Industrial biocatalysis today and tomorrow.* Nature, 2001. **409**: p. 258-267.

66. Pauke, S. and M.G. Wubbolts, *Wnzyme technology and bioprocess engineering.* Current Opinion in Biotechnology, 2002. **13**: p. 111-116.

67. Turner, M.K., *Biocatalysis in organic chemistry (Part I): Past and present.* Trends in Biotechnology, 1995. **13**(5): p. 173-177.

68. Bommarius, A.S. and B.R. Riebel-Bommarius, eds. *Biocatalysis*. 1st ed. 2004, Wiley-VCH, Weinheim: New York. 611.

69. Zaks, A. and A.M. Klibanov, *Enzymatic catalysis in organic media at 100 degrees C.* Science, 1984. **224**(4654): p. 1249-1251.

70. Koskinen, A.M.P. and A.M. Klibanov, eds. *Enzymatic reactions in organic media*. 1st ed. 1996, Blackie academic & Prefessional: Chapman & Hall: London.

71. Wang, P., S. Dai, S.D. Waezsada, A. Tsao, et al., *Enzyme stabilization by covalent binding in nanoporous sol-gel glass for nonaqueous biocatalysis.* Biotechnology and Bioengineering, 2001. **74**(3): p. 249-255.

72. Zacchigna, M., G.D. Luca, L. Lassiani, A. Varnavas, et al., *Properties of methoxy(polyethylene glycol)-lipase from Candida rugosa in organic solvents.* II Farmaco, 1998. **53**: p. 758-763.

73. Castro, G.R. and T. Knubovets, *Homogeneous biocatalysis in organic solvents and water-organic mixtures.* Critical Reviews in Biotechnology, 2003. **23**: p. 195-231.

74. Narayanan, R., *Self-Assembling Multienzyme Systems at Oilwater Interface for Biphasic Biotransformations*, in *Bioproducts and Biosystems Engineering*. 2008, University of Minnesota: Saint Paul. p. 205.

75. Davis, B.G., *Chemical modification of biocatalysts.* Current opinion in Biotechnology, 2003. **14**: p. 379-386.

76. Ohya, Y., T. Sugitou, and T. Ouchi, *Polycondensation of α-hydroxy acids by enzymes or PEG-modified enzymes in organic media.* Journal of Macromolecular Science, Pure and Applied Chemistry, 1995. **A32**: p. 179-190.

77. Wang, P., C.A. Woodward, and E.N. Kaufman, *Poly(ethylene glycol)-modified ligninase enhances pentachlorophenol biodegradation in water-solvent mixtures.* Biotechnology and Bioengineering, 1999. **64**: p. 290-297.

78. Distel, K.A., G. Zhu, and P. Wang, *Biocatalysis using an organic-soluble enzyme for the preparation of poly(lactic acid) in organic solvents.* Bioresource Technology, 2005. **96**: p. 617-623.

79. DeSantis, G. and J.B. Jones, *Probing the altered specificity and catalytic properties of mutant subtilisin chemically modified at position s156c and s166c in the s1 pocket.* Bioorg. Med Chem, 1999. **7**: p. 2293-2301.

80. Tann, C.M., D. Qi, and M.D. Distefano, *Enzyme design by chemical modification of protein scaffolds.* Current opinion in chemical biology, 2001. **5**(6): p. 696-704.

81. Prescott, S.C. and C.G. Dunn, *Industrial Microbiology*. 3rd ed. 1959, New York: McGraw-Hill Book Co., Inc.,. 459.

82. *Dihydroxyacetone* Available from: www.thesynergy.com/supplies/Dihydroxyacetone.pdf

83. Ślepokura, K. and T. Lis, *Crystal structures of dihydroxyacetone and its derivatives.* Carbohydrate Research, 2004. **339**: p. 1995-2007.

84. Yaylayan, V.A., S.H. Majors, and A.A. Ismail, *Investigation of D, L-Glyceraldehyde-Dihydroxyacetone Interconversion by FTIR Spectroscopy.* Carbohydrate Research, 1999. **318**: p. 20-25.

85. Zhu, Y., D. Youssef, C. Porte, A. Rannou, et al., *Study of the Solubility and the Metastable Zone of 1,3-Dihydroxyacetone for the Drowning-out Process.* Journal of Crystal Growth 2003. **257:**: p. 370-377.

86. Waagen, V., T.K. Barua, H.W. Anthonsen, L.K. Hansen, et al., *Dihydroxyacetone Dimers: Solution and Crystal Structure of Stereoisomers of 2,5-Diethoxy-1,4-Dioxane-2,5-Dimethanol.* Tetrahedron Letters, 1994. **50**(33): p. 10055-10060.

87. Mishra, R., S.R. Jain, and A. Kumar, *Microbial production of dihydroxyacetone.* Biotechnology Advances, 2008. **26**: p. 293-303.

88. Brown, D.A., *Skin Pigmentation Enhancers.* Journal of Photochemistry and Photobiology B: Biology, 2001. **63** (1-3): p. 148-161.

89. Akin, F.J. and E. Marlowe, *Non-Carcinogenicity of Dihydroxyacetone by Skin Painting.* JEPTO, 1984. **5**(4-5): p. 349-351.

90. Petersen, A.B., H.C. Wulf, R. Gniadecki, and B. Gajkowska, *Dihydroxyacetone, the Active Browning Ingredient in Sunless Tanning Lotions, Induces DNA Damage, Cell-Cycle Block and Apoptosis in Cultured HaCaT Keratinocytes* Mutation Research, 2004. **560**: p. 173-186.

91. Yourick, J.J., M.L. Koenig, D.L. Yourick, and R.L. Bronaugh, *Fate of Chemicals in Skin after Dermal Application: Does the in Vitro Skin Reservoir affect the Estimate of Systemic Absorption?* Toxicology and Applied Pharmacology, 2004. **195**: p. 309-320.

92. Fesq, H., K. Brockow, K. Strom, M. Mempel, et al., *Dihydroxyacetone in a new formulation-a powerful therapeutic option in vitiligo.* Dermatology, 2001. **203**: p. 241-243.

93. Asawanonda, P., S. Oberlender, and C. Taylor, *The use of dihydroxyacetone for photoprotection in variegate porphyria.* Int J Dermatol, 1999. **38**: p. 916-918.

94. Levy, S., *Cosmetics that imitate a tan.* Dermatol Ther 2001. **14**: p. 215-219.

95. Ahmed, I., *Childhood porphyrias.* Mayo Clin Proc, 2002. **77**: p. 825-836.

96. Nguyen, B. and I. Kochevar, *Factors influencing sunless tanning with dihydroxyacetone.* Brit J Dermatol, 2003. **149**: p. 332-340.

97. Fusaro, R. and E. Rice, *The Maillard reaction: chemistry at the interface of nutrition, aging, and disease.* Ann N Y Acad Sci, 2005. **1043**: p. 174-183.

98. Petersen, A., R. Na, and H. Wulf, *Sunless skin tanning with dihydroxyacetone delays broadspectrum ultraviolet photocarcinogenesis in hairless mice.* Mutat Res Genet Toxicol Environ Mutagen, 2003. **542**: p. 129-138.

99. Hossein, N. and E. Ghelichkhani, *Antagonism of Cyanide Poisoning by Dihydroxyacetone.* Toxicology Letters, 2002. **132**(2): p. 95-100.

100. Hossein, N. and E. Ghelichkhani, *Antidotal Effect of Dihydroxyacetone Against Cyanide Poisoning.* Toxicology Letters, 1998. **95**(Supplement 1): p. 85-84.

101. Enders, D., M. Voith, and A. Lenzen, *The Dihydroxyacetone Unit-a Versatile C3 Building Block in Organic Synthesis.* Angewandte Chemie International Edition, 2005. **44**(9): p. 1304-1325.

102. Zuo, H., B. Zhao, W. Tan, D. Wang, et al., *Synthesis of 1,3-Dihydroxyacetone Derivatives.* Chinese Journal of Organic Chemistry 2004. **24**(3): p. 331-333.

103. Kim, K.S. and S.D. Hong, *Synthesis and Stereoselective Aldol Reaction of Dihydroxyacetone Derivatives.* Tetrahedron Letters, 2000. **41**: p. 5909-5913.

104. Saimoto, H., T. Onitsuka, H. Motobe, S. Okabe, et al., *Reaction of C3 and C4 Ketoses with Alkenals and Alkenones in Water.* Tetrahedron Letters, 2004. **45**(48): p. 8777-8780.

105. Bicker, M., S. Endres, L. Ott, and H. Vogel, *Catalytical Conversion of Carbohydrates in Subcritical Water: A new Chemical Process for Lactic Acid Production.* Journal of Molecular Catalysis A: Chemical, 2005. **239**: p. 151-157.

106. Ciriminna, R. and M. Pagliaro, *Oxidation of Tartronic Acid and Dihydroxyacetone to Sodium Mesoxalate Mediated by TEMPO.* Tetrahedron Letters, 2004. **45**: p. 6381-6383.

107. Porta, F. and L. Prati, *Selective Oxidation of Glycerol to Sodium Glycerate with Gold-on-Carbon Catalyst: an Insight Intoreaction Selectivity.* Journal of Catalysis 2004 **224**: p. 397-403.

108. Demirel, S., K. Lehnert, M. Lucas, and P. Claus, *Use of Renewables for the Production of Chemicals: Glycerol Oxidation Over Carbon Supported Gold Catalysts.* Applied Catalysis B: Environmental, 2007. **70**(1-4): p. 637-643.

109. Hiroshi, K., *Selective Oxidation of Glycerol on a Platinum-Bismuth Catalyst by Using a Fixed Bed Reactor.* Applied Catalysis A: General, 1993. **105**(2): p. 147-158.

110. Michele, B. and G. Pierre, *Selective Oxidation of Alcohols and Adehydes on Metal Catalysts.* Catalysis Today, 2000. **57**(1-2): p. 127-141.

111. Feng, P., J. Zhou, Y. Xu, and Y. Ge, *Production of Dihydroxyacetone by Continuous Cultivation With Membrane Bioreactor.* Food and Fermentation Industries, 2003. **29**(12): p. 40-43.

112. Burton, R.M., *Glycerol Dehydrogenase from Aerobacter aerogenes.* Methods Enzymol., 1955. **1**: p. 397-400.

113. Kong, Y.C., J.W. May, and J.H. Marshal, *Glycerol Oxidation and Triose Redution by Pyridine Nucleotide-linked Enzyme in the Fission Yeast Schizosaccharomyces pombe.* Journal of General Microbiology, 1985. **131**: p. 1571-1579.

114. Nishise, H., A. Nagao, Y. Tani, and H. Yamada, *Further Characterization of Glycerol Dehydrogenase from Cellulomonas sp. NT 3060.* Agric. Biol. Chem., 1984. **48**(6): p. 1603-1609.

115. Leichus, B.N. and J.S. Blanchard, *Isotopic Analysis of the Reaction Catalyzed by Glycerol Dehydrogenase.* Biochemistry, 1994. **33**: p. 14642-14619.

116. Yamada, H., A. Nagao, H. Nishise, and Y. Tani, *Glycerol Dehydrogenase from Cellulomonas sp.NT3060: Purification and Characterization.* Agric.Biol.Chem., 1982. **9**(46): p. 2333-2339.

117. Spencer, P., A. Slade, T. Atkinson, and M.G. Gore, *Studies on the Interactions of Glycerol Dehydrogenase from Bacillus stearothermophilus with Zn^{2+} Ions and NADH.* Biochimica et Biophysica Acta, 1990. **1040**: p. 130-133.

118. Spencer, P., K.J. Bown, M.D. Scawen, T. Atkinson, et al., *Isolation and Characterisation of the Glycerol Dehydrogenase from Bacillus stearothermophilus.* Biochimica et Biophysica Acta, 1989. **994**: p. 270-279.

119. Toews, C.J., *The Kinetics and Reaction Mechanism of the Nicotinamide-Adenine Dinucleotide Phosphate-Specific Glycerol Dehydrogenase of Rat Skeletal Muscle.* Biochem. J., 1967. **105**: p. 1067-1073

120. Amyyama, M., E. Shinagawa, K. Matsushita, and O. Adachi, *Solubilization, Purification and Properties of Membrane-bound Glycerol Dehydrogenase from Gluconobacter industrius.* Agricultural and Biological Chemistry, 1985. **49**(4): p. 1001-1010.

121. Lapenaite, I., B. Kurtinaitiene, J. Razumiene, V. Laurinavicius, et al., *Properties and Analytical Application of PQQ-Dependent Glycerol Dehydrogenase from Gluconobacter sp.33.* Analytical Chimica Acta, 2005. **549**: p. 140-150.

122. www.brenda-enzymes.org.

123. Wang, J., S. Zhu, and C. Xu, *Biochemistry*. 3rd ed. 2002, Beijing: China Higher Education Press.

124. Nishise, H., A. Nagao, Y. Tani, and H. Yamada, *Further Characterization of Glycerol Dehydrogenase from Cellulomonas sp.NT3060.* Biol.Chem., 1984. **6**(48): p. 1603-1609.

125. R.Wichmann and D.Vasic-Racki, *Cofactor Regeneration at the Lab Scale.* Adv Biochem Engin/Biotechnol, 2005. **92**: p. 225-260.

126. Lu, C., Z. Jiang, and J. Wang, *Progress in Regeneration of $NAD(P)^+$ and NAD(P)H.* Chinese Journal of Organic Chemistry, 2004. **24**(11): p. 1366-1379.

127. Zhang, Y., *Bio-catalysis of chiral synthesis*. 2002, Beijing: Chemical Industry Press

128. Chen, H.W., B.S. Fang, and Z.D. Hu, *Optimization of Process Parameters for Key Enzymes Accumulation of 1,3-Propanediol Production from Klebsiella pneumoniae.* Biochemical Engineering Journal 2005. **25**: p. 47-53.

129. Mandler, D. and I. Willner, *Solar Light Induced Formation of Chiral 2-Butanol in an Enzyme-Catalyzed Chemical System.* J.Am. Chem. Soc., 1984. **106**: p. 5352-5353.

130. Suye, S.-I., A. Yasunori, N. Makoto, T. Isao, et al., *Electrochemical Reduction of Immobilized $NADP^+$ on a Polymer Modified Electrode with a Co-polymerized Mediator.* Enzyme and Microbial Technology, 2002. **30**(2): p. 139-144.

131. Hollmann, F., B. Witholt, and A. Schmid, *$[Cp^*Rh(bpy)(H_2O)]^{2+}$: a Versatile Tool for Efficient and Non-Enzymatic Regeneration of Nicotinamide and Flavin Coenzymes.* Journal of Molecular Catalysis B: Enzymatic, 2002. **19-20**: p. 167-176.

132. Dong, S., B. Wang, and B. Liu, *Amperometric glucose sensor with ferrocene as an electron transfer mediator.* Biosensors & Bioelectmnics, 1991. **7**: p. 215-222.

133. Kulys, J.J. and E.J. D'Costa, *Printed amperometric sensor based on TCNQ and cholinesterase.* Biosensors & Bioelectronics, 1991. **6**: p. 109-115.

134. Cass, A.E.G., D.G. Francis, H.A.O. Hill, W.J. Aston, et al., *Ferrocene-mediated enzyme electrode for amperometric determination of glucose.* Analytical Chemistry, 1984. **56**: p. 667-671.

135. Sun, C., W. Song, D. Zhao, Q. Gao, et al., *Tetrabutylammonium-Tetracyanoquinodimethane as Electron-Transfer Mediator in Amperometric Glucose Sensor.* Microchemical Journal, 1996. **53**: p. 296-302.

136. Lau, K.-T., S.A.L.d. Fortescu, L.J. Murphy, and J.M. Slater, *Disposable Glucose Sensors for Flow Injection Analysis Using Substituted 1,4-Benzoquinone Mediators.* Electroanalysis, 2003. **15**(11): p. 975-981.

137. Iwuoha, E.I., A.R. Williams, and L.A. Hall, *Novel Electron Transfer Mediators for Amperometric Bioelectrodes: Introduction of Methylsquarate and Phenylsquarate.* Electroanalysis, 2002. **14**(17): p. 1177-1184.

138. Ganesan, N., A.P. Gadre, M. Paranjape, and J.F. Currie, *Gold layer-based dual crosslinking procedure of glucose oxidase with ferrocene monocarboxylic acid provides a stable biosensor.* Analytical Biochemistry, 2005. **343**: p. 188-191.

139. Bean, L.S., L.Y. Heng, B.M. Yamin, and M. Ahmad, *Photocurable ferrocene-containing poly(2-hydroxyl ethyl methacrylate) films for mediated amperometric glucose biosensor.* Thin Solid Films, 2005. **477**: p. 104-110.

140. Miao, Y., J. Chen, and Y. Hu, *Electrodeposited nonconducting polytyramine for the development of glucose biosensors.* Analytical Biochemistry, 2005. **339**: p. 41-45.

141. Nakabayashi, Y. and H. Yoshikawa, *Amperometric Biosensors for Sensing of Hydrogen Peroxide Besed on Electron Transfer between Horseradish Peroxidase and Ferrocene as a Mediator.* Analytical Sciences, 2000. **16**: p. 609-613.

142. Ghica, M.E. and C.M.A. Brett, *A glucose biosensor using methyl viologen redox mediator on carbon film electrodes.* Analytica Chimica Acta, 2005. **532**: p. 145-151.

143. Liang, L., J. Liu, J. Charles F. Windisch, G.J. Exarhos, et al., *Direct Assembly of Large Arrays of Oriented Conducting Polymer Nanowires.* Angewandte Chemie, International Edition, 2002. **41**(19): p. 3665-3668.

144. Lima, S.H., J. Weia, J. Lina, Q. Lib, et al., *A glucose biosensor based on electrodeposition of palladium nanoparticles and glucose oxidase onto Nafion-solubilized carbon nanotube electrode.* Biosensors and Bioelectronics, 2005. **20**: p. 2341-2346.

145. Liu, G., Y. Lin, V. Ostatna, and J. Wang, *Enzyme nanoparticles-based electronic biosensor.* Chemical Communications, 2005: p. 3481-3483.

146. Lin, Y., F. Lu, Y. Tu, and Z. Ren, *Glucose Biosensors Based on Carbon Nanotube Nanoelectrode Ensembles.* Nano Letters, 2004. **4**(2): p. 191-195.

147. Wang, M., F. Zhao, Y. Liu, and S. Dong, *Direct electrochemistry of microperoxidase at Pt microelectrodes modified with carbon nanotubes.* Biosensors and Bioelectronics, 2005. **21**: p. 159-166.

148. Jia, H., G. Zhu, B. Vugrinovich, W. Kataphinan, et al., *Enzyme-carrying polymeric nanofibers prepared via electrospinning for use as unique biocatalysts.* Biotechnology progress, 2002. **18**(5): p. 1027-1032.

149. Zhao, Y.-D., W.-D. Zhang, H. Chen, and Q.-M. Luo, *Direct electron transfer of glucose oxidase molecules adsorbed onto carbon nanotube powder microelectrode.* Analytical Sciences, 2002. **18**(8): p. 939-941.

150. Musameh, M., J. Wang, A. Merkoci, and Y. Lin, *Low-potential stable NADH detection at carbon-nanotube-modified glassy carbon electrode.* Electrochem. Commun., 2002. **4**: p. 743.

151. Gooding, J.J., R. Wibowo, J.Q. Liu, W. Yang, et al., *Protein electrochemistry using aligned carbon nanotube arrays.* Journal of the American Chemical Society, 2003. **125**: p. 9006.

152. Yu, X., D. Chattopadhyay, I. Galeska, F. Papadimitrakopoulos, et al., *Peroxidase activity of enzymes bound to the ends of single-wall carbon nanotube forest electrodes.* Electrochem. Commun., 2003. **5**(5): p. 408.

153. Shin, M.-C. and H.-S. Kim, *Electrochemical characterization of polypyrrole/glucose oxidase biosensor.* Biosensors and Bioelectronics, 1996. **11**: p. 161-169.

154. Linke, B., W. Kernerl, M. Kiwit, M. Pishko, et al., *Amperometric biosensor for in vivo glucose sensing based on glucose oxidase immobilized in a redox hydrogel.* Biosensors & Bioelectronics, 1994. **9**: p. 151-158.

155. Scheller, F., A. Warsinke, J. Lutter, R. Renneberg, et al., *Multienzyme biosensor*, in *Biosensor and Chemical Sensors*, P.G. Edelman and J. Wang, Editors. 1992.

156. Wollenberger, U., F. Schubert, D. Pfeiffer, and F.W. Scheller, *Enhancing biosensor performance using multienzyme systems.* Trends in biotechnology, 1993. **11**(6): p. 255-262.

157. Kim, N., Y. Choi, S. Jung, and S. Kim, *Effect of initial carbon sources on the performance of microbial fuel cells containing Proteus vulgaris.* Biotechnology and Bioengineering, 2000. **70**(1): p. 109-114.

158. Palmore, G.T.R. and G.M. Whitesides, *Microbial and enzymic biofuel cells.* ACS Symposium Series, 1994. **566**(Enzymatic Conversion of Biomass for Fuels Production): p. 271-90.

159. Lewis, K., *Biochemical fuel cells.* Bacteriological Reviews, 1966. **30**(1): p. 101-13.

160. Katz, E., N.A. Shipway, and I. Willne, *Biochemical fuel cells*, in *Handbook of fuel cells - Fundamentals technology and applications*, W. Vielstich, A. Lamm, and H.A. Gasteiger, Editors. 2003, John Wiley and Sons Ltd: Chichester. p. 355-381.

161. Chaudhuri, S.K. and D.R. Lovley, *Electricity generation by direct oxidation of glucose in mediatorless microbial fuel cells.* Nature Biotechnology, 2003. **21**(10): p. 1229-1232.

162. Bond, D.R. and D.R. Lovley, *Electricity production by geobacter sulfurreducens attached to electrodes.* Applied and Environmental Microbiology, 2003. **69**(3): p. 1548-1555.

163. Kim, H.J., H.S. Park, M.S. Hyun, I.S. Chang, et al., *A mediator-less microbial fuel cell using a metal reducing bacterium, Shewanella putrefaciense.* Enzyme and Microbial Technology, 2002. **30**(2): p. 145-152.

164. Scouten, W.H., J.H.T. Luong, and R.S. Brown, *Enzyme or protein immobilization techniques for applications in biosensor design.* Trends in Biotechnology, 1995. **13**(5): p. 178-85.

165. Habermuller, K., M. Mosbach, and W. Schuhmann, *Electron-transfer mechanisms in amperometric biosensors.* Fresenius' Journal of Analytical Chemistry, 2000. **366**(6-7): p. 560-568.

166. Varfolomeev, S.D., I.N. Kurochkin, and A.I. Yaropolov, *Direct electron transfer effect biosensors.* Biosensors & Bioelectronics, 1996. **11**(9): p. 863-871.

167. Tarasevich, M.R., V.A. Bogdanovskaya, N.M. Zagudaeva, and A.V. Kapustin, *Composite materials for direct bioelectrocatalysis of the hydrogen and oxygen reactions in biofuel cells.* Russian Journal of Electrochemistry, 2002. **38**(3): p. 335.

168. Bullen, R.A., T.C. Arnot, J.B. Lakeman, and F.C. Walsh, *Biofuel cells and their development.* Biosensors & Bioelectronics, 2006. **21**(11): p. 2015-2045.

169. Marcus, R.A., *Electron transfer reactions in chemistry. Theory and experiment.* Reviews of Modern Physics, 1993. **65**(3, Pt. 1): p. 599-610.

170. Marcus, R.A. and N. Sutin, *Electron transfers in chemistry and biology.* Biochimica et Biophysica Acta, Reviews on Bioenergetics, 1985. **811**(3): p. 265-322.

171. Willner, I., V. Heleg-Shabtai, R. Blonder, E. Katz, et al., *Electrical Wiring of Glucose Oxidase by Reconstitution of FAD-Modified Monolayers Assembled onto Au-Electrodes.* Journal of the American Chemical Society, 1996. **118**(42): p. 10321-10322.

172. Guiseppi-Elie, A., C. Lei, and R.H. Baughman, *Direct electron transfer of glucose oxidase on carbon nanotubes.* Nanotechnology, 2002. **13**(5): p. 559-564.

173. Zhao, Y.-D., W.-D. Zhang, H. Chen, and Q.-M. Luo, *Direct electron transfer of glucose oxidase molecules adsorbed onto carbon nanotube powder microelectrode.* Anal. Sci., 2002. **18**(8): p. 939-41.

174. Cai, C. and J. Chen, *Direct electron transfer of glucose oxidase promoted by carbon nanotubes.* Analytical Biochemistry, 2004. **332**(1): p. 75-83.

175. Govil, G. and A. Saran, *Biochemical fuel cells.* Journal of the Indian Chemical Society, 1982. **59**(11-12): p. 1226-8.

176. Heller, A., *Miniature biofuel cells.* Physical Chemistry Chemical Physics, 2004. **6**(2): p. 209-216.

177. Chen, T., S.C. Barton, G. Binyamin, Z. Gao, et al., *A Miniature Biofuel Cell.* Journal of the American Chemical Society, 2001. **123**(35): p. 8630-8631.

178. Mano, N., F. Mao, W. Shin, T. Chen, et al., *A miniature biofuel cell operating at 0.78 V.* Chemical Communications, 2003(4): p. 518-519.

179. Mano, N., F. Mao, and A. Heller, *A Miniature Biofuel Cell Operating in A Physiological Buffer.* Journal of the American Chemical Society, 2002. **124**(44): p. 12962-12963.

180. Mano, N., F. Mao, and A. Heller, *Characteristics of a miniature compartment-less glucose-O2 biofuel cell and its operation in a living plant.* Journal of the American Chemical Society, 2003. **125**(21): p. 6588-6594.

181. Soukharev, V., N. Mano, and A. Heller, *A Four-Electron O2-Electroreduction Biocatalyst Superior to Platinum and a Biofuel Cell Operating at 0.88 V.* Journal of the American Chemical Society, 2004. **126**(27): p. 8368 -8369.

182. Minteer, S.D., N.L. Akers, and C.M. Moore, *Enzyme immobilization for use in biofuel cells and sensors*, in *U.S. Pat. Appl. Publ.* 2004, (St. Louis University, USA). US. p. 33 pp., which.

183. Ogihara, H., S. Takenaka, I. Yamanaka, and K. Otsuka, *Reduction of NO with the carbon nanofibers formed by methane decomposition.* Carbon, 2004. **42**(8-9): p. 1609-1617.

184. Park, C. and R.T.K. Baker, *Catalytic Behavior of Graphite Nanofiber Supported Nickel Particles. 2. The Influence of the Nanofiber Structure.* Journal of Physical Chemistry B, 1998. **102**(26): p. 5168-5177.

185. Gao, C., M.J. Whitcombe, and E.N. Vulfson, *Enzymatic synthesis of dimeric and trimeric sugar-fatty acid esters.* Enzyme and Microbial Technology, 1999. **25**(3-5): p. 264-270.

186. Klefenz, H., *Nanobiotechnology: From molecules to systems.* Engineering in Life Sciences, 2004. **4**(3): p. 211-218.

187. Raffaelle, R.P., B.J. Landi, J.D. Harris, S.G. Bailey, et al., *Carbon nanotubes for power applications.* Materials Science & Engineering, B: Solid-State Materials for Advanced Technology, 2005. **B116**(3): p. 233-243.

188. Wang, Z.-G., Z.-K. Xu, L.-S. Wan, J. Wu, et al., *Nanofibrous membranes containing carbon nanotubes: electrospun for redox enzyme immobilization.* Macromolecular Rapid Communications, 2006. **27**(7): p. 516-521.

189. Sawicka, K., P. Gouma, and S. Simon, *Electrospun biocomposite nanofibers for urea biosensing.* Sensors and Actuators, B: Chemical, 2005. **B108**(1-2): p. 585-588.

190. Rege, K., N.R. Raravikar, D.-Y. Kim, L.S. Schadler, et al., *Enzyme-Polymer-Single Walled Carbon Nanotube Composites as Biocatalytic Films.* Nano Letters, 2003. **3**(6): p. 829-832.

191. Wang, S.G., Q. Zhang, R. Wang, S.F. Yoon, et al., *Multi-walled carbon nanotubes for the immobilization of enzyme in glucose biosensors.* Electrochemistry Communications, 2003. **5**(9): p. 800-803.

192. Davis, J.J., M.L.H. Green, H.A.O. Hill, Y.C. Leung, et al., *The immobilization of proteins in carbon nanotubes.* Inorganica Chimica Acta, 1998. **272**(1,2): p. 261-266.

193. Jia, H., G. Zhu, and P. Wang, *Catalytic behaviors associated with enzymes attached to nanoparticles: the effect of particle mobility.* Biotechnology and Bioengineering, 2003. **84**(4): p. 406-414.

194. Qhobosheane, M., S. Santra, P. Zhang, and W. Tan, *Biochemically functionalized silica nanoparticles.* Analyst (Cambridge, U. K.), 2001. **126**(8): p. 1274-1278.

195. Heilmann, A., N. Teuscher, A. Kiesow, D. Janasek, et al., *Nanoporous aluminum oxide as a novel support material for enzyme biosensors.* Journal of Nanoscience and Nanotechnology, 2003. **3**(5): p. 375-379.

196. El-Zahab, B., H. Jia, and P. Wang, *Enabling multienzyme biocatalysis using nanoporous materials.* Biotechnology and Bioengineering, 2004. **87**(2): p. 178-183.

197. Kim, J.K., J.K. Park, and H.K. Kim, *Synthesis and characterization of nanoporous silica support for enzyme immobilization.* Colloids and Surfaces a-Physicochemical and Engineering Aspects, 2004. **241**(1-3): p. 113-117.

198. Wang, P., S. Dai, S.D. Waezsada, A.Y. Tsao, et al., *Enzyme stabilization by covalent binding in nanoporous sol-gel glass for nonaqueous biocatalysis.* Biotechnology and Bioengineering, 2001. **74**(3): p. 249-255.

199. Kim, J., H. Jia, and P. Wang, *Challenges in biocatalysis for enzyme-based biofuel cells.* Biotechnology Advances, 2006. **24**(3): p. 296-308.

200. Xiao, Y., F. Patolsky, E. Katz, J.F. Hainfeld, et al., *"Plugging into Enzymes": Nanowiring of Redox Enzymes by a Gold Nanoparticle.* Science, 2003. **299**(5614): p. 1877-1881.

201. Bachas, L.G., S.A. Law, V. Gavalas, J.C. Ball, et al., *Development of amperometric biosensors by integrating enzymes with carbon nanotube sol-gel composites*, in *Abstracts of Papers, 223rd ACS National Meeting, Orlando, FL, United States, April 7-11, 2002*. 2002. p. ANYL-064.

202. Nguyen, C.V., L. Delzeit, A.M. Cassell, J. Li, et al., *Preparation of nucleic acid functionalized carbon nanotube arrays.* Nano Letters, 2002. **2**(10): p. 1079-1081.

203. Sotiropoulou, S. and N.A. Chaniotakis, *Carbon nanotube array-based biosensor.* Analytical and Bioanalytical Chemistry, 2003. **375**(1): p. 103-105.

204. Wang, J., M. Musameh, and Y. Lin, *Solubilization of carbon nanotubes by nafion toward the preparation of amperometric biosensors.* Journal of the American Chemical Society, 2003. **125**(9): p. 2408-2409.

205. Xue, H., W. Sun, B. He, and Z. Shen, *Single-wall carbon nanotubes as immobilization material for glucose biosensor.* Synthetic Metals, 2003. **135-136**: p. 831-832.

206. Yu, X., D. Chattopadhyay, I. Galeska, F. Papadimitrakopoulos, et al., *Peroxidase activity of enzymes bound to the ends of single-wall carbon nanotube forest electrodes.* Electrochemistry Communications, 2003. **5**(5): p. 408-411.

207. Chen, J., J. Bao, C. Cai, and T. Lu, *Electrocatalytic oxidation of NADH at an ordered carbon nanotubes modified glassy carbon electrode.* Analytica Chimica Acta, 2004. **516**(1-2): p. 29-34.

208. *Directive 2003/30/EC of The European Parliament and of the Council on the promotion of the use of biofuels or other renewable fuels for transport.*, in *Official Journal of the European Union*.

209. *National Biodiesel Board News Release*.

210. Hornandberg, G.A., J.A. Mattis, and J. Michael Laskowski, *Synthesis of Peptide Bonds by Proteinases. Addition of Organic Cosolvents Shifts Peptide Bond Equilibria toward Synthesis.* Biochemistry, 1978. **17**(24): p. 5220-5227.

211. Kaieda, M., T. Samukawa, A. Kondo, and H. Fukuda, *Effect of Methanol and Water Contents on Production of Biodiesel Fuel from Plant Oil Catalyzed by Various Lipases in a Solvent-Free System.* Journal of Bioscience and Bioengineering, 2001. **91**(1): p. 12-15.

212. Lara, P. and E. Park, *Potential application of waste activated bleaching earth on the production of fatty acid alkyl esters using Candida cylindracea lipase in organic solvent system.* Enzyme and Microbial Technology, 2004 **34**(3-4): p. 270-277.

213. Chang, H.-M., H.-F. Liao, C.-C. Lee, and C.-J. Shieh, *Optimized synthesis of lipase-catalyzed biodiesel by Novozym 435.* Journal of Chemical Technology and Biotechnology, 2005. **80**: p. 307-312.

214. Xu, Y., W. Du, J. Zeng, and D. Liu, *Conversion of Soybean Oil to Biodiesel Fuel Using Lipozyme TL IM in a Solvent-free Medium.* Biocatalysis and Biotransformation, 2004. **22**(1): p. 45-48.

215. Truniger, V. and W. Boos, *Mapping and Cloning of gldA, the Structural Gene of the Escherichia coli Glycerol Dehydrogenase.* Journal of Bacteriology, 1994. **176**(6): p. 1796-1800.

216. *Glycerol Dehydrogenase from Cellulomonas sp.*

217. Pierce, *Coomassie (Bradford) Protein Assay Kit.*

218. R.Blattner, F., V. Burland, G.P. III, H. J.Sofia, et al., *Analysis of the Escherichia cofi genome. IV. DNA sequence of the region from 89.2 to 92.8 minutes.* Nucleic Acids Research, 1993. **21**(23): p. 5408-5417.

219. Hou, H. and D.H. Reneker, *Carbon Nanotubes on Carbon Nanofibers: A Novel Structure Based on Electrospun Polymer Nanofibers.* Advanced Materials, 2004. **16**(1): p. 69-73.

220. Yamada, H., A. Nagao, H. Nishise, and Y. Tani, *Glycerol dehydrogenase from Cellulomonas sp. NT3060: Purification and characterization.* Agricultural and Biological Chemistry, 1982. **46**: p. 2333-2339.

221. Plaisantin, H., R. Pailler, A. Guette, G. Daude, et al., *Conversion of cellulosic fibres into carbon fibres: a study of the mechanical properties and correlation with chemical structure.* . Composites Science and Technology, 2001. **61**: p. 2063-2068.

222. Kim, D.-Y., Y. Nishiyama, M. Wada, and S. Kuga, *Graphitization of highly crystalline cellulose.* Carbon, 2001. **39**: p. 1051-1056.

223. Peng, S., H. Shao, and X. Hu, *Lyocell fibers as the precursor of carbon fibers.* Journal of Applied Polymer Science, 2003. **90**: p. 1941-1947.

224. Polarz, S., B. Smarsly, and J.H. Schattka, *Hierachical porous carbon structures from cellulose acetate fibers.* Chemistry of Materials, 2002. **14**: p. 2940-2945.

225. Li, P., Q. Zhao, X. Zhou, W. Yuan, et al., *Enhanced Distribution and Anchorage of Carbon Nanofibers Grown on Structured Carbon Microfibers.* J. Phys. Chem. C, Article ASAP, 2008.

226. Amatore, C. and E. Maisonhaute, *When voltammetry reaches nanoseconds.* Anal. Chem. , 2005. **77**(15): p. 303A-311A.

227. Baltes, N., L. Thouin, C. Amatore, and J. Heinze, *Imaging Concentration Profiles of Redox-Active Species with Nanometric Amperometric Probes: Effect of Natural Convection on Transport at Microdisk Electrodes.* Angew Chem Int Ed Engl., 2004. **43**(11): p. 1431-1435.

228. Wightman, R.M., *Voltammetry with Microscopic Electrodes in New Domains.* Science, 1988. **240**: p. 415-420.

229. Du, F., W. Huang, Y. Shi, Z. Wang, et al., *Real-time monitoring of NO release from single cells using carbon fiber micro-disk electrodes modified with single-walled carbon nanotubes.* Biosensors & Bioelectronics, 2008. **24**(3): p. 415-421.

230. Bruns, D., *Detection of transmitter release with carbon fiber electrodes.* Methods, 2004. **33**(4): p. 312-321.

231. Robinson, D.L., A. Hermans, A.T. Seipel, and R.M. Wightman, *Monitoring Rapid Chemical Communication in the Brain.* Chemical Reviews 2008. **108**(7): p. 2554-2584.

232. Valcarcel, M., S. Cardenas, and B.M. Simonet, *Role of Carbon Nanotubes in Analytical Science.* Analytical Chemistry, 2007. **79**(13): p. 4788-4797.

233. Zayats, M., B. Willner, and I. Willner, *Design of Amperometric Biosensors and Biofuel Cells by the Reconstitution of Electrically Contacted Enzyme Electrodes.* Electroanalysis, 2008. **20**(6): p. 583 - 601.

234. Aguei, L., P. Yanez-Sedeno, and J.M. Pingarron, *Role of carbon nanotubes in electroanalytical chemistry.* Analytica Chimica Acta, 2008. **622**(1-2): p. 11-47.

235. Kim, J., J.W. Grate, and P. Wang, *Nanobiocatalysis and its potential applications* Trends in biotechnology, 2008. **26**(11): p. 639-646.

236. Viry, L., A. Derré, P. Garrigue, N. Sojic, et al., *Optimized carbon nanotube fiber microelectrodes as potential analytical tools.* Anal. Bioanal. Chem., 2007. **389**: p. 499-505.

237. Vigolo, B., A. Pénicaud, C. Coulon, C. Sauder, et al., *Macroscopic Fibers and Ribbons of Oriented Carbon Nanotubes.* Science, 2000. **290**(5495): p. 1331-1334.

238. Wang, J., R.P. Deo, P. Poulin, and M. Mangey, *Carbon Nanotube Fiber Microelectrodes.* J. Am. Chem. Soc., 2003. **125**(48): p. 14706-14707.

239. Brunauer, S., P.H. Emmett, and E. Teller, *Adsorption of gases in multimolecular layers.* JACS, 1938. **60**: p. 309-319.

240. Brett, C.M.A. and A.M.O. Brett, *Electrochemistry: Principles, Methods, and Applications* 1993, New York: Oxford University Press 472.

241. Walters, R.R., J.F. Graham, R.M. Moore, and D.J. Anderson, *Protein Diffusion Coefficient Measurements by Laminar Flow Analysis: Method and Applications.* Analytical Biochemistry, 1984. **14**: p. 190-195.

242. Wang, Y., S. Serrano, and J.J. Santiago-Aviles, *Conductivity measurement of electrospun PAN-based carbon nanofiber.* Journal of Materials Science Letters, 2002. **21**: p. 1055-1057.

243. Hayes, M.A. and W.G. Kuhr, *Preservation of NADH Voltammetry for Enzyme-Modified Electrodes Based on Dehydrogenase.* Analytical Chemistry, 1999. **71**(9): p. 1720-1727.

244. Kumar, S.A. and S.-M. Chen, *Electroanalysis of NADH using conducting and redox active polymer/carbon nanotubes modified electrodes - a review.* Sensors, 2008. **8**(2): p. 739-766.

245. Ju, H. and D. Leech, *$[Os(bpy)_2(PVI)_{10}ClCl$ polymer-modified carbon fiber electrodes for the electrocatalytic oxidation of NADH.* Analytica Chimica Acta, 1997. **345**: p. 51.

246. Álvarez-González, M.I., S.B. Saidman, M.J. Lobo-Castanon, A.J. Miranda-Ordieres, et al., *Electrocatalytic Detection of NADH and Glycerol by NAD+-Modified Carbon Electrodes.* Analytical Chemistry, 2000. **72**: p. 520-527.

247. Wang, J., A. Kaede, and M. Mustafa, *Carbon-nanotube-modified glassy carbon electrodes for amplified label-free electrochemical detection of DNA hybridization.* Analyst, 2003. **128**: p. 912-916.

248. Musameh, M., J. Wang, A. Merkoci, and Y. Lin, *Low-potential stable NADH detection at carbon-nanotube-modified glassy carbon electrode.* Electrochemistry Communications, 2002. **4**: p. 743.

249. Wang, J. and M. Musameh, *Carbon Nanotube/Teflon Composite Electrochemical Sensors and Biosensors.* Anal. Chem., 2003. **75**: p. 2075-2079.

250. Zhang, M., A. Smith, and W. Gorski, *Carbon Nanotube-Chitosan System for Electrochemical Sensing Based on Dehydrogenase Enzymes.* Analytical Chemistry, 2004. **76**: p. 5045-5050.

251. Moore, R.R., C.E. Banks, and R.G. Compton, *Basal Plane Pyrolytic Graphite Modified Electrodes: Comparison of Carbon Nanotubes and Graphite Powder as Electrocatalysts.* Anal. Chem., 2004. **76**: p. 2677-2682.

252. Valentini, F., A. Salis, A. Curulli, and G. Palleschi, *Chemical Reversibility and Stable Low-Potential NADH Detection with Nonconventional Conducting Polymer Nanotubule Modified Glassy Carbon Electrodes.* Anal. Chem., 2004. **76**: p. 3244-3248.

253. Federica, V. and P. Giuseppe, *Carbon nanotubes as electrode materials for the assembling of new electrochemical biosensors.* Sens. Actuators B, 2004. **100**: p. 117-125.

254. Liu, J., S. Tian, and W. Knoll, *Properties of Polyaniline/Carbon Nanotube Multilayer Films in Neutral Solution and Their Application for Stable Low-Potential Detection of Reduced β-Nicotinamide Adenine Dinucleotide.* Langmuir, 2005. **21**: p. 5596-5599.

255. Riccarda, A., L. Irma, and M. Franco, *Electrocatalytic oxidation of NADH at single-wall carbon-nanotube-paste electrodes: kinetic considerations for use of a redox mediator in solution and dissolved in the paste.* Anal. Bioanal., 2005. **381**(7): p. 1355-1361.

256. Rao, C.N.R., B.C. Satishkumar, A. Govindaraj, and M. Nath, *Nanotubes.* Chem. Phys. Chem., 2001. **2**: p. 78 -105.

257. Pariente, F., F. Tobalina, G. Moreno, L. Hernandez, et al., *Mechanistic Studies of the Electrocatalytic Oxidation of NADH and Ascorbate at Glassy Carbon Electrodes Modified with Electrodeposited Films Derived from 3,4-Dihydroxybenzaldehyde.* Analytical Chemistry, 1997. **69**: p. 4065.

258. Zhu, L., J. Zhai, R. Yang, C. Tian, et al., *Electrocatalytic oxidation of NADH with Meldola's blue functionalized carbon nanotubes electrodes.* Biosensors and Bioelectronics, 2007. **22**: p. 2768-2773.

259. Zhou, D.-m., H.-Q. Fang, H.-y. Chen, H.-x. Ju, et al., *The electrochemical polymerization of methylene green and its electrocatalysis for the oxidation of NADH.* Analytica Chimica Acta, 1996. **329**(1-2): p. 41-48.

260. Polysciences, I., *PolyLink Protein coupling Kit for COOH microspheres.* 2007.

261. Biondi, P.A., E. Passero, S. Soncin, C. Bernardi, et al., *Selective Determination of Dihydroxyacetone in Self-Tanning Creams by HPLC as Pentafluorobenzyloxime Derivative.* Chromatographia, 2007. **65**: p. 65-68.

262. Sawieki, E., R.A. Carnes, and R. Sehumacher, *Spectrophotofluorimetric Determination of 3-Carbon Fragments and Their Precursors with Anthrone. Application to Air Pollution.* Mikrochim. Acta, 1967. **5**: p. 61-68.

263. Raj, C.R. and B.K. Jena, *Efficient electrocatalytic oxidation of NADH at gold nanoparticles self-assembled on three-dimensional sol-gel network.* CHEM. COMMUN., 2005: p. 2005-2007.

264. Grundig, B., G. Wittstock, U. Rudel, and B. Strehlitz, *Mediator-modified electrodes for electrocatalytic oxidation of NADH.* Journal of Electroanalytical Chemistry, 1995. **395**: p. 143.

265. Mano, N. and A. Kuhn, *Immobilized nitro-fluorenone derivatives as electrocatalysts for NADH oxidation.* J. Electroanal. Chem., 1999. **477**: p. 79-88.

266. Wu, Q., M. Maskus, F. Pariente, F. Tobalina, et al., *Electrocatalytic Oxidation of NADH at Glassy Carbon Electrodes Modified with Transition Metal Complexes Containing 1,10-Phenanthroline-5,6-dione Ligands.* Anal. Chem. , 1996. **68**: p. 3688-3696.

267. Wang, P., *Nanoscale biocatalyst systems.* Current Opinion in Biotechnology, 2006. **17**(6): p. 574-579.

268. Schmid, R.D. and V.B. Urlacher, eds. *Modern Biooxidation* 1st ed. 2007, Wiley-VCH.

269. Okuda, K., A.C. Seila, and S.A. Strobel, *Uncovering the Enzymatic pKa of the Ribosomal Peptidyl Transferase Reaction Utilizing a Fluorinated Puromycin Derivative.* Biochemistry, 2005. **44**: p. 6675-6684.

270. Fish, R.H., J.B. Kerr, and C.H. Lo, *NAD(P) mimic for use in enzymic redox reactions* 2002. p. 63

271. Hummel, W., *Large-scale applications of NAD(P)-dependent oxidoreductases: recent developments.* Trends in Biotechnology, 1999. **17**(12): p. 487-492.

272. I.Willner, Y.-M. Yan, B.Willner, and R. Tel-Vered, *Integrated Enzyme-Based Biofuel Cells - A Review.* FUEL CELLS, 2009. **09**(1): p. 7-24.

273. Ivnitski, D., K. Artyushkova, R.A. Rincón, P. Atanassov, et al., *Entrapment of Enzymes and Carbon Nanotubes in Biologically Synthesized Silica: Glucose Oxidase-Catalyzed Direct Electron Transfer.* Small, 2008. **4**(3): p. 357-364.

274. Cooney, M.J., V. Svoboda, C. Lau, G. Martina, et al., *Enzyme catalysed biofuel cells.* Energy Environ. Sci., 2008. **1**: p. 320-337.

275. Matsushita, M., T. Irino, T. Komoda, and Y. Sakagishi, *Determination of proteins by a reverse biuret method combined with the copper-bathocuproine chelate reaction.* Clinica Chimica Acta, 1993. **216**(1-2): p. 103-111.

276. Peigney, A., C. Laurent, E. Flahaut, R.R. Bacsa, et al., *Specific surface area of carbon nanotubes and bundles of carbon nanotubes.* Carbon, 2001. **39**: p. 507-514.

277. Bockris, J.O.M. and S. Srinivasan, *Fuel Cells: Their Electrochemistry*. 1969, New York: McGraw-Hill. 612-619.

278. Aston, W.J. and A.P.F. Turner, *Biosensors and biofuel cells.* Biotechnology & Genetic Engineering Reviews, 1984. **1**: p. 89-120.

279. Katz, E., B. Filanovsky, and I. Willner, *A biofuel cell based on two immiscible solvents and glucose oxidase and microperoxidase-11 monolayer-functionalized electrodes.* New Journal of Chemistry, 1999. **23**(5): p. 481-487.

280. Moore, C.M., N.L. Akers, A.D. Hill, Z.C. Johnson, et al., *Improving the Environment for Immobilized Dehydrogenase Enzymes by Modifying Nafion with Tetraalkylammonium Bromides.* Biomacromolecules, 2004. **5**(4): p. 1241-1247.

281. I.Willner1, Y.-M. Yan, B.Willner, and R. Tel-Vered, *Integrated Enzyme-Based Biofuel Cells - A Review.* FUEL CELLS, 2009. **09**(1): p. 7-24.

282. Grabarek, Z. and J. Gergely, *Zero-length crosslinking procedure with the use of active esters.* Analytical Biochemistry, 1990. **185**(1): p. 131-5.

283. Kawaguchi, S., A. Yekta, and M.A. Winnik, *Surface Characterization and Dissociation Properties of Carboxylic Acid Core-Shell Latex Particle by Photentiometric and Conductometric Titration.* Journal of Colloid and Interface Science, 1995. **176**: p. 362-369.

284. Islam, M., T. Ohashi, T. Yasukawa, H. Shiku, et al., *Use of quinone as a mediator at anode in a glucose /O_2 biofuel cell.* Chem Sens 2004. **20**: p. 744-745.

285. Tsutsui, S., K. Sakamoto, H. Yoshida, and A. Kunai, *Cyclic voltammetry and theoretical calculations of silyl-substituted 1,4-benzoquinones.* Journal of Organometallic Chemistry, 2005. **690**: p. 1324-1331.

286. Kulys, J., T. Buch-Rasmussen, K. Bechgaard, V. Razumas, et al., *Study of the new electron transfer mediators in glucose oxidase catalysis.* Journal of Molecular Catalysis, 1994. **3**(407-420).

287. Gibson, Q.H., B.E.P. Swoboda, and V. Massey, *Kinetics and mechanism of action of glucose oxidase.* Journal of Biological Chemistry, 1964. **239**(11): p. 3927-3934.

288. Marangoni, A.G., *Enzyme kinetics---A modern approach*. 2003, Hoboken, New Jersey: John Wiley &Sons, Inc. . 229.

289. Yan, Y., W. Zheng, L. Su, and L. Mao, *Carbon-Nanotube-Based Glucose/O2 Biofuel Cells.* Advanced Materials, 2006. **18**: p. 2639-2643.

290. Kuwabata, S., R. Tsuda, and H. Yoneyama, *Electrochemical Conversion of Carbon Dioxide to Methanol with the Assistance of Formate Dehydrogenase and Methanol Dehydrogenase as Biocatalysts.* J. Am. Chem. SOC., 1994. **116**: p. 5431-5443.

291. Gattrell, M., N. Gupta, and A. Co, *A review of the aqueous electrochemical reduction of CO_2 to hydrocarbons at copper.* Journal of Electroanalytical Chemistry, 2006. **594** p. 1-19.

292. Centi, G., S. Perathoner, A. Wineab, and M. Gangeri, *Electrocatalytic conversion of CO_2 to long carbon-chain hydrocarbons.* Green Chem., 2007. **9**(671-678).

293. Sullivan, B.P., K. Krist, and H.E. Guard, eds. *Electrochemical and Electrocatalytic Reactions of Carbon Dioxide*. 1993, Elsevier: Amsterdam New York.

294. Mahmood, M.N., D. Masheder, and C.J. Harty, *Use of gas-diffusion electrodes for high-rate electrochemical reduction of carbon dioxide. I. Reduction at lead, indium- and tin-impregnated electrodes.* Journal of Applied Electrochemistry, 1987. **16**(6): p. 1159-1170.

295. Li, H. and C. Oloman, *The electro-reduction of carbon dioxide in a continuous reactor.* Journal of Applied Electrochemistry, 2005. **35**: p. 955-965.

296. Li, H. and C. Oloman, *Development of a continuous reactor for the electro-reduction of carbon dioxide to formate-Part 1:process variables.* JOURNAL OF APPLIED ELECTROCHEMISTRY, 2006. **36**: p. 1105-1115.

297. Yamamoto, T., D.A. Tryk, K. Hashimoto, A. Fujishima, et al., *Electrochemical Reduction of CO2 in the Micropores of Activated Carbon Fibers.* Journal of The Electrochemical Society, 2000. **147**(9): p. 3393-3400.

298. Suzuki, O. and K. Watanabe, *Drugs and Poisons in Humans: A Handbook of Practical Analysis.* Birkhäuser, 2005: p. 123.

299. Yoshitake, H., K. Takahashi, and K.-i. Ota, *Electrochemical Reduction of CO, on Hydrogen-enriched and Hydrogen-depleted Surfaces.* J. Chem. Soc. Faraday Trans. , 1994. **90**(1): p. 155-159.

300. Kanada, R., L. Pan, S. Akita, N. Okazaki, et al., *Synthesis of Multiwalled Carbon Nanocoils Using Codeposited Thin Film of Fe-Sn as Catalyst.* Japanese Journal of Applied Physics, 2008. **47**(4): p. 1949–1951.

301. Hu, R.Z., L. Zhang, X. Liu, M.Q. Zeng, et al., *Investigation of immiscible alloy system of Al-Sn thin films as anodes for lithium ion batteries.* Electrochemistry Communications, 2008. **10**(7): p. 1109-1112

302. Schröder, D., C.A. Schalley, J.N. Harvey, and H. Schwarz, *On the formation of the carbon dioxide anion radical $CO_2^{\cdot-}$ in the gas phase.* International Journal of Mass Spectrometry, 1999 **185/186/187**: p. 25-35.

APPENDIX

A.1 LB (Luria-Bertani) Medium and Plates

A1.1 LB (Luria-Bertani) Medium

a. Dissolving 10 g of Tryptone (BD-Bacto, 251420), 5 g of Yeast Extract (BD-Bacto, 212730) and 10 g of NaCl (Mallinckrodt Chemicals, 758112) into DI water and make the total volume into 1 L.
b. Autoclave on liquid cycle for 30 minutes.
c. Allow solution to cool to ~55 ^{o}C and added Ampicillin (Fluka, 10044) if needed.
d. Store at room temperature or at +4 ^{o}C.

A1.2 LB Agar plates

a. Prepare LB medium as above, but add 15 g/L agar (BD-Bacto, 214010) before autoclaving.
b. Autoclave on liquid cycle for 30 minutes.
c. After autoclaving, cool to ~55 ^{o}C, add antibiotic and pour into 10 cm plates.
d. Let harden, then invert and store at +4 ^{o}C, in the dark.

A.2 S. O. B. Medium (with Antibiotic)

a. Dissolve 20 g tryptone, 5 g yeast extract, and 0.5 g NaCl in 950 ml deionized water.
b. Make a 250 mM KCl solution by dissolving 1.86 g of KCl in 100ml of deionized water. Add 10 ml of this stock KCl solution to the solution in step a.

c. Adjust pH to 7.5 with 5 M NaOH and add deionized water to 1 liter.

d. Autoclave this solution, cool to ~55 ^{o}C, and add 10 ml of sterile 1 M $MgCl_2$. You may also add antibiotic, if needed.

e. Store at +4 ^{o}C. Medium is stable for only 1-2 weeks.

A.3 10X TAE Buffer (pH 8.18~8.29)

Dissolving 48.4 g Tris-Base (Sigma, T1503), 10.9 g Glacial Acetic Acid (FisherSci, A35-500) and 2.92 g EDTA (free acid f.w.292.25) into DI water, and make the total volume into 1L.

A.4 5X TBE buffer (pH 8.13~8.23)

Dissolving 54.0 g Tris base (Sigma, 93352), 27.5 g Boric acid (Sigma, B0394) and 2.92 g EDTA (FisherSci, BP120-500) into DI water, and make the total volume into 1 L.

A.5 1M IPTG Stocking Solution

a. Dissolve 2.83g of isopropylthio-β-galactoside (Invitrogen, 15529019) in 8 ml H_2O;

b. Bring to a final volume of 10ml with molecular biology grade water;

c. Filter sterilize with 0.22um syringe filter;

d. Store in 1ml aliquots at -20 ^{o}C.

A.6 Lysis Buffer

a. Prepare 1 M stock solution of KH_2PO_4 and K_2HPO_4.

b. For 100 ml, dissolve the following reagents in 90 ml of deionized water:

i. 0.3 ml KH_2PO_4

ii. 4.7 ml K_2HPO_4

iii. 2.3 g NaCl

iv. 0.75 g KCl

v. 10 ml glycerol (Sigma, G5516)

vi. 0.5 ml Triton X-100 (Sigma, T9284)

vii. 68 mg imidazole (Fluka, 56750)

c. Mix thoroughly and adjust pH to 7.8 with HCl. Bring the volume to 100 ml. Store at +4 ^{o}C.

A.7 2X SDS-PAGE Sample Buffer

a. Combine the following reagents:

viii.	0.5 M Tris-HCl, pH 6.8	2.5 ml
ix.	Glycerol (100%)	2.0 ml
x.	β-mercaptoethanol	0.4 ml
xi.	Bromophenol Blue	0.02 g
xii.	SDS	0.4 g

b. Bring the volume to 10 ml with sterile water

c. Aliquot and freeze at -20 ^{o}C until needed.

A.8 Electrophoresis Stain and Destain Solutions

A8.1 Coomassie Blue Staining Stock Solution

Dissolving 0.25g of Coomassie Brilliant Blue R250, 400 ml of methanol and 70 ml of acetic acid into DI H_2O, and make the final volume to 1L.

A8.2 Destain Solution I

Dissolving 400 ml of methanol and 70 ml of acetic acid into DI H_2O and make the final volume to 1L.

A8.3 Destain Solution II

Dissolving 50 ml of methanol and 70 ml of acetic acid into DI H_2O and make the final volume to 1L.

A.9 1X Running Buffer

Mixing 50 ml 20x MOPS SDS Running Buffer and 950 ml DI water.

A.10 1X Running Buffer + Antioxidant

Mixing 200 ml of 1X Running Buffer (above) and 500 µl antioxidant.

A.11 20X NuPAGE® Transfer Buffer

To prepare 20X NuPAGE® Transfer Buffer, dissolve the following reagents in 100 ml of deionized water:

	Concentration (1X)
Bicine	10.2 g 25 mM

Bis-Tris (free base) 13.1 g 25 mM

EDTA 0.75 g 1 mM

Chlorobutanol* 0.025 g 0.05 mM

Mix well and adjust the volume to 125 ml with deionized water. The pH of the buffer is 7.2, and store at room temperature. The buffer is stable for 6 months at room temperature. For transfer, dilute the 20X NuPAGE® Transfer Buffer. *Chlorobutanol is used as a preservative.

A.12 10× TBST

90 g NaCl

100 ml 1 M Tris·Cl, pH 7.5

10 g Tween 20

Add H_2O to 1 liter

For 1× TBST dilute 1 part 10× TBST with 9 parts water prior to use

Store indefinitely at room temperature

A.13 5× Native Purification Buffer

Prepare 200 ml solution (250 mM NaH_2PO_4, pH 8.0, 2.5 M NaCl):

a. Add Sodium phosphate, monobasic 7 g and NaCl 29.2 g to 180 ml deionized water; Mix well and adjust the pH with NaOH to pH 8.0.
b. Bring the final volume to 200 ml with deionized water.
c. Store buffer at room temperature.

A.14 1X Native Purification Buffer

To prepare 100 ml 1X Native Purification Buffer, combine:

a. 80 ml of sterile distilled water;

b. 20 ml of 5X Native Purification Buffer;

c. Mix well and adjust pH to 8.0 with NaOH or HCl.

A.15 Native Binding Buffer:

Use 30 ml of the 1X Native Purification Buffer (Without Imidazole) for use as the Native Binding Buffer (used for column preparation, cell lysis, and binding).

A.16 Native Wash Buffer

To prepare 50 ml Native Wash Buffer with 20 mM imidazole, combine:

a. 50 ml of 1X Native Purification Buffer**;**

b. 335 µl of 3 M Imidazole, pH 6.0;

c. Mix well and adjust pH to 8.0 with NaOH or HCl.

A.17 Native Elution Buffer

To prepare 15 ml Native Elution Buffer with 250 mM imidazole, combine:

a. 13.75 ml of 1X Native Purification Buffer;

b. 1.25 ml of 3 M Imidazole, pH 6.0;

c. Mix well and adjust pH to 8.0 with NaOH or HCl.

A.18 Standard Curve of Protein Concentration of Bradford Method

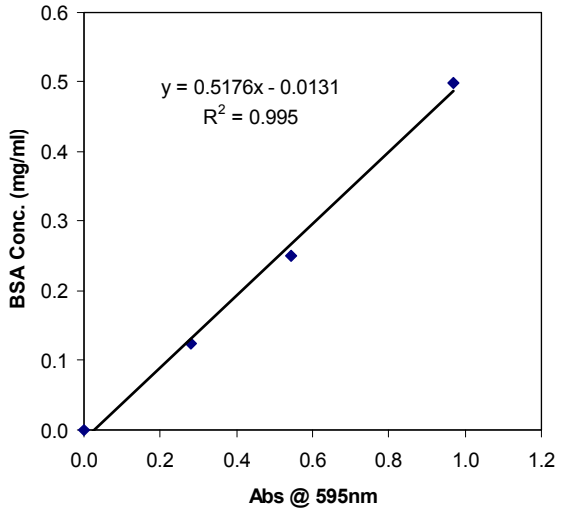

A.19 Calibration curve of DHA concentration by spectrophotofluorimetry

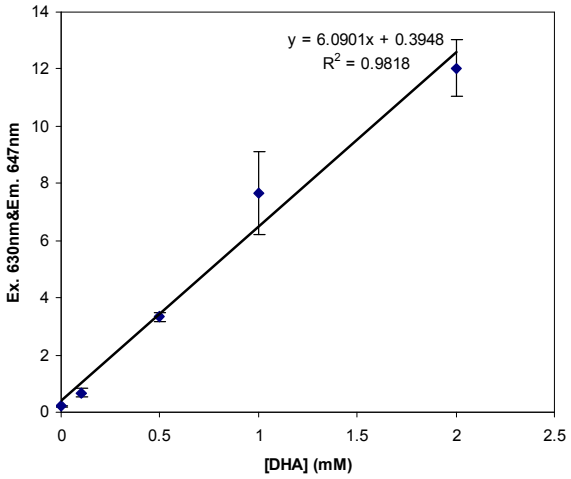

A.20 BET surface area measurements for the samples

Surface Area and Pore Size Distribution Lab.

ASAP 2000 V3.03 A

SAMPLE DIRECTORY/NUMBER: SAC /24
SAMPLE ID: Number 2
SUBMITTER: St Paul
OPERATOR: RAC
UNIT NUMBER: 1
ANALYSIS GAS: Nitrogen

START 12:40:11 01/09/09
COMPL 15:45:19 01/09/09
REPRT 09:38:57 01/12/09
SAMPLE WT: 0.1041 g
FREE SPACE: 54.3215 cc
EQUIL INTRVL: 5 sec

ANALYSIS LOG

RELATIVE PRESSURE	PRESSURE (mmHg)	VOL ADSORBED (cc/g STP)	ELAPSED TIME (HR:MN)	SATURATION PRESS.(mmHg)
			0:38	747.747
0.0592	44.268	7.8140	0:41	
0.0793	59.265	8.2363	0:43	
0.1198	89.601	8.9158	0:44	
0.1398	104.583	9.2201	0:46	
0.1599	119.560	9.4545	0:47	
0.1996	149.260	10.1295	0:48	
0.2499	186.862	10.8387	0:50	
0.2999	224.288	11.6339	0:51	
0.3500	261.781	12.4435	0:53	
0.3998	299.011	13.2551	0:54	
0.4497	336.354	14.0955	0:56	
0.4997	373.791	14.9381	0:58	
0.5496	411.062	15.8688	0:59	
0.5996	448.524	16.9062	1:01	
0.6495	485.811	18.1215	1:02	
0.6994	523.201	19.6286	1:04	
0.7396	553.294	21.0346	1:06	
0.7694	575.588	22.3433	1:08	
0.7996	598.187	23.8280	1:09	
0.8194	613.030	24.9872	1:11	
0.8395	628.042	26.2995	1:13	
0.8593	642.874	27.8101	1:14	
0.8744	654.190	29.1289	1:16	
0.8892	665.293	30.6593	1:18	
0.9044	676.686	32.3733	1:19	
0.9140	683.910	33.7969	1:21	
0.9245	691.797	35.4344	1:23	
0.9321	697.454	36.8020	1:24	
0.9393	702.848	38.2200	1:26	
0.9460	707.916	39.7857	1:28	
0.9521	712.524	41.4138	1:29	
0.9581	717.039	43.1576	1:31	
0.9627	720.442	45.0558	1:33	
0.9676	724.160	47.0484	1:35	
0.9697	725.717	48.2125	1:36	
0.9734	728.494	50.3537	1:38	
0.9760	730.500	51.9040	1:40	
0.9790	732.750	53.5618	1:41	
0.9805	733.934	54.8534	1:43	
0.9836	736.220	56.7885	1:45	
0.9837	736.318	57.9646	1:46	

SAMPLE DIRECTORY/NUMBER: SAC /24
SAMPLE ID: Number 2
SUBMITTER: St Paul
OPERATOR: RAC
UNIT NUMBER: 1
ANALYSIS GAS: Nitrogen

START 12:40:11 01/09/09
COMPL 15:45:19 01/09/09
REPRT 09:38:57 01/12/09
SAMPLE WT: 0.1041 g
FREE SPACE: 54.3215 cc
EQUIL INTRVL: 5 sec

ANALYSIS LOG

RELATIVE PRESSURE	PRESSURE (mmHg)	VOL ADSORBED (cc/g STP)	ELAPSED TIME (HR:MN)	SATURATION PRESS.(mmHg)
0.9875	739.168	60.3082	1:48	
0.9938	743.972	69.9185	1:55	
0.9937	744.013	75.4675	2:01	
0.9776	731.943	69.4285	2:04	
0.9650	722.674	62.9920	2:08	
0.9523	713.093	56.3336	2:12	
0.9521	712.955	55.4043	2:13	
0.9388	703.060	50.3330	2:17	
0.9252	692.929	45.9128	2:20	
0.9094	681.128	42.1099	2:23	
0.9048	677.653	40.9590	2:25	
0.8867	664.134	38.0634	2:27	
0.8749	655.332	36.3198	2:29	
0.8580	642.709	34.3058	2:32	
0.8385	628.125	32.4728	2:34	
0.8188	613.376	30.5849	2:36	
0.7981	597.918	28.9741	2:38	
			2:39	749.143
0.7700	576.829	27.0886	2:41	
0.7359	554.328	25.2939	2:43	
0.6996	524.121	23.3588	2:45	
0.6500	486.948	21.4335	2:47	
0.6000	449.486	19.8253	2:49	
0.5500	412.008	18.4623	2:51	
0.5000	374.572	17.2347	2:53	
0.4516	338.325	16.1871	2:55	
0.3999	299.585	15.2163	2:57	
0.3501	262.247	12.2858	2:59	
0.3007	225.240	11.4687	3:00	
0.2502	187.415	10.6164	3:02	
0.2002	149.988	9.9217	3:04	
0.1461	109.481	9.0403	3:05	

Surface Area and Pore Size Distribution Lab.
ASAP 2000 V3.03 A PAGE 3

SAMPLE DIRECTORY/NUMBER: SAC /24
SAMPLE ID: Number 2
SUBMITTER: St Paul
OPERATOR: RAC
UNIT NUMBER: 1
ANALYSIS GAS: Nitrogen

START 12:40:11 01/09/09
COMPL 15:45:19 01/09/09
REPRT 09:38:57 01/12/09
SAMPLE WT: 0.1041 g
FREE SPACE: 54.3215 cc
EQUIL INTRVL: 5 sec

ISOTHERM PLOT
+ ADS, + DES

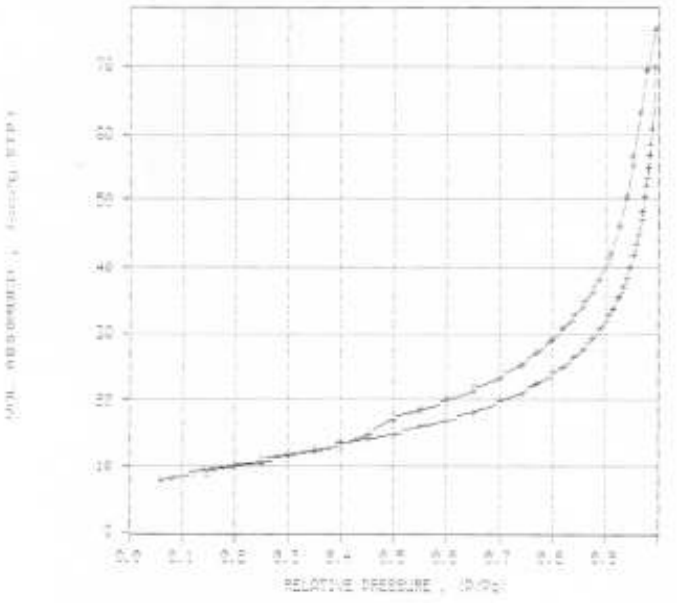

Surface Area and Pore Size Distribution Lab.

ASAP 2000 V3.03 A PAGE 4

SAMPLE DIRECTORY/NUMBER: SAC /24
SAMPLE ID: Number 2
SUBMITTER: St Paul
OPERATOR: RAC
UNIT NUMBER: 1
ANALYSIS GAS: Nitrogen

START 12:40:11 01/09/09
COMPL 15:45:19 01/09/09
REPRT 09:38:57 01/12/09
SAMPLE WT: 0.1041 g
FREE SPACE: 54.3215 cc
EQUIL INTRVL: 5 sec

BET SURFACE AREA REPORT

BET SURFACE AREA:	36.4354	+/-	0.2414	sq. m/g
SLOPE:	0.118402	+/-	0.000784	
Y-INTERCEPT:	0.001075	+/-	0.000105	
C:	111.139191			
VM:	8.369810	cc/g STP		
CORRELATION COEFFICIENT:	9.99934E-01			

RELATIVE PRESSURE	VOL ADSORBED (cc/g STP)	1/ [VA(Po/P - 1)]
0.0592	7.8140	0.008053
0.0793	8.2363	0.010451
0.1198	8.9158	0.015268
0.1599	9.4545	0.020127
0.1996	10.1295	0.024616

Surface Area and Pore Size Distribution Lab.
ASAP 2000 V3.03 A PAGE 5

SAMPLE DIRECTORY/NUMBER: SAC /24
SAMPLE ID: Number 2
SUBMITTER: St Paul
OPERATOR: RAC
UNIT NUMBER: 1
ANALYSIS GAS: Nitrogen

START 12:40:11 01/09/09
COMPL 15:45:19 01/09/09
REPRT 09:38:57 01/12/09
SAMPLE WT: 0.1041 g
FREE SPACE: 54.3215 cc
EQUIL INTRVL: 5 sec

BET PLOT

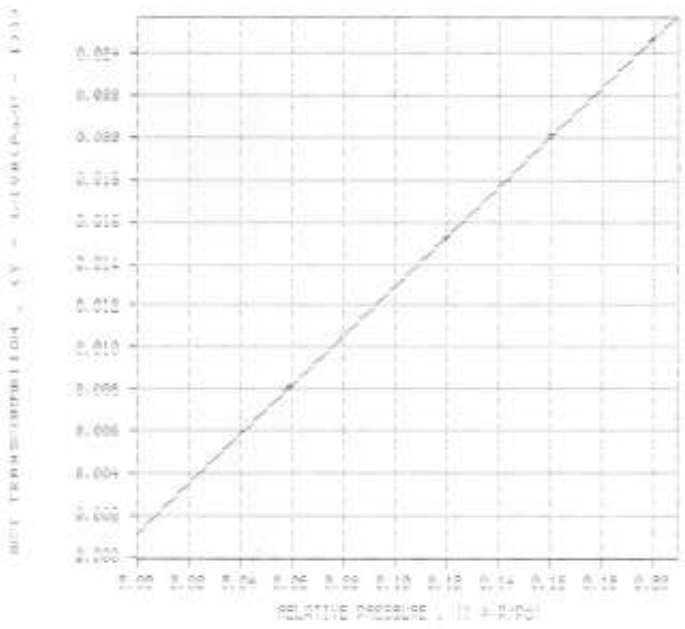

Surface Area and Pore Size Distribution Lab.

ASAP 2000 V3.03 A PAGE 6

SAMPLE DIRECTORY/NUMBER: SAC /24
SAMPLE ID: Number 2
SUBMITTER: St Paul
OPERATOR: RAC
UNIT NUMBER: 1
ANALYSIS GAS: Nitrogen

START 12:40:11 01/09/09
COMPL 15:45:19 01/09/09
REPRT 09:38:57 01/12/09
SAMPLE WT: 0.1041 g
FREE SPACE: 54.3275 cc
EQUIL INTRVL: 5 sec

MICROPORE ANALYSIS REPORT

MICROPORE VOLUME:	0.000714	cc/g
MICROPORE AREA:	2.2208	sq. m/g
EXTERNAL SURFACE AREA:	34.2147	sq. m/g
SLOPE:	2.211965 +/-	0.039193
Y-INTERCEPT:	0.461440 +/-	0.155357
CORRELATION COEFFICIENT:	9.998638-01	

RELATIVE PRESSURE	STATISTICAL THICKNESS,(nm)	VOL ADSORBED (cc/g STP)
0.0793	0.351	8.2363
0.1398	0.397	9.2201
0.1996	0.437	10.1295
0.2999	0.501	11.6379
0.4497	0.606	14.0955

THICKNESS VALUES USED IN THE LEAST-SQUARES ANALYSIS WERE BETWEEN 0.350 AND 0.500 nm.

$$t = \left[\frac{13.9900}{0.0340 - \log(P/Po)} \right]^{0.500}$$

SURFACE AREA CORRECTION FACTOR IS 1.000.

Surface Area and Pore Size Distribution Lab.

ASAP 2000 V3.03 A PAGE 7

SAMPLE DIRECTORY/NUMBER: SAC /24
SAMPLE ID: Number 2
SUBMITTER: St Paul
OPERATOR: RAC
UNIT NUMBER: 1
ANALYSIS GAS: Nitrogen

START 12:40:11 01/09/09
COMPL 15:45:19 01/09/09
REPRT 09:38:57 01/12/09
SAMPLE WT: 0.1041 g
FREE SPACE: 54.3275 cc
EQUIL INTRVL: 5 sec

t-PLOT

+ fitted, + non-fitted

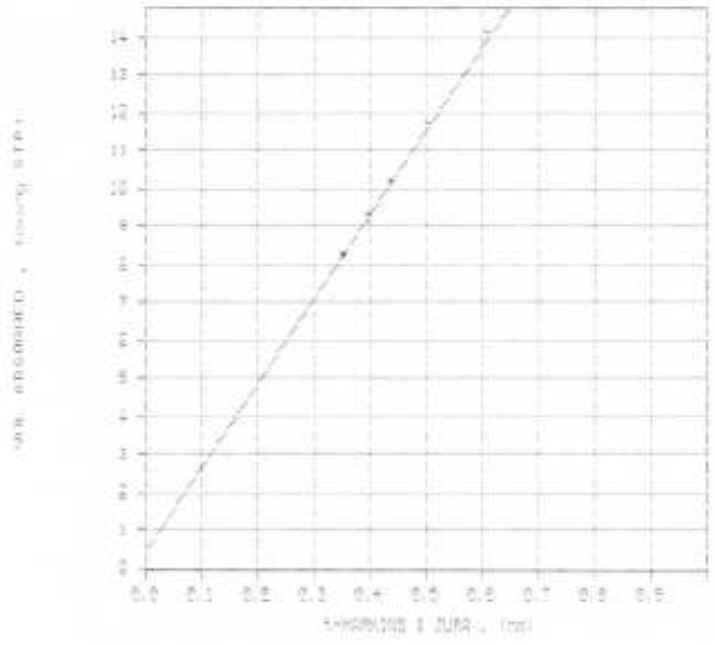

Surface Area and Pore Size Distribution Lab.

ASAP 2000 V3.03 A PAGE 8

SAMPLE DIRECTORY/NUMBER: SAC /24
SAMPLE ID: Number 2
SUBMITTER: St Paul
OPERATOR: RAC
UNIT NUMBER: 1
ANALYSIS GAS: Nitrogen

START 12:40:11 01/09/09
COMPL 15:45:19 01/09/09
REPRT 09:38:57 01/12/09
SAMPLE WT: 0.1041 g
FREE SPACE: 54.3215 cc
EQUIL INTRVL: 5 sec

BJH ADSORPTION PORE DISTRIBUTION REPORT

PORE DIAMETER RANGE (nm)		AVERAGE DIAMETER (nm)	INCREMENTAL PORE VOLUME (cc/g)	CUMULATIVE PORE VOLUME (cc/g)	INCREMENTAL PORE AREA (sq. m/g)	CUMULATIVE PORE AREA (sq. m/g)
311.6-	156.2	186.9	0.015729	0.015729	0.337	0.337
156.2-	120.6	153.8	0.003317	0.019547	0.114	0.451
120.6-	119.8	120.2	0.001969	0.021516	0.066	0.518
119.8-	101.5	109.1	0.003183	0.024701	0.117	0.633
101.5-	94.1	97.5	0.002152	0.026852	0.088	0.721
94.1-	82.7	87.6	0.002754	0.029607	0.126	0.847
82.7-	74.6	78.2	0.002601	0.032207	0.133	0.980
74.6-	65.8	69.6	0.003622	0.035829	0.208	1.188
65.8-	61.7	63.6	0.001981	0.037810	0.125	1.313
61.7-	53.7	57.1	0.003385	0.041195	0.237	1.550
53.7-	48.1	50.6	0.003268	0.044463	0.259	1.808
48.1-	42.2	44.7	0.002991	0.047454	0.268	2.076
42.2-	37.5	39.6	0.002822	0.050275	0.285	2.361
37.5-	33.5	35.3	0.002735	0.053010	0.310	2.672
33.5-	30.0	31.6	0.002491	0.055501	0.316	2.987
30.0-	27.1	28.4	0.002428	0.057929	0.342	3.329
27.1-	23.9	25.3	0.002931	0.060860	0.463	3.792
23.9-	21.6	22.6	0.002592	0.063452	0.458	4.250
21.6-	18.7	19.9	0.003118	0.066570	0.626	4.876
18.7-	16.6	17.5	0.002843	0.069413	0.650	5.526
16.6-	14.8	15.6	0.002469	0.071882	0.633	6.159
14.8-	13.1	13.8	0.002848	0.074731	0.830	6.988
13.1-	11.7	12.3	0.002523	0.077274	0.822	7.810
11.7-	10.5	11.0	0.002263	0.079537	0.821	8.631
10.5-	9.2	9.7	0.002928	0.082465	1.201	9.833
9.2-	8.1	8.6	0.002646	0.085111	1.233	11.065
8.1-	7.1	7.5	0.002837	0.087948	1.512	12.577
7.1-	6.0	6.4	0.003127	0.091074	1.939	14.517
6.0-	5.3	5.6	0.002510	0.093585	1.800	16.316
5.3-	4.6	4.9	0.002143	0.095727	1.750	18.066
4.6-	4.1	4.3	0.001956	0.097682	1.800	19.867
4.1-	3.7	3.9	0.001776	0.099459	1.827	21.693
3.7-	3.3	3.5	0.001886	0.101344	2.156	23.850
3.3-	3.0	3.2	0.001869	0.103213	2.365	26.215
3.0-	2.7	2.9	0.001920	0.105133	2.685	28.900
2.7-	2.5	2.6	0.001890	0.107023	2.922	31.822
2.5-	2.2	2.3	0.001417	0.108440	2.427	34.249
2.2-	2.0	2.1	0.001868	0.110308	3.621	37.870

Surface Area and Pore Size Distribution Lab.

ASAP 2000 V3.03 A PAGE 9

SAMPLE DIRECTORY/NUMBER: SAC /24
SAMPLE ID: Number 2
SUBMITTER: St Paul
OPERATOR: RAC
UNIT NUMBER: 1
ANALYSIS GAS: Nitrogen

START 12:40:11 01/09/09
COMPL 15:45:19 01/09/09
REPRT 09:38:57 01/12/09
SAMPLE WT: 0.1041 g
FREE SPACE: 54.3215 cc
EQUIL INTRVL: 5 sec

BJH(D) ADSORPTION PORE VOLUME PLOT

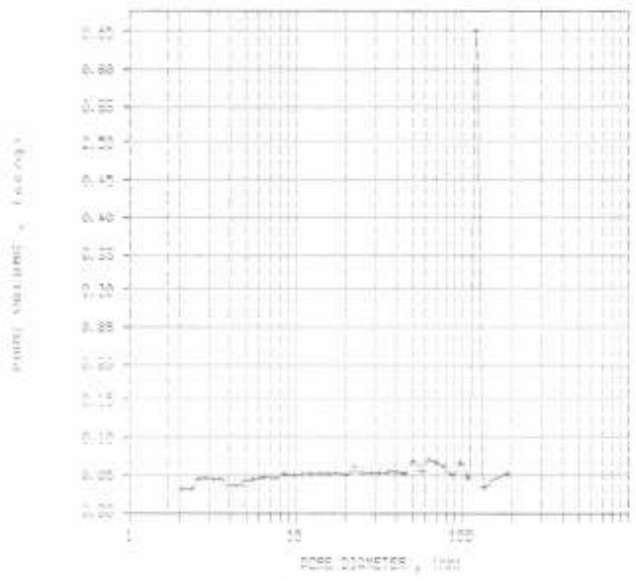

SAMPLE DIRECTORY/NUMBER: SAC /24
SAMPLE ID: Number 2
SUBMITTER: St Paul
OPERATOR: RAC
UNIT NUMBER: 1
ANALYSIS GAS: Nitrogen

START 12:40:11 01/09/09
COMPL 15:45:19 01/09/09
REPRT 09:38:57 01/12/09
SAMPLE WT: 0.1041 g
FREE SPACE: 54.3215 cc
EQUIL INTRVL: 5 sec

BJH DESORPTION PORE DISTRIBUTION REPORT

PORE DIAMETER RANGE (nm)		AVERAGE DIAMETER (nm)	INCREMENTAL PORE VOLUME (cc/g)	CUMULATIVE PORE VOLUME (cc/g)	INCREMENTAL PORE AREA (sq. m/g)	CUMULATIVE PORE AREA (sq. m/g)
88.1-	57.0	66.0	0.011085	0.011085	0.672	0.672
57.0-	42.1	47.2	0.011652	0.022736	0.986	1.658
42.1-	41.9	42.0	0.001670	0.024406	0.159	1.817
41.9-	33.0	36.4	0.008948	0.033354	0.985	2.802
33.0-	27.1	29.5	0.007809	0.041163	1.073	3.875
27.1-	22.5	24.4	0.006847	0.048109	1.124	4.999
22.5-	21.4	21.9	0.002705	0.050214	0.384	5.383
21.4-	18.1	19.4	0.005218	0.055432	1.073	6.456
18.1-	16.4	17.2	0.003191	0.058623	0.744	7.201
16.4-	14.5	15.3	0.003680	0.062303	0.961	8.162
14.5-	12.8	13.5	0.003462	0.065765	1.026	9.187
12.8-	11.4	12.0	0.003425	0.069189	1.143	10.331
11.4-	10.2	10.7	0.003019	0.072208	1.126	11.456
10.2-	9.0	9.5	0.003559	0.075768	1.499	12.955
9.0-	7.9	8.4	0.003444	0.079211	1.647	14.603
7.9-	6.8	7.3	0.003687	0.082898	2.028	16.631
6.8-	5.8	6.2	0.003651	0.086549	2.349	18.980
5.8-	5.0	5.3	0.003027	0.089576	2.265	21.244
5.0-	4.4	4.7	0.002532	0.092108	2.172	23.416
4.4-	3.9	4.1	0.002289	0.094397	2.228	25.643
3.9-	3.5	3.7	0.005954	0.100351	6.509	32.152
3.5-	3.1	3.3	0.003741	0.104091	4.583	36.736
3.1-	2.8	2.9	0.001339	0.105430	1.834	38.569
2.8-	2.5	2.6	0.000992	0.106423	1.513	40.082
2.5-	2.2	2.4	0.001087	0.107510	1.849	41.932
2.2-	2.0	2.1	0.000403	0.107912	0.748	42.700
2.0-	1.7	1.8	0.000819	0.108732	1.776	44.476

Surface Area and Pore Size Distribution Lab.
ASAP 2000 V3.03 A PAGE 11

SAMPLE DIRECTORY/NUMBER: SAC /24
SAMPLE ID: Number 2
SUBMITTER: St Paul
OPERATOR: RAC
UNIT NUMBER: 1
ANALYSIS GAS: Nitrogen

START 12:40:11 01/09/09
COMPL 15:45:19 01/09/09
REPRT 09:38:57 01/12/09
SAMPLE WT: 0.1041 g
FREE SPACE: 54.3215 cc
EQUIL INTRVL: 5 sec

BJH Single DESORPTION PORE VOLUME PLOT

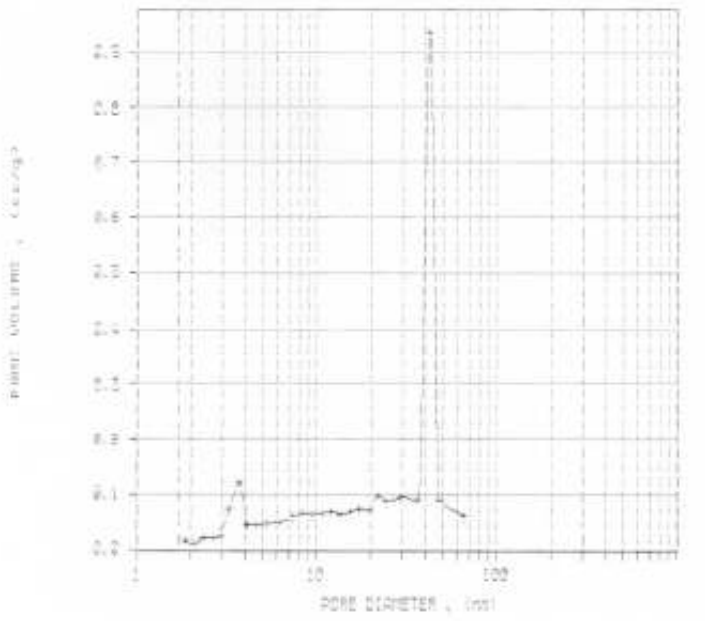

SAMPLE DIRECTORY/NUMBER: SAC /24
SAMPLE ID: Number 2
SUBMITTER: St Paul
OPERATOR: RAC
UNIT NUMBER: 1
ANALYSIS GAS: Nitrogen

START 12:40:11 01/09/09
COMPL 15:45:19 01/09/09
REPRT 09:38:57 01/12/09
SAMPLE WT: 0.1041 g
FREE SPACE: 54.3215 cc
EQUIL INTRVL: 5 sec

DIGISORB 2500-STYLE ADSORPTION PORE VOLUME DISTRIBUTION REPORT

RANGE PORE DIAMETER,A	AVERAGE DIA.,A	PORE VOLUME (cc/g)	CUMULATIVE PORE VOLUME	SURFACE AREA (sq. m/g)	CUMULATIVE SURFACE AREA
500.-500.	550.0	0.005007	0.005007	0.364	0.364
500.-450.	475.0	0.002771	0.007778	0.233	0.597
450.-400.	425.0	0.002928	0.010706	0.276	0.873
400.-350.	375.0	0.003350	0.014056	0.357	1.230
350.-300.	325.0	0.003834	0.017890	0.472	1.702
300.-280.	290.0	0.001621	0.019511	0.224	1.926
280.-260.	270.0	0.001799	0.021309	0.266	2.192
260.-240.	250.0	0.001994	0.023304	0.319	2.511
240.-220.	230.0	0.002255	0.025558	0.392	2.903
220.-200.	210.0	0.002214	0.027772	0.422	3.325
200.-180.	190.0	0.002513	0.030286	0.529	3.854
180.-160.	170.0	0.002885	0.033171	0.679	4.533
160.-150.	155.0	0.001403	0.034574	0.362	4.895
150.-140.	145.0	0.001572	0.036145	0.434	5.329
140.-130.	135.0	0.001808	0.037953	0.536	5.864
130.-120.	125.0	0.001824	0.039777	0.584	6.448
120.-110.	115.0	0.001834	0.041611	0.707	7.156
110.-100.	105.0	0.002776	0.044387	0.829	7.985
100.- 95.	97.5	0.000953	0.044940	0.391	8.375
95.- 90.	92.5	0.001245	0.046185	0.539	8.914
90.- 85.	87.5	0.001301	0.047486	0.595	9.509
85.- 80.	82.5	0.001390	0.048876	0.674	10.183
80.- 75.	77.5	0.001309	0.050185	0.676	10.858
75.- 70.	72.5	0.001512	0.051697	0.834	11.692
70.- 65.	67.5	0.001499	0.053196	0.888	12.580
65.- 60.	62.5	0.001778	0.054974	1.138	13.718
60.- 55.	57.5	0.001656	0.056630	1.152	14.877
55.- 50.	52.5	0.001845	0.058475	1.406	16.276
50.- 45.	47.5	0.001992	0.060467	1.677	17.954
45.- 40.	42.5	0.002224	0.062691	2.093	20.047
40.- 35.	37.5	0.002588	0.065279	2.760	22.807
35.- 30.	32.5	0.003359	0.068638	4.134	26.941
30.- 25.	27.5	0.004252	0.072889	6.184	33.125
25.- 20.	22.5	0.004450	0.077339	7.911	41.037

SAMPLE DIRECTORY/NUMBER: SAC /24
SAMPLE ID: Number 2
SUBMITTER: St Paul
OPERATOR: RAC
UNIT NUMBER: 1
ANALYSIS GAS: Nitrogen

START 12:40:11 01/09/09
COMPL 15:45:19 01/09/09
REPRT 09:38:57 01/12/09
SAMPLE WT: 0.1041 g
FREE SPACE: 54.3215 cc
EQUIL INTRVL: 5 sec

SUMMARY REPORT

AREA

BET SURFACE AREA:	36.4354	sq. m/g
SINGLE POINT SURFACE AREA AT P/Po 0.1998:	35.2951	sq. m/g
BJH CUMULATIVE ADSORPTION SURFACE AREA OF PORES BETWEEN 1.7000 AND 300.0000 nm DIAMETER:	37.8701	sq. m/g
BJH CUMULATIVE DESORPTION SURFACE AREA OF PORES BETWEEN 1.7000 AND 300.0000 nm DIAMETER:	44.4756	sq. m/g
MICROPORE AREA:	2.2208	sq. m/g

VOLUME

SINGLE POINT TOTAL PORE VOLUME OF PORES LESS THAN 119.7707 nm DIAMETER AT P/Po 0.9830:	0.087840	cc/g
BJH CUMULATIVE ADSORPTION PORE VOLUME OF PORES BETWEEN 1.7000 AND 300.0000 nm DIAMETER:	0.110308	cc/g
BJH CUMULATIVE DESORPTION PORE VOLUME OF PORES BETWEEN 1.7000 AND 300.0000 nm DIAMETER:	0.106732	cc/g
MICROPORE VOLUME:	0.000714	cc/g

PORE SIZE

AVERAGE PORE DIAMETER (4V/A BY BET):	9.6436	nm
BJH ADSORPTION AVERAGE PORE DIAMETER (4V/A):	11.6512	nm
BJH DESORPTION AVERAGE PORE DIAMETER (4V/A):	9.7790	nm